UNIVERSIDADE ESTADUAL DE CAMPINAS
INSTITUTO DE GEOCIÊNCIAS

RAISA FAGUNDES DE FIGUEIRÊDO

PETROLOGIA, GEOCRONOLOGIA E GEOFÍSICA DAS ROCHAS ALCALINAS MESOZOICAS DO NORTE DO CRÁTON AMAZÔNICO

PETROLOGY, GEOCHRONOLOGY AND GEOPHYSICS OF THE MESOZOIC ALKALINE ROCKS FROM NORTHERN AMAZONIAN CRATON

CAMPINAS
2020

RAISA FAGUNDES DE FIGUEIRÊDO

PETROLOGIA, GEOCRONOLOGIA E GEOFÍSICA DAS ROCHAS ALCALINAS MESOZOICAS DO NORTE DO CRÁTON AMAZÔNICO

PETROLOGY, GEOCHRONOLOGY AND GEOPHYSICS OF THE MESOZOIC ALKALINE ROCKS FROM NORTHERN AMAZONIAN CRATON

TESE APRESENTADA AO INSTITUTO DE GEOCIÊNCIAS DA UNIVERSIDADE ESTADUAL DE CAMPINAS PARA OBTENÇÃO DO TÍTULO DE DOUTORA EM CIÊNCIAS NA ÁREA DE GEOLOGIA E RECURSOS NATURAIS

ORIENTADOR: PROF. DR. TICIANO JOSÉ SARAIVA DOS SANTOS
COORIENTADOR: PROF. DR. ROGÉRIO GUITARRARI AZZONE

ESTE EXEMPLAR CORRESPONDE À VERSÃO FINAL DA TESE DEFENDIDA PELA ALUNA RAISA FAGUNDES DE FIGUEIRÊDO E ORIENTADA PELO PROF. DR. TICIANO JOSÉ SARAIVA DOS SANTOS E COORIENTADA PELO PROF. DR. ROGÉRIO GUITARRARI AZZONE

CAMPINAS
2020

Ficha catalográfica
Universidade Estadual de Campinas
Biblioteca do Instituto de Geociências
Marta dos Santos - CRB 8/5892

F469p

Figueirêdo, Raisa Fagundes de, 1991-
Petrologia, geocronologia e geofísica das rochas alcalinas mesozoicas do norte do Cráton Amazônico / Raisa Fagundes de Figueirêdo. – Campinas, SP : [s.n.], 2020.

Orientador: Ticiano José Saraiva dos Santos.
Coorientador: Rogério Guitarrari Azzone.
Tese (doutorado) – Universidade Estadual de Campinas, Instituto de Geociências.

1. Rochas igneas alcalinas. 2. Gretas (Geologia). 3. Crátons – Amazônia. 4. Roraima. 5. Escudo das Guianas. I. Santos, Ticiano José Saraiva dos, 1964-. II. Azzone, Rogério Guitarrari. III. Universidade Estadual de Campinas. Instituto de Geociências. IV. Título.

Informações para Biblioteca Digital

Título em outro idioma: Petrology, geochronology and geophysics of the Mesozoic alkaline rocks from northern Amazonian Craton
Palavras-chave em inglês:
Alkalic igneous rocks
Rifts (Geology)
Cratons - Amazon River Region
Roraima (Brazil)
Guiana Highlands
Área de concentração: Geologia e Recursos Naturais
Titulação: Doutora em Ciências
Banca examinadora:
Ticiano José Saraiva dos Santos [Orientador]
Elson Paiva de Oliveira
Excelso Ruberti
Sérgio de Castro Valente
Emilson Pereira Leite
Data de defesa: 23-09-2020
Programa de Pós-Graduação: Geociências

Identificação e informações acadêmicas do(a) aluno(a)
- ORCID do autor: https://orcid.org/0000-0001-5725-3349
- Currículo Lattes do autor: http://lattes.cnpq.br/6712137084816477

UNIVERSIDADE ESTADUAL DE CAMPINAS
INSTITUTO DE GEOCIÊNCIAS

AUTORA: RAISA FAGUNDES DE FIGUEIREDO

PETROLOGIA, GEOCRONOLOGIA E GEOFÍSICA DAS ROCHAS ALCALINAS MESOZOICAS DO NORTE DO CRÁTON AMAZÔNICO

ORIENTADOR: PROF. DR. TICIANO JOSÉ SARAIVA DOS SANTOS
COORIENTADOR: PROF. DR. ROGÉRIO GUITARRARI AZZONE

Aprovado em: 23 / 09 / 2020

EXAMINADORES:

Prof. Dr. Ticiano José Saraiva dos Santos - Presidente

Prof. Dr. Elson Paiva de Oliveira

Prof. Dr. Emilson Pereira Leite

Prof. Dr. Excelso Ruberti

Prof. Dr. Sérgio de Castro Valente

A Ata de Defesa assinada pelos membros da Comissão Examinadora consta no processo de vida acadêmica da aluna.

Campinas, 23 de setembro de 2020.

BIOGRAFIA

Roraimense, possui graduação em Geologia pela Universidade Federal de Roraima – UFRR (2013). Durante a graduação participou de projetos de iniciação científica na área de Estratigrafia. Estagiou na Companhia de Pesquisa de Recursos Naturais (CPRM) durante os anos de 2010 e 2011, onde adquiriu experiência com SIG e mapeamento geológico.

Em 2014 ingressou no programa de pós-graduação em Geociências, nível mestrado, na Unicamp. O projeto de mestrado englobou estudos na área de geofísica, petrologia e geocronologia. Participou do programa de estágio docente – PED como monitora da disciplina de Mineralogia para Química (2015). O mestrado lhe rendeu uma publicação no Journal of South America Earth Sciences (2018).

Em 2016 ingressou no doutorado, dando continuidade à área de pesquisa do mestrado. O projeto incluiu novos métodos e ampliou a área geográfica. Participou duas vezes do programa de estágio docente – PED como monitora da disciplina de Mineralogia II (2016 e 2018).

DEDICATÓRIA

Dedico essa tese a minha mãe
em reconhecimento a todo seu esforço
de três décadas.

AGRADECIMENTOS

Durante todo esse tempo, muitas pessoas contribuíram para que essa tese chegasse a um formato final. Mas para que eu chegasse a fazer parte da Unicamp, foi necessária uma vida inteira de esforços e incentivos da minha mãe. Por isso, ela é a primeira pessoa a quem eu agradeço. Além de uma mãe incrível, ela é uma mulher maravilhosa e uma excelente professora (mesmo que ela não saiba). Foi a primeira pessoa a me ensinar o valor de um senso crítico. Sem isso, jamais estaria finalizando um doutorado. Minha eterna gratidão.

Aos meus queridos orientadores, Ticiano e Rogério, que sempre estiveram dispostos a me ajudar no que fosse necessário. Ticiano que me abriu as portas da Unicamp, acreditou em mim e na minha ideia desde o começo. Rogério que também agarrou a ideia, me ensinou e me incentivou muito, sempre paciente e disponível mesmo em outra cidade. Foram muitos anos de confiança, apoio e grandes discussões.

Ao meu querido Pan por toda a paciência e incentivo, principalmente nas etapas finais do doutorado (uma loucura só). Mesmo sem conhecer muito o meu trabalho, sabia que eu seria capaz de finalizá-lo. Estava sempre disposto a ouvir eu falar (durante horas) sobre geologia, laboratório, cráton, oceano e tudo que tinha direito. Muita gratidão por tudo!

A SGM Mineração e a Amazon Stone por toda a assistência durante os trabalhos de campo. Agradeço especialmente ao Marcelo Almeida e ao Mide Vasconcelos que não mediram esforços para que chegássemos as entranhas da floresta amazônica. Ao Zazá que estava lá sempre disposto a ser o mateiro da vez.

Aos amigos Alice Bosco, Paola Melo, Igor Camargo, Matheus Scalabrin, Aquila Mesquita, João Motta, Verônica Trevisan e Thais de Paula pelas valiosas discussões (e desabafos) durante todo esse período de pós-graduação. As minhas queridas amigas Patrícia Silva, Alcione Moreira, Mayara Messias, Thais Fernandes e Aline Silva que Campinas me deu a oportunidade de conhecer e que foram sempre um apoio nas horas difíceis. Galera, vocês são demais! Muita gratidão a vida por tê-los conhecido.

A CPRM pelos dados aerogeofísicos disponibilizados que foram peças chave para que o trabalho alcançasse um bom resultado. A CAPES pela minha bolsa de doutorado que permitiu a minha sobrevivência em Campinas.

O presente trabalho foi realizado com apoio da Coordenação de Aperfeiçoamento de Pessoal de Nível Superior - Brasil (CAPES) - Código de Financiamento 001.

Foto: Claudia Andujar.

"Os anos tranquilos na bacia do rio Catrimâni, em Roraima, foram interrompidos pelo desenvolvimento da Amazônia durante o governo militar. Entre 1973 e 1976, a construção da rodovia Perimetral Norte, no lugar exato em que Andujar desenvolvia seu trabalho, espalhou um rastro de doenças e conflitos que os Yanomami até então desconheciam. Em 1975, pesquisas aéreas revelaram a existência de minérios nobres na terra indígena, atraindo garimpeiros e mineradoras. Desmatamento, poluição e epidemias marcaram as décadas seguintes, com a omissão de Brasília, que pretendia "integrar" os índios para transformá-los em força de trabalho".

Trecho extraído da exposição fotográfica de Claudia Andujar, no Museu da Imagem e do Som, São Paulo, 2019.

Curadoria de Thyago Nogueira.

RESUMO

A Província Alcalina de Roraima (PAR) corresponde a um magmatismo relacionado a um ambiente de rift, encaixado em importantes falhas e zonas de cisalhamento da porção centro-sul do Escudo das Guianas. Trata-se da primeira província alcalina proposta para o Escudo das Guianas e ao único registro de magmatismo alcalino cretáceo intrudindo o embasamento paleo e mesoproterozoico do norte do Cráton Amazônico. A província é constituída por rochas insaturadas em sílica, predominantemente nefelina sienito e fonolito que ocorrem como grandes e pequenos corpos plutônicos e diques, enquanto as rochas básicas são restritas a raros diques de lamprófiro, tefrito e tefrifonolito. Neste trabalho, são apresentados novos dados petrográficos, geoquímicos, isotópicos e geocronológicos com o intuito de verificar se as rochas são de fato cogenéticas e propor um modelo de origem para a província. Além disso, foram analisados os dados aerogeofísicos para sete plutons *foid* sieníticos da PAR, bem como a assinatura aeromagnética do seu embasamento. As rochas estudadas são nefelina normativa, com afinidades peralcalinas e metaluminosas, e mineralogia que varia de miaskítica a agpaítica. Os dados geoquímicos e petrográficos sugerem que as rochas evoluíram principalmente por cristalização fracionada. A possível relação entre as rochas félsicas e básicas foi avaliada a partir de modelagem termodinâmica utilizando o MELTS, a qual sugere que alguns fonolitos e sienitos podem ser o resultado da cristalização de 51-68% de um magma tefrítico. Os dados petrográficos, geoquímicos, isotópicos e geocronológicos indicam que processos de contaminação crustal afetaram a petrogênese das rochas estudadas. Os dados de geocronologia forneceram idades entre ~100 e 116 Ma para a PAR, indicando que a atividade magmática alcalina no Escudo das Guianas aconteceu durante um curto período do Cretáceo. As assinaturas isotópicas das amostras menos contaminadas sugerem que a fonte está relacionada a mistura de dois componentes mantélicos, uma provável mistura entre um componente enriquecido e outro empobrecido. Além disso, as idades T_{DM} variam entre 548 e 657 Ma, intervalo que coincide com as idades modelo dos basaltos da *Central Atlantic Magmatic Province (CAMP)* no Escudo das Guianas, sugerindo um mesmo evento de metassomatismo mantélico para os magmas alcalino e toleítico, associado aos esforços distensivos mesozoicos. As rochas estudadas são caracterizadas por altas concentrações de eU, eTh e K, além de amplitudes baixas a altas na imagem ASA em comparação as rochas do embasamento. Sendo assim, as interpretações dos dados aerogeofísicos aliados aos dados de campo funcionaram como um importante guia prospectivo para as rochas félsicas da PAR, além de permitirem compreender o arcabouço estrutural da região. Os dados magnetométricos mostraram as estruturas relacionadas aos diferentes eventos tectônicos que afetaram a região, tais como Transamazônico, K'Mudku e a reativação mesozoica. A ascensão do magmatismo alcalino cretáceo está estreitamente associada a reativação dessas estruturas pré-cambrianas NE e NW e, posteriormente, a movimentos transcorrentes E-W. Além disso, ao correlacionar as estruturas com os dados geocronológicos disponíveis, conclui-se que o *emplacement* da PAR coincide com a movimentação tectônica do início da abertura do Oceano Atlântico Equatorial.

Palavras-chave: Escudo das Guiana; Cretáceo; Cráton Amazônico; Roraima; magmatismo alcalino.

ABSTRACT

The Roraima Alkaline Province (RAP) is rift-related magmatism emplaced into main faults and shear zones central-southern part of Guyana Shield, northern Amazonian Craton. It corresponds to the first alkaline province proposed to Guyana Shield, which timing of emplacement coincides with early rifting stage in the Equatorial Atlantic. The RAP encompasses mainly felsic rocks, mostly foid syenites and phonolites as large and small plutons or dykes, while basic rocks are confined to scarce lamprophyre, tephrite and tephriphonolite dykes. In this paper, we combine petrographic, geochemical and isotopic evidence, as well as U-Pb ages, to evaluate whether indeed these rocks are cogenetic and propose a model for the origin of the RAP. Besides, we analysed airborne radiometric and magnetometric data from seven foid and foid-bearing syenites from RAP, as well as the aeromagnetic signature of the Precambrian basement to understand its relationships with the alkaline magmatism. The studied rocks are nepheline-normative, from metaluminous to peralkaline affinity and with mineralogy that varies from miaskitic to agpaitic. The geochemical patterns indicate that the rock-types seem to be controlled mainly by fractional crystallisation and the increase in peralkalinity conditions is attributed to the extensive fractionation of feldspar. The possible relationship between basic and felsic magma was evaluated by MELTS thermodynamic modelling which demonstrated that some phonolites and syenites may be the result of 51–68% crystallization of a tephritic magma. Geochemical, isotopic, geochronological and petrographic features show that crustal assimilation process played a role in the genesis of the studied rocks. The U-Pb ages obtained for RAP range from ~100 to 116 Ma, indicating that alkaline magmatic activity in central Guyana Shield was a short-lived event. The Sr-Nd isotopic signatures suggest a mixture of the depleted and enriched mantle as responsible for generating those rocks. Furthermore, depleted-mantle model ages present relatively short intervals, between 548 to 657 Ma, which coincides with model ages for tholeiites of Central Atlantic Magmatic Province in Guyana Shield, suggesting the same metasomatic event for Mesozoic alkaline and tholeiite magmatism. Therefore, the lithospheric mantle metasomatism took place shortly before magmatism, triggered by an extensional tectonic environment regarding the Tacutu rift and the Atlantic opening. Gamma-ray spectrometry data allowed us to delineate the area of high favourability to other alkaline bodies. The rocks are characterized by high concentrations of eU, eTh and K relative to the host basement and exhibit mostly low to intermediate amplitude in the ASA image. Therefore, interpretations of gamma-ray spectrometry and magnetic data constrained by field observations proved to be efficient in prospecting alkaline rocks and deciphering the regional structures in remote regions and areas of the limited outcrop. The major deformational events in the central Guyana Shield, such as Paleoproterozoic Trans-Amazonian, Mesoproterozoic K'Mudku and Mesozoic reactivation, provides a framework from which we can derive the magnetic framework of the area and insights over its structures, as well as understand their relationships with the alkaline magmatism. Alkaline magmatism occurs associated with reactivations of Precambrian NE and NW-trending weakness zones and, subsequently, E-W strike-slip faults during early rifting stage in the Equatorial Atlantic Ocean.

Keywords: Guyana Shield; Cretaceous; Amazonian Craton; Roraima; alkaline magmatism.

LISTA DE FIGURAS

LISTA DE TABELAS

SUMÁRIO

CAPÍTULO 1 – ASPECTOS INTRODUTÓRIOS

1. Apresentação

Vasto número de províncias ígneas, associadas a diferentes contextos magmáticos, são descritas ao redor do mundo. O termo "província ígnea" vem sendo utilizado para agrupar rochas ígneas que possuem afinidade petrográfica ou geoquímica, que ocorrem em uma área geográfica delimitada e que se formaram durante um dado intervalo de atividade magmática (Rock, 1981; Bates e Jackson, 1987). Essas províncias variam desde alguns plugs até enormes volumes de magma (Rock, 1981). Trata-se de um conceito muito útil para agrupar uma associação de rochas que estão relacionadas a um evento tectonotermal específico ou a uma sequência de eventos (Gillespie et al., 2008).

As centenas de corpos ígneos alcalinos e carbonatíticos na Plataforma Sul-Americana, ligados aos eventos do meso-cenozoico, foram divididos em diferentes províncias (Gomes e Comin-Chiaramonti, 2017). Dentre todas as ocorrências alcalinas, Ulbrich e Gomes (1981) reconhecem oito tipos de associações petrográficas principais, predominando variedades insaturadas em sílica. Almeida (1983) agrupou as ocorrências alcalinas da Plataforma Sul-Americana em 12 províncias. A sua distribuição espacial no Brasil está estreitamente relacionada a reativação de zonas de fraqueza pré-cambrianas, desde o Permiano Superior no Cráton Amazônico, a Triássico nas outras regiões (Ulbrich e Gomes, 1981; Almeida, 1986). Posteriormente, Riccomini et al. (2005) reúnem em 15 províncias todas as ocorrências na porção centro-sudeste da Plataforma Sul-Americana, e destacam que elas são estruturalmente controladas por descontinuidades ao redor de importantes bacias sedimentares.

Morbidelli et al. (1995) mostram que, nas suítes alcalinas e alcalinas-carbonatíticas do Brasil, existe uma preponderância de corpos intrusivos evoluídos, com corpos cumuláticos máficos a ultramáficos subordinados. Petrologicamente, a cristalização fracionada tem sido reportada como o principal processo de evolução magmática, relacionando tipos mais primitivos e mais evoluídos de uma mesma associação (Morbidelli et al., 1995; Gomes e Comin-Chiaramonti, 2017). Processos de contaminação crustal também têm sido descritos para algumas ocorrências brasileiras, tais como Ponte Nova (Azzone et al.,

2016), Fortaleza (Macciotta et al., 1990), Itatiaia (Brotzu et al., 1997) e Cananeia (Spinelli e Gomes, 2009).

Sob um contexto mais amplo, os dados geocronológicos para as intrusões alcalinas brasileiras variam desde o Paleoproterozoico até o Cenozoico. A predominância desse magmatismo ocorreu durante o intervalo 250 - 50 Ma, com picos entre o Permiano e o Triássico (250-240 Ma), no Cretáceo Inferior (~130 Ma) e entre o Cretáceo Superior e o Eoceno (90-50Ma) (Gomes e Comin-Chiaramonti, 2005). A atividade alcalina mais recente está limitada ao nordeste brasileiro, entre 50 e 7 Ma, associada ao último estágio de abertura do Atlântico (Sial, 1987; Macciotta et al., 1990; Silveira, 2006; Ngonge et al., 2016). Já as ocorrências mais antigas estão restritas ao Complexo de Angico dos Dias, borda do Cráton São Francisco, com idades em torno de 2,01 Ga (Silva et al., 1988; Gomes et al., 1990), e as ocorrências no Cráton Amazônico com idades entre o Meso e Neoproterozoico (referências na Tabela 2.1).

Embora o controle estrutural para essas rochas seja claro, os modelos geodinâmicos para sua geração ainda são muito debatidos. Para Gibson et al. (1995) e Thompson et al. (1998), o magmatismo alcalino meso-cenozoico no sudeste brasileiro está relacionado a presença de uma pluma sob a litosfera subcontinental. Esta hipótese é parcialmente sustentada por reconstruções paleogeográficas que mostram que a Província do Alto Paranaíba estava localizada na atual Pluma de Trindade. Por outro lado, dados isotópicos e geocronológicos não suportam esta teoria, levando alguns autores a interpretarem o magmatismo alcalino como produto da fusão de um manto litosférico metassomatizado, mas sem o envolvimento de plumas, ligado principalmente à reativação de antigas zonas de fraqueza (Riccomini et al., 2005; Gomes et al., 2011; Guarino et al., 2013).

Especificamente para as ocorrências alcalinas intrusivas no embasamento do Cráton Amazônico, apenas duas províncias são definidas: Províncias Alcalinas de Velasco e Candelária – Bolívia, ambas de idade cretácea e localizadas no Escudo Brasil Central (Fletcher and Beddoe-Stephens, 1987; Comin-Chiaramonti et al., 2005, Riccomini et al., 2005). Até o momento, não existe nenhuma província alcalina proposta para o Escudo das Guianas. Contudo, alguns complexos alcalinos e alcalinos-carbonatíticos são descritos nos dois seguimentos do Cráton Amazônico. Esses complexos são constituídos por uma ampla variedade de rochas, desde insaturadas a supersaturadas em sílica, máficas e félsicas, as quais apresentam forte controle estrutural e idades predominantemente meso e neoproterozoicas (referências na Tabela 2.1).

A maioria das rochas alcalinas no Escudo das Guianas datam do Mesoproterozoico, entre 1000 e 1500 Ma, intervalo no qual Cordani et al. (2010) associam a importantes eventos tectônicos na região. Estes autores atribuem a geração de magma alcalino no cráton a *hot spots* e plumas, cuja ascensão se deu por meio de zonas de fraqueza pré-existentes. Independentemente da idade, essas rochas estão associadas a importantes estruturas que cortam todo o cráton (Ulbrich e Gomes, 1981; Cordani et al., 2010). Rossoni et al. (2017) afirmam que o Complexo Carbonatítico de Seis Lagos, com idade de 1328 Ma, foi controlado por um importante lineamento E-W e estruturas NE-SW e WNW-ESE secundárias que aparecem na porção oeste do cráton. Além de Seis Lagos, o Complexo Alcalino de Maicuru, de idade mais recente (589 Ma), está encaixado ao longo de importantes sistemas de falhas NE-SW e NW-SE que cortam a porção leste do Escudo das Guianas (Gomes et al., 1990; Costa et al., 1991).

Nas últimas décadas, alguns trabalhos chamaram atenção para ocorrências de rochas alcalinas cretáceas no Escudo das Guianas. Os primeiros registros, na porção brasileira, deram-se com os projetos Norte da Amazônia e RADAM, durante a década de 1970. Primeiramente foi descrito um plúton de nefelina sienito, cortado por diques de fonolito, o qual foi denominado de Sienito Catrimâni (Salas e Santos, 1974; Montalvão et al., 1975). Posteriormente, o Serviço Geológico do Brasil – CPRM em conjunto com o DNPM (atual ANM), mapearam novas ocorrências de rochas alcalinas com ajuda de importantes projetos aerogeofísicos, descritas em Borges (1990) e Brandão e Freitas (1994). Nessa fase foram descobertas as rochas localizadas a cerca de 150 km a norte do Sienito Catrimâni, as quais foram descritas na literatura como Suíte ou Complexo Apiaú (Borges, 1990; Brandão e Freitas, 1994; Reis et al., 1999; Reis et al., 2004; Figueiredo, 2016 e Figueiredo et al., 2018).

Neste contexto, o objetivo principal dessa tese é a proposição de uma nova província ígnea alcalina cretácea, a qual foi denominada de Província Alcalina de Roraima, integrando novos dados geológicos, petrológicos e geocronológicos. Trata-se da primeira província alcalina proposta para o Escudo das Guianas. Visto que a maior parte dela se localiza em uma área de acesso muito limitado, buscou-se definir a provável extensão desse magmatismo alcalino por meio de métodos aerogeofísicos.

A tese está organizada em formato de artigos, apresentados nos capítulos 2 e 3 e seguidos por considerações finais integradas. O capítulo 2 apresenta o artigo que define a Província Alcalina de Roraima, dividindo-a em duas subprovíncias, no qual discute a evolução geológica por meio de dados petrográficos, geoquímicos, isotópicos e

geocronológicos. Nesse artigo constam os dados de 6 plutons de sienitos insaturados e 15 diques de composições variadas mapeados durante o doutorado e compilados de Figueiredo (2016).

No capítulo 3 é apresentado o artigo com dados aerogeofísicos para a Província Alcalina de Roraima e seu embasamento pré-cambriano. Nele são reveladas as assinaturas aeromagnetométrica e aerogamaespetromética das rochas alcalinas de maior expressão na província. Além disso, discute-se a evolução tectônica da porção central do Escudo das Guianas que favoreceu a ascensão do magma alcalino durante o Cretáceo.

2. Localização e acesso

A área de estudo está localizada na porção central do estado de Roraima, extremo norte do Brasil, e compreende uma região com aproximadamente 85.000 km^2. Entretanto os trabalhos de campo ocorreram apenas nos municípios de Mucajaí e Iracema, onde afloram as rochas alcalinas e onde é possível acessá-las. A maior parte da zona oeste da área corresponde a terra indígena Yanomami e a áreas de preservação ambiental, e não foram visitadas durante os trabalhos de campo. As duas regiões em que afloram as rochas alcalinas estão a cerca de 150 km uma da outra, sendo aqui denominadas de subprovíncias Apiaú (ao norte) e Catrimâni (ao sul), nomes referentes a vilarejos locais e importantes rios.

A subprovíncia Apiaú é a região onde mais aflora rochas alcalinas. Portanto, é também a área com maior amostragem nesta tese, onde se tem maior facilidade de acesso, mais infraestrutura e mais exposição de rochas. Por ser uma grande área, pode ser acessada por várias vias. Localiza-se a cerca de 100 km da capital Boa Vista, sendo o acesso pela BR-174 por 60 km sentido sul até a cidade de Mucajaí. Ao passar pela cidade, segue-se pela RR-325 por 16 km até a rodovia MUC-445 (antiga vicinal 7), continuando por aproximadamente 15 km até a vila Campos Novos. A partir daí, é possível o acesso por várias vicinais, tais como vicinal 3 e 12 (Figura 1.1).

O acesso a subprovíncia Catrimâni, ao sul, é feito por rodovias e hidrovias. Boa parte da região encontra-se encoberta por uma cobertura sedimentar que a transforma ou em uma área alagadiça na época de chuvas ou uma área não navegável em época de seca. O percurso total até a intrusão Catrimâni é de aproximadamente 400 km. O acesso é feito a partir da capital Boa Vista até a cidade de Caracaraí, pela BR-174, sentido sul, por 146 km. A partir de Caracaraí, o transporte passa a ser hidroviário. Partindo do porto de Caracaraí,

navega-se por um trecho de aproximadamente 170 km pelo Rio Branco, sentido sul, até a confluência com o Rio Catrimâni. O trecho no Rio Catrimâni é de 60 km, sentido noroeste, até a confluência com o Igarapé Uixi. Posteriormente, segue-se no Igarapé Uixi, sentido norte, por aproximadamente 20 km até próximo a intrusão Catrimâni, onde o acesso passa a ser terrestre por cerca de 5 km. Entretanto, o trecho de caminhada pode aumentar se o nível do Igarapé Uixi estiver muito baixo.

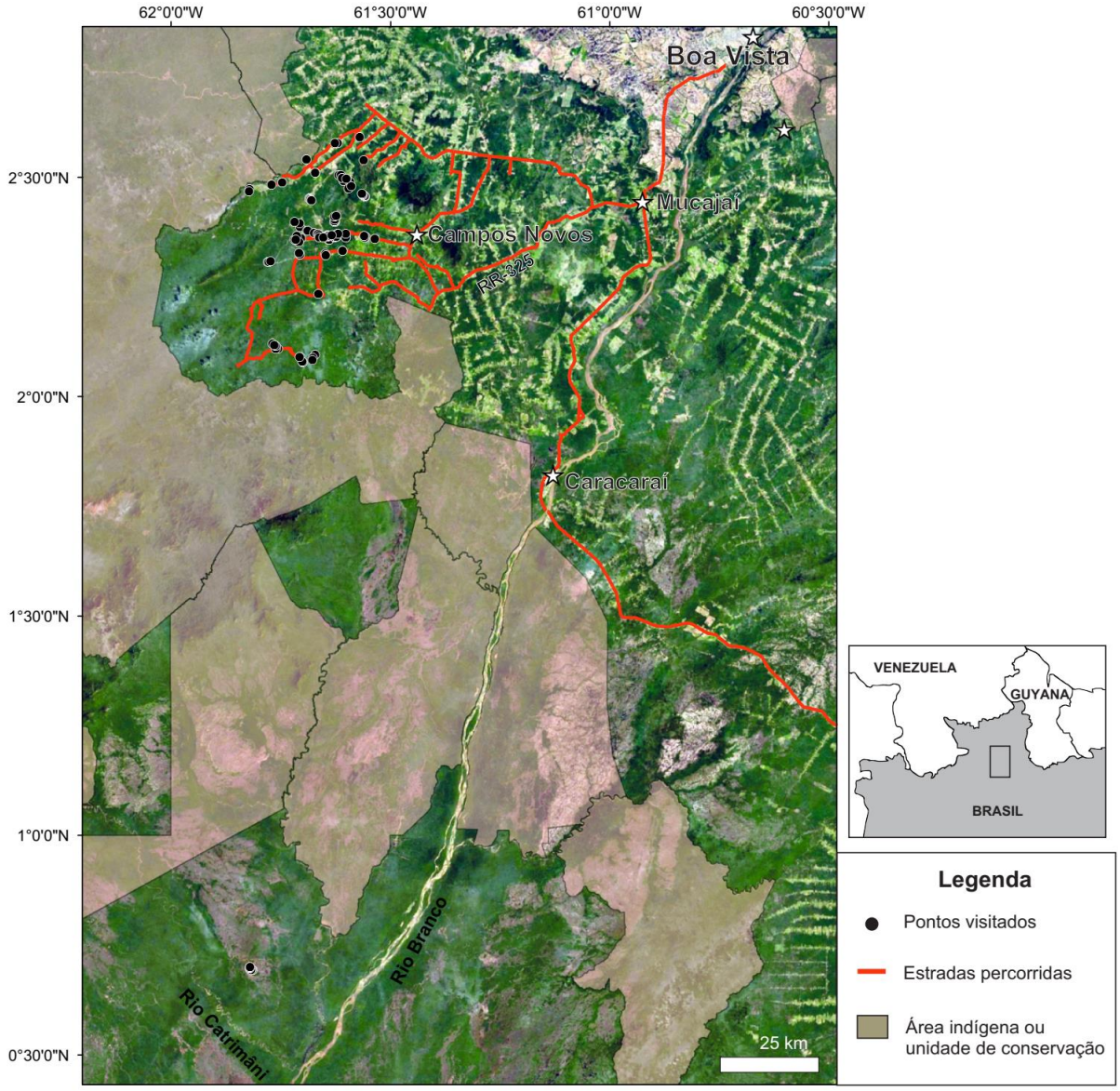

Figura 1.1: Mapa de localização da região estudada com as vias de acesso.

3. Geologia Regional

O Cráton Amazônico corresponde a uma das maiores áreas cratônicas do mundo, limitado a leste, sul e sudeste por faixas móveis neoproterozoicas geradas durante o Ciclo Brasiliano (Santos, 2003; Tassinari e Macambira, 2004). A noroeste e sudoeste é recoberto por bacias foreland relacionadas a Cordilheira dos Andes (Cordani et al., 2009). O Cráton Amazônico é dividido em Escudo das Guianas e Escudo Brasil Central ou Guaporé (Almeida, 1983), separados pelas bacias Paleozoicas do Amazonas e Solimões. O Escudo das Guianas corresponde a parte norte do cráton e abrange Brasil, Colômbia, Venezuela, Guiana, Suriname e Guiana Francesa. É composto por um embasamento de rochas graníticas e metamórficas, possuindo um importante registro do Arqueano ao Mesoproterozoico (Kroonemberg et al., 2016).

A evolução tectônica do Cráton Amazônico ainda é muito incerta, e vem sendo discutida na forma de províncias geocronológicas (Figura 1.2). Tassinari e Macambira (1999, 2004), propõem que parte dessas províncias se formaram a partir de materiais derivados do manto e evoluíram através de uma sucessão de arcos magmáticos, enquanto outras estão associadas a processos colisionais envolvendo reciclagem da crosta mais antiga. Santos et al. (2000, 2006) sugerem que as províncias seriam geradas por acresção crustal relacionada a processos orogenéticos e por retrabalhamento da crosta arqueana. A porção estudada do Escudo das Guianas localiza-se no norte da província Tapajós-Parima e na faixa K'Mudku de Santos et al. (2000, 2006) ou na província Maroni-Itacaiúnas de Tassinari e Macambira (1999, 2004).

Os diversos processos tectônicos que atuaram no Cráton Amazônico contribuíram para a formação de zonas de fraqueza profundas, as quais serviram de conduto para magmas alcalinos (Cordani et al., 2010). Com exceção das rochas cretáceas da Província Alcalina de Roraima, as ocorrências alcalinas do cráton datam do Meso ao Neoproterozoico (ver Tabela 2.1). Independentemente da idade, essas rochas estão associadas a importantes estruturas que cortam todo o cráton (Ulbrich e Gomes, 1981) e cuja origem mantélica é atribuída a *hot spots* e plumas (Cordani et al., 2010). Além disso, Teixeira (1978) associam o magmatismo alcalino do Cráton Amazônico ao magmatismo máfico também registrado.

Na parte centro-sul do Escudo das Guianas estão localizadas as rochas cretáceas da Província Alcalina de Roraima. A província é composta predominantemente por rochas félsicas, tais como monzonito, sienito, sienito com nefelina e nefelina sienito, traquito e fonolito, enquanto as rochas básicas são restritas a estreitos diques de nefelinito (Salas and Santos, 1974; Montalvão et al., 1975; Borges, 1990; Brandão and Freitas, 1994; Reis et al., 2004; Figueiredo, 2016). As rochas apresentam idades U-Pb que variam de 111 a 116 Ma (Figueiredo et al., 2018) e Rb-Sr de 100 Ma (Montalvão et al., 1975).

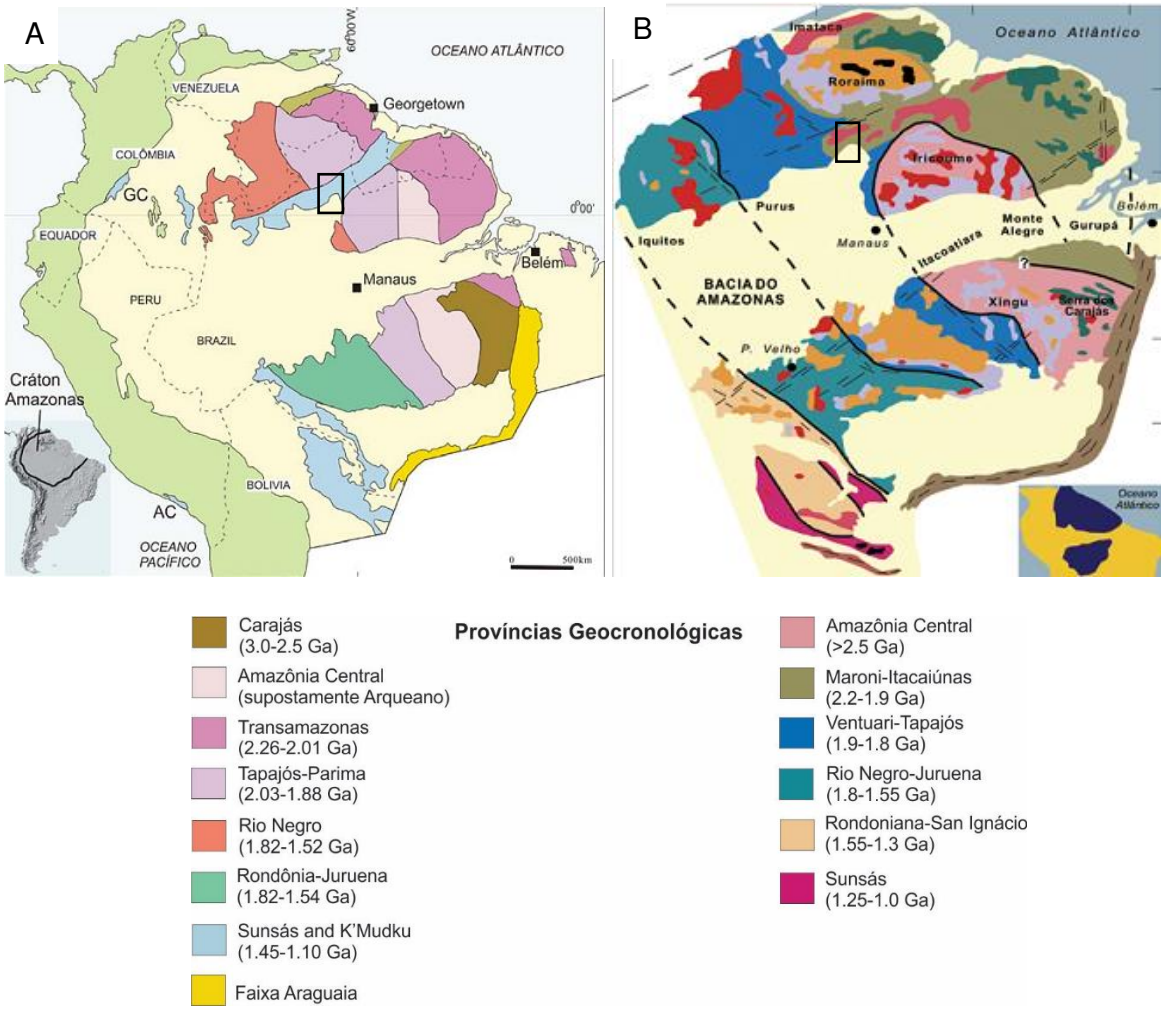

Figura 1.2: Compartimentação geocronológica do Cráton Amazônico. A) Modelo proposto por Santos et al. (2000, 2006a); B) Modelo proposto por Tassinari e Macambira (1999, 2004). O retângulo preto corresponde a área de estudo, inserida entre a Província Tapajós-Parima e a faixa K'Mudku, ou ainda na Província Maroni-Itacaiúnas, de acordo com os modelos existentes.

3.1 O embasamento pré-cambriano

As rochas alcalinas afloram ao longo de importantes falhas e zonas de cisalhamento de um terreno estruturalmente complexo do Escudo das Guianas. A principal e mais antiga feição estrutural corresponde ao Cinturão Cauarane–Coeroeni, descrito como uma estrutura sinuosa NW–SE/NE–SW (Fig. 3.1) que inclui rochas paleoproterozoicas supracrustais de fácies anfibolito a granulito (Kroonemberg, 1976; Delor et al., 2003; Fraga et al., 2009). Imediatamente ao sul do cinturão, predominam granitoides Orosirianos (1.96-1.91 Ga) e gnaisses de alto potássio, cálcio-alcalinos, metamorfisados em 1,91 Ga (Gaudette et al., 1996; Fraga, 2002; Reis et al., 2003; Costa, 2005; Fraga et al., 2009). Lentes de charnockitos e granulitos paleoproterozoicos também afloram nessa porção (Fraga et al. 2009). Ao sul do cinturão, é descrita uma associação de anortosito, gabro, mangerito e granito rapakivi, com idades em torno de 1,5 Ga (Gaudette et al., 1996; Fraga, 2002; Reis et al., 2003; Fraga et al., 2009; Heinonen et al., 2012).

O Cinturão Cauarane-Coeroeni é considerado um reflexo da orogenia transamazônica, entretanto sua evolução tectônica ainda é incerta. De acordo com Fraga et al. (2009, 2017), o cinturão é o resultado do fechamento de uma bacia orogênica em torno de 2 Ga, formada devido a colisão de arcos magmáticos de 2.04-2.03 Ga com blocos riacianos. Por outro lado, Kroonenberg et al. (2016) sugerem que o cinturão evoluiu a partir da formação de uma bacia rift, seguido por metamorfismo de alto grau em 2.07-2.05 Ga e 1.99-1.95 Ga, durante o Transamazônico. Além disso, colocam que a subducção ocorreu para norte e que o final da colisão ocorreu entre 2.03–2.00 Ga e o magmatismo pós-orogênico em 1.98 Ga.

O evento tectônico K'Mudku, desencadeado no Mesoproterozoico (1.49 and 1.15 Ga), afetou a porção central do Escudo das Guianas. Este evento gerou um cinturão de cisalhamento NE-SW que trunca o Cinturão Cauarane-Coeroeni e cruza o escudo do Suriname ao estado do Amazonas (Fig. 3.1., Gibbs e Barron, 1993; Santos et al., 2000, 2006). Esse evento é interpretado como uma flexura tectônica, de médio a alto grau metamórfico, decorrente da colisão Sunsás, na porção sudoeste do Cráton Amazônico (Santos et al., 2000, 2006). Por outro lado, Fraga (2002) e Fraga et al. (2009) argumentam que o evento K'Mudku resultou em zonas de cisalhamento rúptil-dúctil, com obliteração total ou parcial das estruturas pré-existentes, desenvolvidas por um mecanismo de transpressão em condições de baixo grau metamórfico.

3.2 Bacia do Tacutu

Reativações mesozoicas das estruturas geradas no Paleo e Mesoproterozoico foram responsáveis pelo desenvolvimento do rift Tacutu (Crawford et al., 1985; Eiras e Kinoshita, 1988) e ascensão do magmatismo alcalino. A Bacia do Tacutu é um aulacógeno em formato de meio-gráben alongado na direção NE-SW, que se estende por 300 km entre o Brasil e a Guiana, atingindo de 30 a 50 km de largura (Figura 1.3). As grandes falhas de Lethem e Kanuku estabelecem os limites sul/sudeste da bacia, enquanto as falhas Surumu, Maú e Pirara delimitam a borda norte, sendo consideradas as ombreiras do rift, facilmente identificadas por afloramentos de rochas vulcânicas (Silva e Porsani, 2006; Vaz *et al*., 2007).

O arcabouço estratigráfico da bacia compreende rochas sedimentares e vulcânicas, chegando a ultrapassar seis mil metros de espessura (Berrangé e Dearnley, 1975; Crawford *et al.*, 1984; Eiras e Kinoshita, 1988; Vaz *et al*., 2007). As seções sísmicas mostram um espessamento predominantemente de noroeste para sudeste, refletindo o forte controle tectônico da borda sudeste, onde se encontram os maiores rejeitos e maior espessura sedimentar (Vaz *et al*., 2007). No Mioceno a bacia foi afetada por um evento transcorrente que atingiu toda a seção vulcânica e sedimentar, resultando na formação de dobras e estruturas em flor positiva, além de reativação de antigos falhamentos (Eiras e Kinoshita, 1988).

A fase inicial do rift é marcada pelo magmatismo toleítico da *Central Atlantic Magmatic Province - CAMP* no início do Triássico, com diques por volta de 200 Ma e derrames vulcânicos no assoalho da bacia entre 153 e 135 Ma (Marzoli et al., 1999; Leal et al., 2000; Reis et al., 2006). A estratigrafia proposta para a bacia engloba na base os basaltos da Formação Apoteri (Vaz et al., 2007), seguido discordantemente por sedimentos clásticos finos (siltitos, folhelhos e dolomitos) da Formação Manari. A terceira sequência é a Formação Pirara, constituída por halitas, seguida de siltitos vermelhos da Formação Tacutu. O topo da sequência rifte corresponde a arenitos, e com menor frequência conglomerados e pelitos, da Formação Serra do Tucano, marcando o final da sedimentação da Bacia do Tacutu durante o Cretáceo Inferior, concomitante à cristalização das rochas alcalinas (Vaz et al., 2007; Figueiredo et al., 2018).

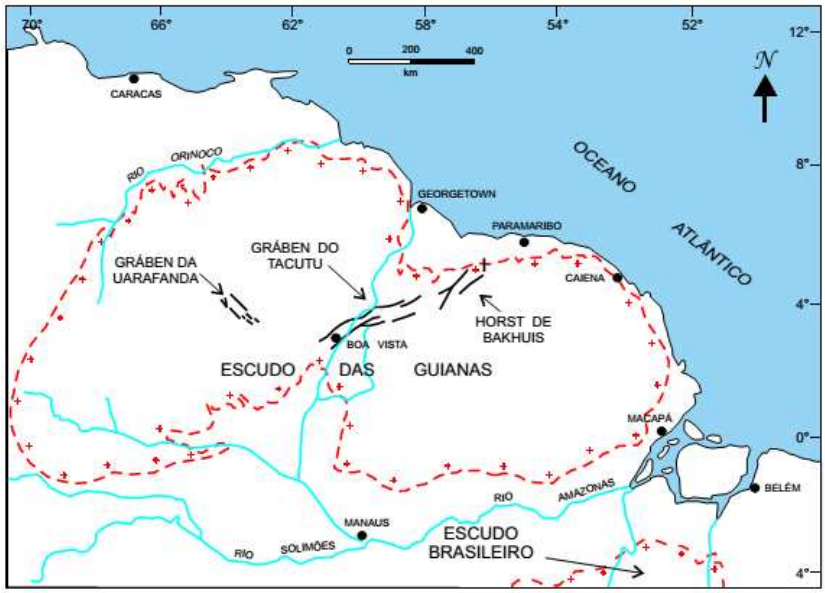

Figura 1.3: Localização da Bacia do Tacutu na porção central do Escudo das Guianas (Silva e Porsani, 2006).

4. Materiais e Métodos

4.1 Trabalhos de Campo

Os trabalhos de campo visaram mapear as rochas alcalinas e coletar amostras para as análises apresentadas no capítulo 2. Os trabalhos de campo foram organizados em duas etapas: a primeira ocorreu em abril de 2016, durante 18 dias, e a segunda em março de 2017 por 12 dias, totalizando 30 dias de campo. É importante salientar que os 30 dias correspondem apenas ao período de mapeamento, sem considerar os contratempos durante a logística. Algumas dificuldades, descritas a seguir, forçaram o retorno à capital Boa Vista diversas vezes, o que reduziu bastante o período de campo.

Os trabalhos de campos foram viabilizados pelas empresas SGM mineração e Amazon Stone, que forneceram todo o apoio de transporte, hospedagem e pessoal. Os campos foram concentrados nos municípios de Mucajaí e Iracema, em Roraima, onde o acesso é feito por pequenas estradas de terra, algumas delas construídas pela própria SGM. Embora essa região esteja se tornando um polo pecuarista, boa parte ainda é encoberta pela densa floresta amazônica, e, por isso, o acesso a alguns pontos visitados foi através de abertura de picadas. Além disso, a vegetação da área sofre com queimadas sazonais que favorecem o aparecimento de plantas daninhas (juquira) difíceis de serem retiradas, tornando a abertura de picadas um processo muito demorado.

Os principais desafios enfrentados durante os trabalhos de campo foram as limitações relacionadas a infraestrutura, aos conflitos de terra e a presença de animais selvagens. As estradas secundárias, conhecidas como vicinais, não são asfaltadas e sofrem com a falta de manutenção. Ademais, as pontes são de madeira, algumas vezes improvisadas, e comumente são danificadas durante as épocas de cheias. Em virtude do desmatamento ilegal e dos conflitos históricos de terra no estado, muitos proprietários não permitiram a entrada em suas fazendas. Essa questão afetou muito o mapeamento, pois impossibilitou a amostragem em muitos alvos. Além disso, essa região da floresta é repleta de enormes bandos de porcos selvagens, conhecidos popularmente como queixadas. Esses animais andam em bandos de pelo menos 100, chegando a 300 porcos, e são muito agressivos quando se sentem ameaçados.

O sul da área de estudo, onde está localizada a intrusão Catrimâni, é uma das regiões de mais difícil acesso em Roraima, sendo parte dela acessada apenas por vias fluviais. Encoberta pela Bacia do Solimões, com uma cobertura sedimentar que transforma a região ou em uma área alagadiça ou uma área muito seca, limitando o acesso a períodos bem específicos. Na época alagadiça o acesso terrestre se torna comprometido, e na época da seca, os rios secam a ponto de deixarem de ser navegáveis. Portanto, o acesso é feito apenas no início da época de chuvas. Infelizmente, não foi possível viabilizar a logística para campo no Catrimâni e a aquisição dos dados deu-se devido ao apoio da empresa Amazon Stone ao ceder amostras daquela região.

Figura 1.4: A) Acampamento provisório em projeto de pesquisa mineral da SGM mineração; B) Geólogo e auxiliar de campo da Amazon Stone que integraram a equipe de campo; C) Funcionários da Amazon Stone em trabalho de campo na região do rio Catrimâni; D) Parte da estrada particular da SGM mineração onde o acesso é feito por meio de quadriciclo; E) Bando de porcos selvagens atravessando uma estrada de terra próximo a vila Campos Novos; F) Pontes de madeira, típicas das estradas da região, comprometidas em virtude de grandes cheias.

4.2 Petrografia

Ao todo foram descritas 62 lâminas de amostras superficiais que correspondem a plutons de composição *foid* sienítica, diques de composição variada, além das rochas graníticas do embasamento. As lâminas foram confeccionadas no Instituto de Geociências da USP. A petrografia macro e microscópica consistiu na identificação da assembleia mineral e texturas referentes aos diferentes estágios magmáticos. A descrição microscópica foi realizada utilizando microscópio petrográfico Carl Zeiss, modelo Axiolab, do Laboratório de Microscopia do Instituto de Geociências da Unicamp. O reconhecimento das fases complexas e exóticas se deu a partir de análises em MEV-EDS. Estas análises foram realizadas no Laboratório de Microscopia Eletrônica do Instituto de Geociências da Unicamp, utilizando-se o microscópio LEO 430i Zeiss com um espectrômetro de energia dispersiva (EDS) acoplado da Oxford Instruments.

4.3 Geoquímica de rocha total

Foram selecionadas 33 amostras da Província Alcalina de Roraima para análises geoquímicas de elementos maiores, menores e traços. As análises dos óxidos de elementos maiores e menores foram feitas por fluorescência de raio-X através de um espectrômetro sequencial (Philips, PW2404). Para isso, foram confeccionadas pastilhas prensadas pela mistura de 9 g de amostra e 1,5 g cera em pó, e discos de vidro constituídos por uma mistura de amostra com metaborato e tetraborato de lítio. Os procedimentos seguidos estão descritos em Vendemiatto e Enzweiler (2001).

As análises de elementos traço foram realizadas por um ICP-Q-MS equipado com uma célula de colisão, seguindo o protocolo de Cotta e Enzweiler (2011). Para a diluição das amostras, uma mistura de 100g de amostra com HF/HNO_3 foi fechada e aquecida a 180ºC por 4 dias. Depois foi acrescentado $HClO_4$ e evaporado a 150ºC por mais 4 horas. Todas as análises foram realizadas no Laboratório de Geoquímica Analítica e no Laboratório de Geologia Isotópica do Instituto de Geociências da Unicamp.

4.4 Geoquímica isotópica

As análises da composição isotópica de Sr-Nd para 13 amostras foram realizadas no Centro de Pesquisas Geocronológicas do Instituto de Geociências da USP. Os detalhes da separação química e dos métodos analíticos estão descritos em Souza (2009) e Petronilho (2009). As razões isotópicas de Sr foram determinadas por um espectrômetro de massa de ionização térmica (TIMS – Thermo Triton), enquanto os isótopos de Nd foram medidos por um ICP-MS Thermo-Neptune. As razões medidas foram normalizadas para $^{86}Sr/^{88}Sr = 0,1194$ e $^{146}Nd/^{144}Nd = 0,7219$ e $^{143}Nd/^{144}Nd = 0,7219$. Elas foram calculadas usando os materiais de referência o isótopo de Sr NBS 987 (Média: 0.710248 ± 0.000017; n = 100) e isótopo de Nd JNDi-1 (Média: 0.512100 ± 0.000005; n = 20). Os valores de $^{87}Sr/^{86}Sr$ e $^{143}Nd/^{144}Nd$ iniciais foram corrigidos para 116 Ma.

4.5 Geocronologia

A aquisição dos dados geocronológicos foi uma das etapas mais desafiadoras desta tese em virtude das características físicas e químicas das rochas. Foram encontrados minerais para datação U-Pb apenas em alguns dos plutons de composição sienítica. Os diques estudados apresentam granulação muito fina e largura centimétricas, o que dificulta muito encontrar minerais para datação. Em alguns deles, foram identificados cristais muito pequenos de zircão (<10 um) em MEV, inviáveis para análises geocronológicas. Dentre as amostras preparadas, foram encontrados minerais para datação U-Pb em cinco delas: três amostras com zircão e duas com badeleíta.

Os procedimentos para separação de zircão consistiram na britagem das amostras em britador de mandíbulas, moagem em moinho de discos de tungstênio, concentração mineral por densidade em bateia, separação magnética através de ímãs de neodímio e separador Frantz e, por fim, catação em lupa binocular. Já os procedimentos para separação de badeleíta consistiram em britagem, moagem, banho ultrassônico, concentração de minerais pesados na mesa de Wilfley, separação magnética manual e catação em lupa binocular. Entretanto, a separação de badeleíta foi uma etapa mais complexa e será explicada em detalhes a seguir:

1. **Britagem e moagem** - A britagem de amostra foi feita num britador de mandíbulas (assim como na separação de zircão, Fig.1.5A). Posteriormente foi feita a moagem em um

moinho de discos de tungstênio, com o mínimo de abertura possível entre os discos (Fig.1.5B). Para amostras de granulação mais fina, recomenda-se também a moagem no moinho de disco de anéis, durante 2 a 4 minutos (Fig.1.5C). Embora muitos grãos de badeleíta possam ser fragmentados durante a moagem, Heaman (2007) mostra que a pulverização no moinho de anéis é capaz de liberar mais badeleítas e aumentar a recuperação dos grãos menores (<30 um). Portanto, essa é uma etapa primordial para uma separação mineral satisfatória;

2. **Banho ultrassônico** - Cerca de 300 a 400 g do pó de rocha foram misturados com água e gotas de detergente neutro até obter uma textura de lama (Fig.1.5D). Essa mistura foi então colocada em banho ultrassônico durante 20 min (Fig.1.5E). Conforme Söderlund e Johansson (2002), o banho ultrassônico com adição de detergente facilita o umedecimento completo do pó e reduz a adesão entre as partículas;

3. **Concentração mineral por gravidade** - A concentração de minerais pesados foi feita em uma mesa vibratória de Wilfley utilizando a metodologia *water-based* descrita em Söderlund e Johansson (2002). Essa técnica baseia-se no princípio que os grãos maiores se movem numa velocidade muito maior ao longo da mesa vibratória do que os grãos menores. Mesmo apresentando densidade de 5,7 g/cm3, a badeleíta comporta-se como uma fase mineral menos densa devido à alta razão superfície/volume.

Cerca de 1 colher de sopa rasa da mistura, resultante da etapa anterior, é colocada na parte superior da mesa vibratória. O tempo para começar a coleta varia de 4 a 8 minutos, dependendo da amostra. A coleta é feita com auxílio de uma pisseta e um Becker (Fig.1.5F). Esse processo se repete até que toda a amostra seja derramada na mesa.

Como a mesa vibratória de Wilfley do Instituto de Geociências da Unicamp possui dimensões menores (90 x 50 cm) que a utilizada em Söderlund e Johansson (2002) (127 x 61 cm), foram feitos testes para constatar se a técnica *water-based* era eficiente para essas condições, bem como para definir os parâmetros que deveriam ser modificados para melhor eficácia na separação mineral. Para isso, utilizou-se de areia essencialmente quartzosa e cristais de badeleíta anteriormente separados. A areia foi moída no moinho de anéis, até a obtenção de um pó fino não homogêneo, com o intuito de parecer o máximo possível com uma amostra real. Para cada teste foram utilizados cerca de 3 colheres de sopa de areia, sendo adicionados 10 cristais de badeleíta provenientes do carbonatito de Jacupiranga (Matheus, 2019).

Os principais parâmetros variáveis na mesa de Wilfley são o fluxo de água e seu ângulo de inclinação. Dos testes realizados, o que apresentou melhor eficácia teve uma recuperação de 70% dos grãos de badeleíta. Para chegar nesse resultado, substituiu-se a mangueira original da mesa por outra com saídas de água de diâmetros menores, de forma a lavar toda a mesa com menor vazão de água (Fig. 1.6A e B). As saídas originais, por serem muito grandes, lavavam a mesa muito rapidamente, ocasionando perda significativa de material.

Vários ângulos de inclinação da mesa foram testados (2° a 10°), de forma a analisar o efeito da inclinação na recuperação da badeleíta. Os testes demonstraram melhor eficácia ao ajustar a mesa vibratória para 6º. Para os ângulos muito baixos, houve um espalhamento do material na porção lateral esquerda da mesa (Fig. 1.6C), além de demorar muito tempo para atravessá-la, sem concentração efetiva. A recuperação para esses ângulos foi em torno de 30%. Já para ângulos elevados, a lavagem foi muito rápida, apresentando também uma baixa recuperação ~ 30%. Devido ao menor tamanho da mesa, foi necessário coletar mais material do final do concentrado do que o indicado por Söderlund e Johansson (2002).

4. **Separação magnética** - Após a etapa de concentração mineral na mesa vibratória, os minerais magnéticos foram removidos utilizando de um ímã de mão fraco (Fig.1.5G). É importante que esse processo seja feito logo após a etapa da mesa, sem secar a amostra, pois os grãos de badeleíta tendem a aderir ao vidro depois de secos. Só depois a amostra é colocada sob uma lâmpada quente (Fig.1.5H) A badeleíta ficará no concentrado não magnético;

5. **Catação** - A identificação e catação da badeleíta foram feitas manualmente na lupa binocular (Fig.1.5I). A identificação é uma etapa que requer treino até a familiarização com os grãos. A badeleíta apresenta variações nas cores e opacidade dependendo do litotipo, causando dificuldades na sua individualização. Entretanto, seu brilho característico, o aspecto de "relevo alto" (ao transmitir e refletir a luz da lupa), bem como uma clivagem na direção do eixo C do cristal, auxiliam muito na identificação (Fig.1.7). Os cristais selecionados são colados em fita dupla face e analisados em MEV-EDS. É crucial que, ao colocar os grãos na fita, eles fiquem nivelados. Isso é importante para que, depois de colocar a resina, todos os grãos fiquem próximos a superfície do mount e sejam expostos com o lixamento e polimento.

Tanto os grãos de zircão quanto de badeleíta foram coletados da fração de pesados, montados em resina epóxi e lixados e/ou polidos até se obter uma superfície plana. Os mounts de badeleíta foram levemente lixados com lixa nº 2500 e polidos com pasta diamantada 0-1. Para grãos muito pequenos (<30um), recomenda-se apenas o polimento suficiente para retirar a cola da fita dupla face. O lixamento e polimento são extremamente delicados, visto que muitos grãos podem ser perdidos nessas etapas por serem frágeis e pequenos.

Apesar do aprimoramento das técnicas de concentração de badeleíta, a recuperação dos grãos é muito dependente do litotipo. Para carbonatito e sienito, em 400g da amostra, a recuperação pode ultrapassar 30 grãos, enquanto para um shonkinito a recuperação é bem menor, em média 15 a 20 grãos, sendo necessário uma quantidade maior de amostra para compor o mount (Matheus, 2019).

As idades U-Pb de zircão e badeleíta foram obtidas por *Laser Ablation Sector Field Inductively Coupled Plasma Mass Spectrometry* (LA-SF-ICP-MS) do Laboratório de Geologia Isotópica do Instituto de Geociências da UNICAMP. O equipamento utilizado foi um Thermo Scientific Element XR acoplado a um sistema de *laser ablation* Excite 193 Photon Machines. O diâmetro do spot do laser foi de 25 µm. Como materiais de referência foram utilizados zircão 91500 e badeleíta Phalaborwa, enquanto zircão Peixe e badeleíta Kovdor foram utilizados como padrão interno. A redução dos dados foi realizada pelo software IOLITE, e o cálculo das idades foi feito através do ISOPLOT (Ludwig, 1991).

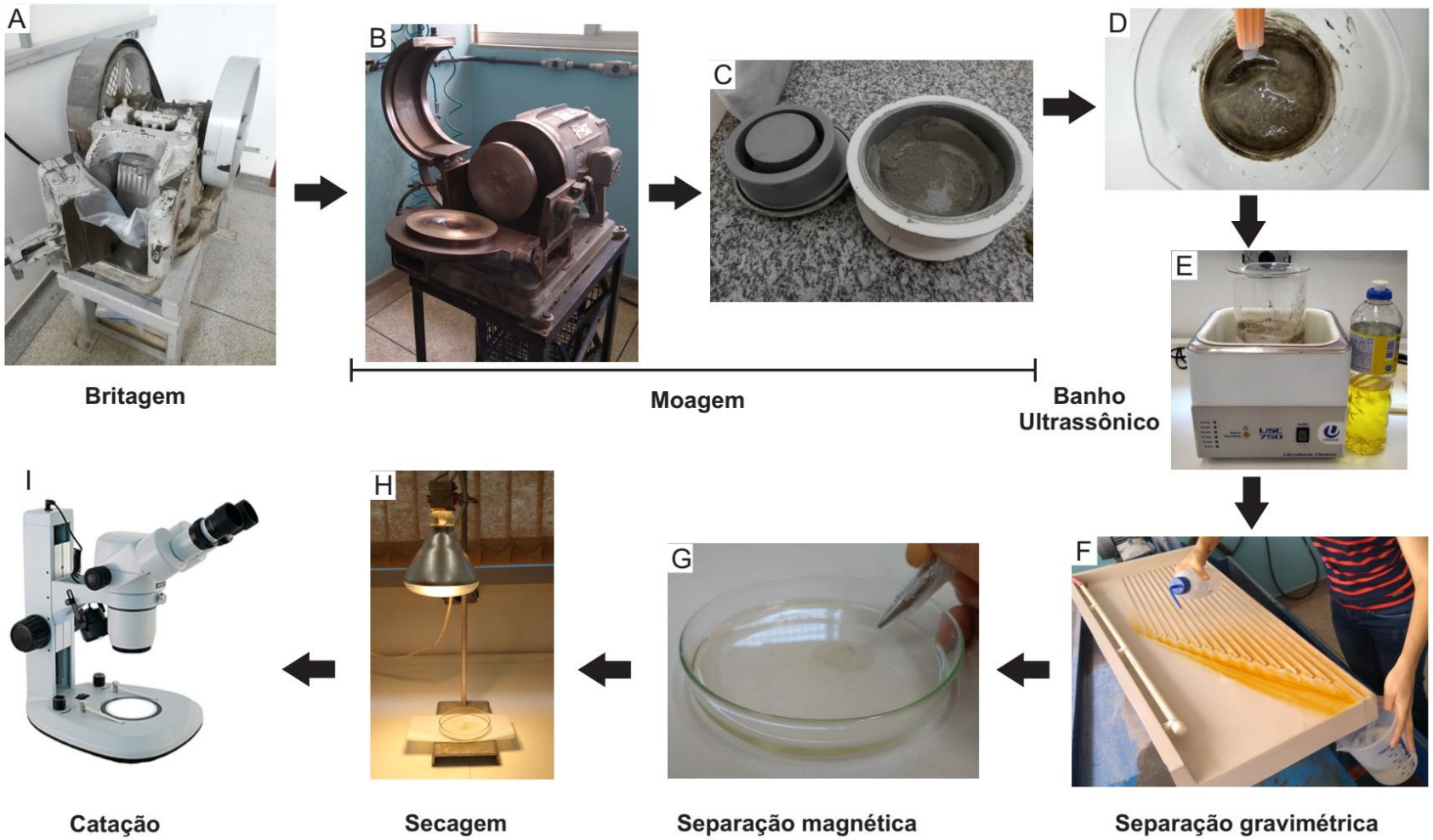

Figura 1.5: Procedimentos adotados para separação de badeleíta no Laboratório de Geocronologia da Unicamp. A) britagem de amostras com até 5cm de diâmetro; B) moinho de disco para redução de grãos; c) moinho de anéis para pulverização de amostra; D-E) mistura do pó da amostra com água e detergente em Becker para banho ultrassônico; F) separação gravimétrica da mistura em mesa Wilfley; G) separação magnética do concentrado de pesados obtidos na mesa Wilfley; H-I) secagem e catação em lupa binocular dos grãos de badeleíta.

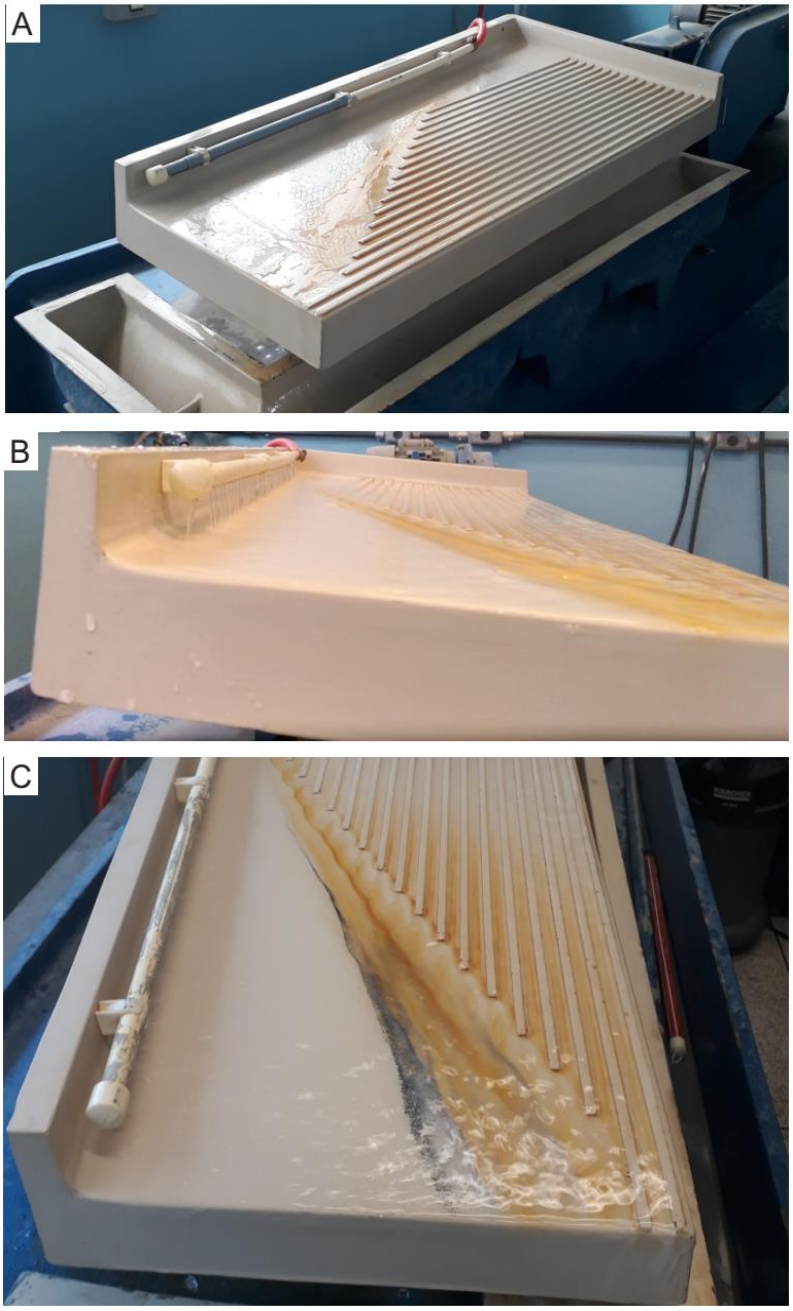

Figura 1.6: Fotos da mesa vibratória de Wilfley do Instituto de Geociências da Unicamp. A) Saídas finais da mangueira fechadas com fita adesiva na tentativa de diminuir o volume de água; B) Mangueira adaptada com saídas de água de diâmetros menores; C) Mesa ajustada para 3º, mostrando um espalhamento do material na porção lateral esquerda.

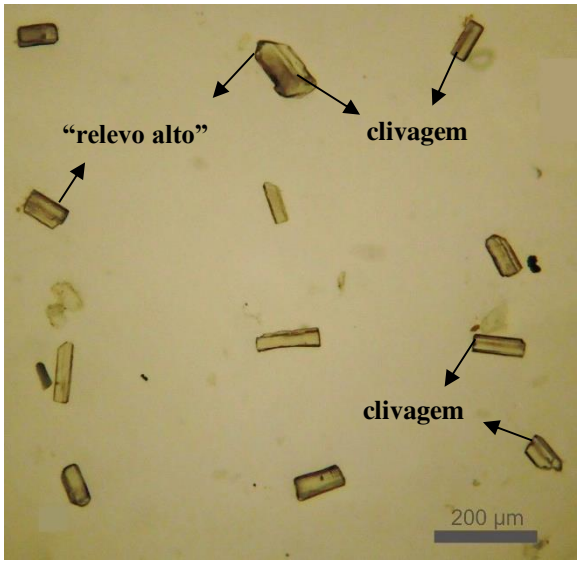

Figura 1.7: Badeleítas coletadas do carbonatito de Jacupiranga (Matheus, 2019) e utilizadas para os testes. Observe o aspecto de “relevo alto” e a clivagem no eixo C dos cristais, características que auxiliam muito a identificação da badeleíta.

4.6 Geofísica

A área de estudo insere-se nos limites de 4 projetos aerogeofísicos: Parima-Uraricoera (1058), Catrimâni-Aracá (1107), Centro-Leste de Roraima (1108) e Sudeste de Roraima (1109) e (Figura 1.8). Os levantamentos aerogeofísicos foram realizados pelo Serviço Geológico do Brasil – CPRM durante dos anos 2001, 2010, 2011 e 2012. A direção das linhas de voo de todos os levantamentos foi N-S, com espaçamento de 500 m, linhas de controle perpendiculares (E-W) com espaçamento de 10 km, altura de voo de 100 m. A base de dados foi cedida pela CPRM em forma de arquivo digital XYZ, cujo X e Y correspondem às coordenadas UTM (*Datum* WGS-84 – Zona 20N) e Z as medidas de magnetometria (nT) e gamaespectrometria (cps). Os parâmetros utilizados em cada levantamento estão detalhados na Tabela 1.1.

Os dados aerogeofísicos foram processados no *software* Oasis Montaj (GEOSOFT) e interpolados numa malha regular de 125 x 125 metros (1/4 do espaçamento da linha de voo). Para os dados de gamaespectrometria foi utilizado o método interpolador da curvatura mínima, e para magnetometria o método bidirecional. Foram aplicados alguns filtros para diminuir as tendências na direção da linha de voo, tais como *Butterworth low pass filter* e *directional cosine*.

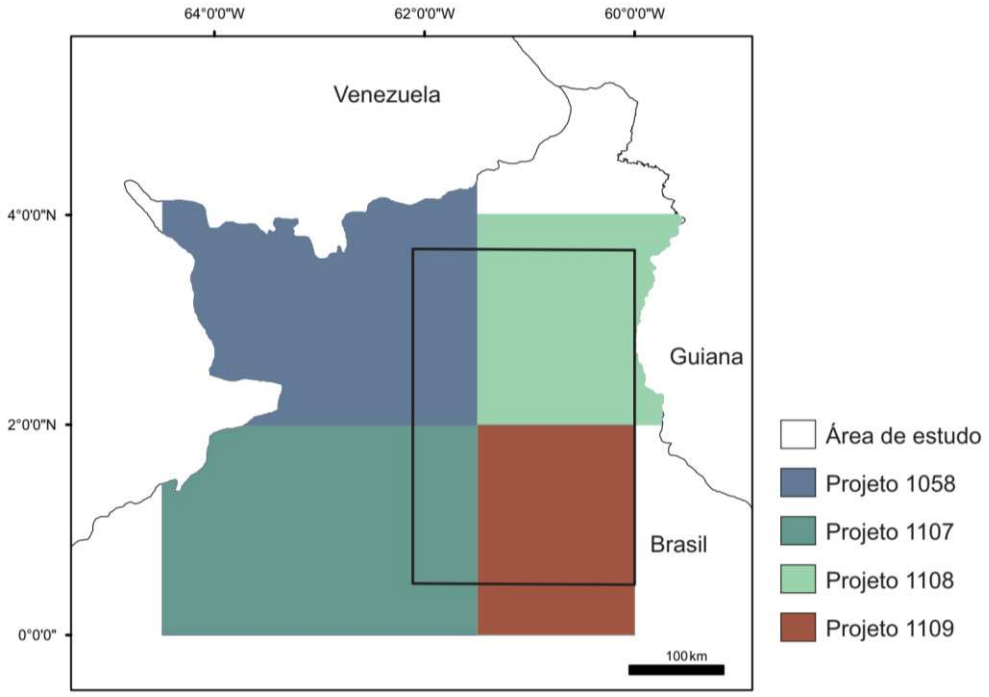

Figura 1.8: Área de abrangência de cada aerolevantamento utilizado para compor os produtos geofísicos estudados.

Tabela 1.1: Parâmetros adotados para cada aerolevantamento que compõe a área de estudo.

Parâmetros	***1058 - Parima-Uraricoera***	***1107 - Catrimâni-Aracá***	***1108 - Centro-Leste de Roraima***	***1109 - Sudeste de Roraima***
Ano	2001	2012	2011	2010
Direção da linha de voo	N-S	N-S	N-S	N-S
Espaçamento das linhas de voo	500 m	500 m	500 m	500 m
Direção das linhas de controle	E-W	E-W	E-W	E-W
Espaçamento das linhas de controle	10 km	10 km	10 km	10 km
Altura média do voo	100 m	100 m	100 m	100 m
Velocidade do voo	200 and 250 km/h	238-289 km/h (5 aircrafts)	234-242 km/h (3 aircrafts)	270 km/h
Taxa de amostragem	0.1 s (magnetometer) 1 s (spectrometer)	0.1 s (magnetometer) 1 s (spectrometer)	0.1 s (magnetometer) 1 s (spectrometer)	0.1 s (magnetometer) 1 s (spectrometer)

5. Referências bibliográficas

Almeida, F. F. M., 1983. Relações tectônicas das rochas alcalinas mesozoicas da região meridional da plataforma sul-americana. Revista Brasileira de Geociências 13,139-158.

Almeida, F.F.M., 1986. Distribuição regional e relações tectônicas do magmatismo pós-paleozóico no Brasil. Revista Brasileira de Geociências 16, 325-349.

Azzone, R. G., Munoz, P. M., Enrich, G. E. R., Alves, A., Ruberti, E., Gomes, C. B. 2016. Petrographic, geochemical and isotopic evidence of crustal assimilation processes in the Ponte Nova alkaline mafic-ultramafic massif, SE Brazil. Lithos, 260, 58–75.

Bailey, D.K. 1987. Mantle metasomatism – perspective and prospect. In: Fitton JG, Upton BGJ (eds) Alkaline rocks. Geol Soc Spec Publi 30: 1-14.

Bates, R.L., Jackson, J.A. 1987. Glossary of Geology. 3rd Edition, American Geological Institute, Alexandria, 788 p.

Berrangé J.P. & Dearnley R. 1975. The apoteri volcanic formation – tholeiitic flows in the North Savannas Graben of Guyana and Brazil. Sttutgart, Geologische Rundschau, 64 (1): 883-899.

Borges, F.R., 1990. Projeto Serra do Repartimento. Technical report, CPRM, 30 pp.

Brandão, R.L., Freitas, A.F.F., 1994. Serra do Ajarani: Folha NA.20-X- C- VI. Technical report, CPRM, 153 pp.

Brotzu P., Gomes C.B., Melluso L., Morbidelli L., Morra V., Ruberti E. 1997. Petrogenesis of coexisting SiO2-undersaturated to SiO2- oversaturated felsic igneous rocks: the alkaline complex of Itatiaia, southeastern Brazil. Lithos, 40:133-156.

Cordani U.G., Teixeira W., D'Agrella-Filho M.S., Trindade R.I. 2009. The position of the Amazonian Craton in supercontinents. Gondwana Research, 15: 396–407.

Cordani, U.G., Fraga, L.M., Tassinari, C.C.G., Brito-Neves, B.B., 2010. On the origin and tectonic significance of the intra-plate events of Grenvillian-type age in South America: A discussion. Journal of South American Earth Science 29, 143-159.).

Costa, M. L., Fonseca, L. R., Angélica, R. S., Lemos, V. P., Lemos, R. L. 1991. Geochemical exploration of the Maicuru alkaline-ultramafic-carbonatite complex, northern Brazil. Journal of Geochemical Exploration, 40(1–3), 193–204.

Costa, S.S., 2005. Delimitação do arcabouço tectônico do Cinturão Guiana Central, estado de Roraima, com base na análise integrada dos dados geofísicos, geológicos, isotópicos e imagens de satélite. PhD thesis, University of Campinas, 189 pp.

Cotta, A.J.B., Enzweiler, J., 2011. Classical and new procedures of whole rock dissolution for Trace Element determination by ICP-MS. Geostandards and Geoanalytical Research, 1-24.).

Crawford F. D., Szelewski C. E., Alvey G. D. 1984. Geology and exploration in the Takutu Graben of Guyana. Beaconsfield, Journal Petroleum Geology, 8 (1): 5-36.

Delor C., de Roever E.W.F, Lafon J.M., Lahondere D., Rossi P., Cocherie A., Potrel A. 2003. The Bakhuis ultra-high-temperature granulite belt (Suriname): II. Implications for the late Transamazonian crustal stretching in a revised Guiana Shield framework. Géologie de la France 2-3-4: 207–230.

De Min, A., Piccirillo, E.M., Marzoli, A., Bellieni, G., Renne, P.R., Ernesto, M., Marques, L.S. 2003. The Central Atlantic Magmatic Province (CAMP) in Brazil: petrology, geochemistry, 40Ar/39Ar ages, paleomagnetism and geodynamic implications. In: Hames, W., McHone, J.G., Renne, P.R., Ruppel, C. (eds.). The Central Atlantic Magmatic Province. AGU Geophysical Monograph, 136, p. 91-128.

Eiras, J.F., Kinoshita, E.M., 1988. Evidências de movimentos transcorrentes na Bacia do Tacutu. Boletim de Geociências da Petrobras 2, 193-208.

Figueiredo, R.F., 2016. Contexto tectônico do Complexo Alcalino Apiaú– Roraima: Aerogeofísica, petrologia e geocronologia U-Pb. M.S. thesis, University of Campinas, 102 pp.

Figueiredo, R. F. de, Santos, T. J. S., Tonetto, E. M. 2018. Petrology, geochemistry and U-Pb zircon and baddeleyite ages of the alkaline rocks from the central-southern Guyana Shield, northern Amazonian Craton. Journal of South American Earth Sciences, 86, 461–474.

Fletcher, C.J.N., Beddoe-Stephens, B. 1987. The petrology, chemistry and crystallization history of the Velasco alkaline province, eastern Bolivia. In: Fitton, J.G., Upton, B.G.J. (Eds.) Alkaline igneous rocks. Geological Society Special Publication 30, 403-413.

Fraga, L.M.B., 2002. A associação anortosito-mangerito-granito rapakivi (AMG) do Cinturão Guiana Central, Roraima, e suas encaixantes paleoproterozóicas: evolução estrutural, geocronologia e petrologia. PhD thesis, Federal University of Pará, 351 pp.

Fraga, L.M., Dall'Agnol, R., Costa, J.B.S., Macambira, M.J.B., 2009. The Mesoproterozoic Mucajaí anorthosite-mangerite-rapakivi granite complex, Amazonian Craton, Brazil. The Canadian Mineralogist 47, 1469-1492.

Fraga L.M.B., Cordani U., Kroonenberg S., De Roever E., Nadeau S., and Maurer V.C. 2017. U-PB SHRIMP new data on the high-grade supracrustal rocks of the Cauarane Coeroeni Belt - insights on the tectonic Eo-Orosirian evolution of the Guiana Shield. In: 15º Simpósio De Geologia da Amazônia, anais, 486-490.

Gaudette, H. E., Olszewski Jr., W. J., Santos, J.O.S., 1996. Geochronology of Precambrian rocks from the northern part of Guiana Shield, State of Roraima, Brazil. Journal of South American Earth Sciences 9, 183- 195.

Guarino, V., Wu, F. Y., Lustrino, M., Melluso, L., Brotzu, P., Gomes, C. de B., Svisero, D. P. 2013. U-Pb ages, Sr-Nd- isotope geochemistry, and petrogenesis of kimberlites, kamafugites and phlogopite-picrites of the Alto Paranaíba Igneous Province, Brazil. Chemical Geology, 353, 65–82.

Gibson, S.A., Thompson, R.N., Leonardos, O.H., Dickin, A.P., Mitchell, J.G., 1995. The Late Cretaceous impact of the Trindade mantle plume: Evidence from large volume, mafic potassic magmatism in SE Brazil. Journal of Petrology 36, 189-229.).

Gibbs A.K., Barron C.N. 1993. Geology of the Guiana shield. Oxford University Press (Oxford): 246 pp.

Gillespie, M.R., Stephenson, D., Millward, D. 2008. BGS classification of lithodemic unit: Proposals for classifying units of intrusive rocks. *British Geological Survey Research Report RR/08/05*.

Gomes, C.B., Ruberti, E., Morbidelli, L., 1990. Carbonatite complexes from Brazil: A review. Journal of South American Earth Sciences 3, 51-63.

Gomes, C.B., Comin-Chiaramonti, P., 2005. An introduction to the alkaline and alkaline-carbonatitic magmatism in and around the Paraná Basin. In: Comin-Chiaramonti, P., Gomes, C.B. (Eds.), Mesozoic to Cenozoic Alkaline Magmatism in the Brazilian Platform. Edusp/Fapesp, São Paulo, pp. 21-29.

Gomes, C. B., E. Ruberti, P. Comin-Chiaramonti, and R. G. Azzone. 2011. "Alkaline Magmatism in the Ponta Grossa Arch, SE Brazil: A Review." Journal of South American Earth Sciences 32(2): 152–68.

Gomes, C. B., Comin-Chiaramonti, P. 2017. Magmatismo alcalino continental da região meridional da Plataforma Brasileira. São Paulo: Edusp. 595 p.

Heaman, L. M., Easton, R. M., Hart, T. R., Hollings, P., MacDonald, C. A., Smyk, M. C. 2007. Further refinement to the timing of Mesoproterozoic magmatism, Lake Nipigon region, Ontario. Canadian Journal of Earth Sciences, 44(8), 1055–1086.

Heinonen, A.P., Fraga, L.M., Rämö, O.T., Dall'Agnol, R., Mänttäri, I., Andersen, T., 2012. Petrogenesis of the igneous Mucajaí AMG complex, northern Amazonian craton - Geochemical, U-Pb geochronological, and Nd-Hf-O isotopic constraints. Lithos 151, 17–34.

Kroonenberg, S. B., De Roever, E. W. F., Fraga, L. M., Reis, N. J., Faraco, T., Lafon, J. M., Wong, T. E. 2016. Paleoproterozoic evolution of the Guiana Shield in Suriname: A revised model. Geologie En Mijnbouw/Netherlands Journal of Geosciences, 95(4), 491–522.

Leal, A.B.M., Girardi, V.A.V., Leal, L.R.B., 2000. Petrologia e geoquímica do magmatismo básico mesozoico da Suíte Básica Apoteri, estado de Roraima. Geochimica Brasiliensis 14, 155-174.

Ludwig, K.R. 1991. ISOPLOT; a plotting and regression program for radiogenic-isotope data; version 2.53. USGS Open-File Report 91-445.

Macciotta, G., Almeida, A., Barbieri, M., Beccaluva, L., Brotzu, P., Coltorti, M., Conte, A., Garbarino, C., Gomes, C. B., Morbidelli, L., Ruberti, E., Siena, F., & Traversa, G. 1990. Petrology of the tephrite-phonolite suite and cognate xenoliths of the Fortaleza district (Ceará, Brazil). European Journal of Mineralogy, 2(5), 687–710.

Marzoli A., Renne P.R., Piccirillo E.M., Ernesto M., Bellieni G., De Min A. 1999. Extensive 200-Million-Year-Old Continental Flood Basalts of the Central Atlantic Magmatic Province. Science 284, 616–618.

Matheus, G.F. 2019. Geocronologia U-Pb em badeleíta aplicado às rochas alcalinas do sul do estado de São Paulo. Dissertação de mestrado. Instituto de Geociências – Universidade Estadual de Campinas, 98 p.

Montalvão, R. M.G., Muniz, M. C., Issler R. S., Dall'Agnol R., Lima M. I. C., Fernandes P. E. C. A, Silva G. G. 1975. Projeto Radam Brasil 8v: Folha NA.20- Boa Vista e parte das folhas NA.21 - Tumucumaque, NB.20 – Roraima e NB.21. DNPM, Rio de Janeiro, 403 pp.

Morbidelli, L., Gomes, C.B., Beccaluva, L., Brotzu, P., Conte, A.M., Ruberti, E., Traversa, G., 1995. Mineralogical, petrological and geochemical aspects of alkaline and alkaline carbonatite associations from Brazil. Earth Sciences Review 39, 135-168.).

Ngonge, E. D., de Hollanda, M. H. B. M., Pimentel, M. M., Oliveira, D. C. 2016. Petrology of the alkaline rocks of the Macau Volcanic Field, NE Brazil. Lithos, 266–267, 453–470.

Petronilho L.A. 2009. Método Sm-Nd no CPGeo-IGc-USP: procedimentos analíticos atualmente em rotina. In: Simpósio 45 anos de Geocronologia no Brasil, Boletim de Resumos Expandidos, 116-118.

Reis, N. J., Fraga, L.M., Faria, M.S.G., Almeida, M. E., 2003. A geologia de Roraima. Géologie de la France 2-3-4, 121-134.

Reis N.J., Faria M.S.G., Almeida M.E., Oliveira M.A. 2004. Folhas NA.20-Boa Vista e NB.20-Roraima. In: Schobbenhaus, C., Gonçalves, J.H., Santos, J.O.S., Abram, M.B., Leão Neto, R., Matos, G.M.M., Vidotti, R.M., Ramos, M.A.B., Jesus, J.D.A.de. (Eds.) Carta Geológica do Brasil ao Milionésimo, Sistema de Informações Geográficas-SIG, Programa Geologia do Brasil. CPRM, Brasília, CD-ROM.

Reis, N.J, Szatmari, P, Wanderley Filho, J.R, York, D, Evensen, N.M, Smith, P.E., 2006. Dois eventos de magmatismo máfico mesozóico na fronteira Brasil-Guiana, Escudo das Guianas: enfoque à região do rifte Tacutu-North Savannas, in: 43º Congresso Brasileiro de Geologia, Aracaju, 459–46.

Riccomini, C., Velázquez, V.F., Gomes, C.B., 2005. Tectonic controls of the Mesozoic and Cenozoic alkaline magmatism in Central-Southeastern Brazilian Platform. In: Comin-Chiaramonti, P., Gomes, C.B. (Eds.), Mesozoic to Cenozoic Alkaline Magmatism in the Brazilian Platform. Edusp/Fapesp, São Paulo, pp. 31 - 55.

Rock, N. M.S. 1981. "How Should Igneous Rocks Be Grouped?" Geological Magazine 118(5): 449–61.

Rossoni, M. B., Bastos Neto, A. C., Souza, V. S., Marques, J. C., Dantas, E., Botelho, N. F., Pereira, V. P. 2017. U-Pb zircon geochronologycal investigation on the Morro dos Seis Lagos Carbonatite Complex and associated Nb deposit (Amazonas, Brazil). Journal of South American Earth Sciences, 80, 1–17.

Salas, N. J., Santos, J. O. S., 1974. Determinações geocronológicas pelo método da birrefringência em phonolite na área do Projeto Norte da Amazônia, in: 28º Congresso Brasileiro de Geologia, Porto Alegre, 221-224.

Santos, J. O. S., Hartmann, L. A., Gaudette, H. E., Groves, D. I., Mcnaughton, N. J., Fletcher, I. R., 2000. A new understanding of the Provinces of the Amazon Craton based on integration of field mapping and U-Pb and Sm-Nd Geochronology. Gondwana Research 3, 453-488.

Santos, J.O.S., Faria, M.S.G., Riker, S.R., Souza, M.M., Hartmann, L.A., Almeida, M.E., McNaughton, N.J., Fletcher, I.R., 2006b. A faixa colisional K'Mudku (idade Greenvilliana) no norte do Cráton Amazonas: reflexo intracontinental do orógeno Sunsás na margem ocidental do Cráton, in: 9º Simpósio de Geologia da Amazônia, Belém, CD-ROM.

Santos J.O.S. 2003. Geotectônica dos Escudos das Guianas e Brasil Central. In: Bizzi L.A., Schobbenhaus C., Vidotti R.M., Gonçalves J.H (Eds.) Geologia, Tectônica e Recursos Minerais do Brasil: texto, mapas e SIG. Brasilia, CPRM, p. 169–226.

Sial, A.N. 1987. The Tertiary alkaline province of Fortaleza, State of Ceará, Brazil: oxygen isotopes and REE-geochemistry. Geoch. BrasiL, 1, 41-51.

Spinelli, F.P., Gomes, C.B. 2009. A ocorrência alcalina de Cananeia, litoral sul do Estado de São Paulo: petrologia e geoquímica. Revista Brasileira de Geociências, 39:304-323.

Silveira, F.V., 2006. *Magmatismo cenozóico da porção central do Rio Grande do Norte, NE do Brasil.* Tese (doutorado). Universidade Federal do Rio Grande do Norte, Natal, 220 pp.

Silva, A.B., Liberal, G.S., Grossi Sad, J.H., Issa Filho, A., Rodrigues, C.S. and Riffel, B.F. (1988) Geologia e petrologia do complexo Angico dos Dias (Bahia, Brasil), uma associac¸a˜o carbonatitica Precambriana. Geochimica Brasiliensis, 2, 81 –108.

Silva, M.G, Porsani M.J. 2006. Aplicação de balanceamento espectral e DMO no processamento sísmico da Bacia do Tacutu. Revista Brasileira de Geofísica, 24: 273–290.

Söderlund, U., Johansson, L., 2002. A simple way to extract baddeleyite (ZrO2). Geochemistry, Geophysics and Geosystems 3, 1-7.

Souza S.L. 2009. Métodos radiométricos Rb-Sr e Sm-Nd no CPGeoIGc-USP. In: Simpósio 45 anos de Geocronologia no Brasil, Boletim de Resumos Expandidos, 137-139.

Tassinari, C. C. G., Macambira, M. J. B., 1999. Geochronological Provinces of the Amazonian Craton. Episodes 22, 174-182.

Tassinari, C.C.G., Macambira M.J.B., 2004. A evolução tectônica do Cráton Amazônico. In: Neto, V. M.; Bartorelli, A.; Carneiro, C.D.R.; Neves, B.B.B. (Eds.), Geologia do Continente Sul-Americano: Evolução da obra de Fernando Flávio Marques de Almeida. Beca, São Paulo, 471-485.

Teixeira, W., 1978. Significação tectônica do magmatismo anorogênico básico e alcalino na região amazônica. M.S thesis, University of São Paulo, 99 p.

Thompson, R.N., Gibson, S.A., Mitchell, J.G., Dickin, A.P., Leonardos, O.H., Brod, J.A., Greenwood, J.C., 1998. Migrating Cretaceous–Eocene magmatism in the Serra do mar Alkaline Province, SE Brazil: melts from the deflected Trindade mantle plume? Journal of Petrology 39, 1493–1526.

Ulbrich, H.H.G.J, Gomes, C.B., 1981. Alkaline rocks from continental Brazil. Earth-Science Reviews 17, 135–154.

Vaz, P.T., Wanderley Filho, J.R., Bueno, G.V. 2007. Bacia do Tacutu. Boletim de Geociências da Petrobras 15, 289–297.

Vendemiatto, M.A., Enzweiler, J., 2001. Routine control of accuracy in silicate rock analysis by X-Ray Fluorescence Spectrometry. Geostandards and Geoanalytical Research. 25, 283-291.

CAPÍTULO 2 – RORAIMA ALKALINE PROVINCE: A NEW CRETACEOUS ALKALINE PROVINCE IN AMAZONIAN CRATON

Abstract

The Roraima Alkaline Province - RAP is rift-related magmatism located over 200 km into main faults and shear zones of central Guyana Shield, northern Amazonian Craton. It corresponds to the first alkaline province proposed to Guyana Shield. The RAP encompasses mainly felsic rocks, mostly foid syenites and phonolites as large and small plutons or dykes, while basic rocks are confined to scarce lamprophyre, tephrite and tephriphonolite dykes. In this paper, we combine petrographic, geochemical and isotopic evidence, as well as U-Pb ages, to evaluate whether indeed these rocks are cogenetic and propose a model for the origin of the RAP. The studied rocks are nepheline-normative, from metaluminous to peralkaline affinity and with mineralogy that varies from miaskitic to agpaitic. The geochemical patterns indicate that the rock-types seem to be controlled mainly by fractional crystallisation. Moreover, the increase in peralkalinity conditions is attributed to the extensive fractionation of feldspar. The possible relationship between basic and felsic magma was evaluated by MELTS thermodynamic modelling which demonstrated that some phonolites and syenites may be the result of 51–68% crystallization of a tephritic magma. Geochemical, isotopic, geochronological and petrographic features show that crustal assimilation process played a role in the genesis of the studied rocks. The U-Pb ages obtained and compiled for RAP range from ~100 to 116 Ma, indicating that alkaline magmatic activity in central Guyana Shield was a short-lived event. The Sr-Nd isotopic signatures suggest a mixture of the depleted and enriched mantle as responsible for generating those rocks. Furthermore, depleted-mantle model ages present relatively short intervals, between 548 to 657 Ma, which coincides with model ages for tholeiites of Central Atlantic Magmatic Province in Guyana Shield, suggesting the same metasomatic event for Mesozoic alkaline and tholeiite magmatism. Therefore, the lithospheric mantle metasomatism took place shortly before magmatism, triggered by an extensional tectonic environment regarding the Tacutu rift and the Atlantic opening.

Keywords: alkaline rocks; Tacutu rift; Guyana Shield.

1. Introduction

Alkaline magmatism is often associated, in space and time, with extensional tectonic and more specifically with rifting events, although alkaline rocks occur in different tectonic environments including subduction zone magmatic suites in convergent margins (Fitton and Upton, 1987; Pirajno, 2015). Despite the importance of rift-related magmatism, questions about the causal mechanism of the rifting and magmatism remain controversial. The main thoughts are related to (i) passive rifting caused by an extension, whose MORB-type melts became enriched through interaction with an enriched sub-continental lithospheric mantle (Dunworth, 2001; Wilson and Downes, 1991, 1992), and (ii) active rifting in which the magmatic products were originated by partial melting of enriched sub-lithospheric plume material (Gibson et al., 2006; Torsvik et al., 2008).

Continental rifts provide the most important occurrences of alkaline rocks, usually grouped in alkaline provinces, as observed in the East African Rift (Baker, 1987; Rooney, 2017). Rock (1981) suggests the term "province" refer to cotemporal/cospatial magmatism which covers since a few plugs to enormous magma volume, with ages falling within a narrow range. Thus, many alkaline provinces are reported worldwide. It occurs, for instance, in the Paraná-Edenteka Province (Peate, 1997; Comin-Chiaramonti et al., 2011), Kola Province (Kogarko, 1987; Downes et al., 2005) and Circum-Mediterranean Anorogenic Cenozoic Igneous Province (Lustrino and Wilson, 2007), where cogenetic associations of wide range compositions, in a specific geographical area, are within a coherent tectonomagmatic framework.

Several alkaline provinces are described to the Brazilian platform. Almeida (1983) grouped into twelve provinces the alkaline occurrences around Paraná and Santos basins. Moreover, Riccomini et al. (2005) grouped the central-southeastern Brazilian occurrences into 15 provinces and argued that they are controlled by crustal discontinuities along the borders of sedimentary basins. Nevertheless, magma genesis is much debated in the literature. Gibson et al. (1995, 1999) put forward that the widespread Late Cretaceous alkaline magmatism in southeastern Brazil is caused by impingement of the Trindade plume underneath the subcontinental lithosphere. In contrast, another line of research holds that magmas are derived from a sublithospheric mantle source, without interaction with a convective mantle (Riccomini et al., 2005; Gomes et al., 2011; Guarino et al., 2013).

Although several alkaline occurrences have been reported to the Amazonian Craton, there are only two alkaline provinces – Velasco and Candelaria in Bolivia – proposed within the southern part (Fletcher and Beddoe-Stephens, 1987; Comin-Chiaramonti et al., 2005). The alkaline and alkaline-carbonatitic rocks within the Amazonian Craton have a wide range of composition, including undersaturated to oversaturated plutons and mafic to felsic dykes (ref. in Table 2.1). They have been emplaced mainly toward critical NE-SW and NW-SE shear zones and most of them are dating from Mesoproterozoic (Ulbrich and Gomes, 1981). Mesozoic alkaline rocks have been described to the Guyana Shield, northern Amazonian Craton (Salas and Santos, 1974; Montalvão et al., 1975; Figueiredo et al., 2018).

In the last decades, some authors have drawn attention to alkaline occurrences in the Guyana Shield and their close spatial-temporal relationships with the Atlantic opening (Salas and Santos, 1974; Montalvão et al., 1975; Ulbrich and Gomes, 1981; Borges, 1990; Brandão and Freitas, 1994; Figueiredo, 2016; Figueiredo et al., 2018). In this context, this paper aims to develop a general model for the geological evolution of the Mesozoic rift-related magmatism within the northern Amazonian Craton, hereafter referred to as the Roraima Alkaline Province - RAP (formerly called the Apiaú Alkaline Complex and Catrimâni Syenite). We have compiled all the available geochemical, geological, geochronological and petrological data from the literature, together with our unpublished data for the RAP and the crystalline basement.

2. Alkaline magmatism in Amazonian Craton

The Amazonian Craton is one of the largest cratonic areas in the world, covering approximately 430,000 km^2, and extending along with French Guyana, Suriname, Guyana, Venezuela, Brazil, Colombia and Bolivia (Tassinari et al., 2000). It is split into two shields (Guyana and Central Brazil/Guaporé) separated by the Phanerozoic Amazon and Solimões Basins. The region has still a limited knowledge owing to complex issues as the rainforest cover and limited infrastructure. In this way, the Precambrian terranes have been recognised mainly based on geochronological data ranging from Archean to Neoproterozoic. Nevertheless, the geochronological provinces have controversial issues regarding geographical boundaries, tectonic setting and age intervals of those terranes (Teixeira et al.,1989; Tassinari et al., 2000; Tassinari and Macambira, 1999, 2004, Santos et al., 2000).

In this context, the alkaline rocks and associated carbonatites in Amazonian Craton are emplaced in Precambrian terranes (Ulbrich and Gomes, 1981). Rare alkaline occurrences are found into the craton, which most of them are poorly understood and were only studied by projects of recognition of Amazon during the 1970s in Brazil. The Fig.2.1 shows the location of alkaline rocks within the Amazonian Craton, which the details are described in Tab.2.1.

The alkaline and alkaline-carbonatitic rocks within Amazonian Craton have been emplaced mainly toward important NE-SW and NW-SE shear zones that crosscut the entire craton (Cordani et al., 2010; Rossoni et al., 2017; Figueiredo, 2016). They have a wide range of composition, including undersaturated to oversaturated plutons and mafic to felsic dykes (see Tab.2.1). Most of these rocks are dating from Mesoproterozoic, mainly between 1000 and 1500 Ma. Cordani et al. (2010) claim that this interval corresponds to important tectonic events of Grenville-type age into the craton and suggest that the formation of alkaline magmatism in Amazon could be attributed partially to hot spot and plumes. Moreover, the authors assert that the tectonic processes occurring at the active margin (Rondonia-San Ignacio and Sunsás belts) may have contributed to the formation of weakness zones, facilitating the emplacement of the alkaline magmatism. Teixeira (1978) made an extensive survey of geochronological data of alkaline rocks and associated them with mafic magmatism into the Amazonian Craton.

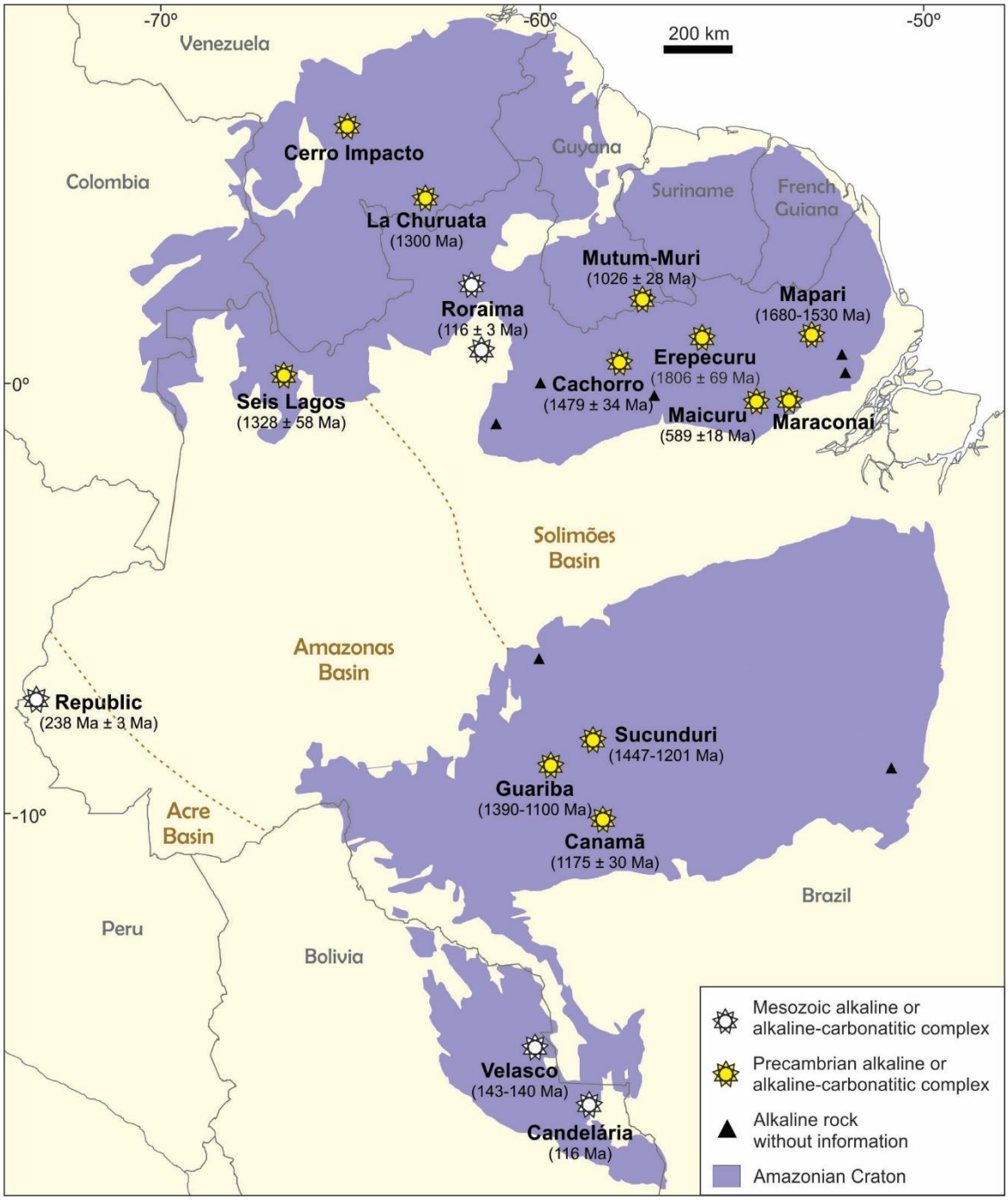

Figure 2.1: Localization of the alkaline and alkaline-carbonatitic complexes into the Amazonian Craton. We also located the undefined alkaline rocks that have been mapped by the Brazilian Geological Survey, and which further information is not available. In this sketch map are summarised all ages (see references in Table 2.1), with different colours to Mesozoic and Precambrian occurrences.

Table 2.1: Some general features of the alkaline and alkaline-carbonatitic occurrences in the Amazonian Craton.

Shield	Country	Locality	Age	Geological Features	Rock Type	References
Guyana Shield	Brazil	Republic - AC	238 ± 3 K-Ar	These rocks have been emplaced in the Acre Basin and the dykes have trends N-S and NE-SW.	A plug of quartz syenite and dykes of quartz trachyte	Barros et al. (1977); Teixeira (1978).
		Cachorro - PA	1479 ± 34 Rb-Sr	An elongated NW-SE outcrop (25 km long by 5 km wide) with NE-SW fault system.	Quartz syenite	Oliveira et al. (1975); Teixeira (1978).
		Erepecuru - PA	1806 ± 69 Rb-Sr	Two near-circular outcrops of 2 km diameter.	Hastingsite syenite	Oliveira et al. (1975); Teixeira (1978).
		Maicuru - PA	589 +18 Ma Rb-Sr	Tectonically, the Maicuru Complex seems to have been emplaced in the Guyana basement along with major NE-SW and NW-SE fault systems that cross the region.	The complex is covered by lateritic materials. The subsurface is composed by pyroxenites with subordinate dunites, carbonatite veins that cut all rocks types, including isolated apatitic bodies. Fenites occur in a narrow zone along the border of the complex.	Ulbrich and Gomes (1981); Lemos and Costa, 1987; Gomes et al. (1990); Costa et al (1991); Angélica and Costa (1993).
		Maraconai - PA	Not dated	Two oval-shaped intrusions, the largest covering about 25 km^2 and the smaller one about 8 km^2.	Deeply weathered; petrography unknown, but ultramafic alkaline and related rocks are probably dominant.	Issler et al (1974); Ulbrich and Gomes (1981); Costa et al (1991).
		Mapari - AP	1680-1530 Rb-Sr	Three small circular intrusions with diameters varying from 200 to 500 m.	Nepheline syenite, syenite and alkali syenite	Lima et al (1974); Teixeira (1978).
		Roraima - RR	116 ± 3 U-Pb	Formerly described as Sienito Catrimâni and Apiaú Alkaline Complex/Suite. Strongly controlled by NE and NW lineaments.	Nepheline syenitic varieties with or without agpaitic minerals are the main rock type, besides dykes of phonolite, trachyte, tephriphonolite, tephrite and nephelinite.	Santos and Salas (1974); Montalvão et al. (1975); Reis et al (1999); Figueiredo et al. (2018) and this work.

		Seis Lagos - AM	1328 ± 58 U-Pb	Three approximately circular bodies. The emplacement of the complex was controlled by an E-W lineament, but NE-SW and WNW-ESE structures are also found.	Lateritic crust, carbonate breccia and siderite carbonatite (composed by siderite, barite and gorceixite, and minor monazite and pyrochlore.	Issler and Silva (1980); Ulbrich and Gomes (1981); Justo and Souza (1986); Gomes et al. (1990); Rossoni et al. (2017).
	Venezuela	Cerro Impacto	Not dated (Probable Early to Middle Proterozoic)	A complex of 6 by 2 km, it is central of three discontinuous N-trending ridges that stand out within an irregularly shaped depression that has a diameter of 20 km. The circular structure is surrounded by a set of radial fractures visible in the radar imagery. The emplacement is probably related to significant NE faults.	Most of the area is covered by a 200-300-m-deep laterite containing anomalous amounts of Nb and REE that are inferred to be derived from weathering of a carbonatite. Tonalite, granodiorite, and granite showing signs of fenitization are adjacent to the carbonatite.	Aarden et al. (1973); Premoli and Kroonenberg (1984); Woolley (1987); Brooks et al. (1993).
		La Churuata	1300 Rb-Sr	Some circular structures as much as 5 km in diameter.	Saturated syenites, quartz-syenites, nepheline syenites, and granites. No carbonatite has been identified.	Soares (1985); Brooks et al.(1993).
	Boarder Brazil - Guyana	Mutum - Muri	1026 ± 28 K-Ar	There are at least three circular structures which occupy a small isolated mountain straddling the boundary between Guyana/Suriname and Brazil. The emplacement is probably related to significant NE faults.	Nepheline syenite is dominant rock besides tinguaite and inferred carbonatite. Fenitisation (Na metasomatism) affected rocks in the surroundings.	Issler at al (1975); Teixeira (1978); Premoli and Kroonenberg (1984); Kroonenberg et al.(2016).
Central Brazil - Guaporé	Brazil	Canamã - MT	1175 ± 30 Rb-Sr; 1169 ± 57 K-Ar	A large intrusion oval shape (21 by 12 km) controlled by a NW-SE fault.	Alkali syenite, nordmakite.	Silva et al (1974); Basei (1974); Teixeira (1978); Ulbrich and Gomes (1981)
		Guariba - AM	1390 - 1100 Rb-Sr	Tentatively associated with the Sucunduri alkaline	Syenite, quartz syenite and riebeckite syenite.	Teixeira (1978); Leal et al (1978).
		Sucunduri - AM	1447 ± 15 1201 ± 31 Rb-Sr	A large elongated NNW-SSE dome-like (21 km by 5 km).	Plugs of nepheline syenite, egirine-nepheline syenite, eudialyte-pegmatite, and trachyte and phonolite dykes and flows.	Iwanuch (1976); Ulbrich and Gomes (1981).

Bolivia	Velasco	143-140 Rb-Sr	It comprises a volcanic suite, a series of 14 interfering ring plutons, dykes and a carbonatite complex (Cerro Manomó) emplaced along a narrow NE belt.	Intrusive rocks consist of nepheline syenites, syenites, quartz syenites and granites; effusive types range from trachyphonolites to trachytes, whereas the dykes show both silica oversaturated and silica-undersaturated varieties	(Fletcher and Beddoe-Stephens, 1987); Comin-Chiaramonti et al. (2005)
	Candelaria	116 K-Ar	The province is controlled by E-W to WNW-ESE trending faults of the Early Tertiary Mercedes Rift, with more than 100 km in length.	Nepheline syenites, quartz syenites, nordmarkites, phonolites, foyaites, pulaskites and trachyte dykes and lavas.	(Litherland et al., 1986); Comin-Chiaramonti et al. (2005)

3. Geological background of the Cretaceous alkaline intrusions in the Guyana Shield

The alkaline intrusions are located in the central part of Roraima State, north of Brazil. The first records of alkaline rocks in the region were given by the Norte da Amazônia and RADAM projects, which intended to make a recognition of the Amazon during the 1970s in Brazil. They have described a nepheline syenite pluton (Salas and Santos, 1974; Montalvão et al., 1975) crosscut by phonolite, regarding the Catrimâni subprovince in this paper. Afterwards, the Brazilian Geological Survey - CPRM and the current National Mining Agency (former DNPM), mapped new occurrences of alkaline rocks with the aid of important airborne geophysical surveys (Borges, 1990; Brandão and Freitas, 1994) which have been described by many authors as either Apiaú Alkaline Suite or Apiaú Alkaline Complex (Reis et al., 2004; Figueiredo, 2016 and Figueiredo et al., 2018).

The Cretaceous alkaline occurrences in Guyana Shield have been described as monzonite, syenite, nepheline-bearing syenite and nepheline syenite plutons, plus foidite, tephriphonolite, trachytes and phonolites dykes (Salas and Santos, 1974; Montalvão et al., 1975; Borges, 1990; Brandão and Freitas, 1994; Figueiredo, 2016; Figueiredo et al., 2018). These alkaline rocks date from 111-116 Ma U-Pb (Figueiredo et al., 2018) to 100 Ma Rb-Sr (Montalvão et al., 1975). There is a preponderance of felsic rocks, mostly foid syenites and their hypabyssal equivalents, while basic rocks are confined to scarce lamprophyre, nephelinite and tephrite dykes. Most of them are mapped into northern area and are related mainly to NE-SW faults and the intersection with NW-SE and E-W structures.

In this paper, we have studied six foid and foid-bearing syenite plutons plus 16 dykes from central Guyana Shield. We found out others lithologies such as lamprophyre, tephrite, tephriphonolite, sodalite nepheline syenites which have never been described before. The studied outcrops are often as rock blocks, and sometimes dykes are inferred. Among them, three plutons have been previously mapped, but there were only few pieces of information about them. Also, we have compiled the data for more nine plutons described in Borges (1990) whose we cannot able to access. Some of the alkaline rocks previously mapped there is no information available and are referred to as undifferentiated alkaline rocks in this paper.

In northern are, we have studied five intrusions, as hereafter referred to as Pupunha, Piauí, Campos Novos, Queixada and Gavião (Fig. 2.3). A summary of their features is described in Table 2.2. The Pupunha is one of the most significant intrusions from the area (3.5 x 1.5 km) and is composed by nepheline-bearing syenite and alkali syenite. This alkaline body was dated by Figueiredo et al. (2018) and presented U-Pb ages of 111 and 116 Ma. The Piauí intrusion is an elongated elevation (1.3 x 0.7 km) constituted by nepheline-bearing syenite and trachyte dyke. The Campos Novos intrusion is a circular alkaline body (1 km diameter) composed by nepheline syenite plus tepriphonolite dyke. To the west, very close, there is the Gavião intrusion, the smallest alkaline body from the area (500 m diameter) which is composed by sodalite nepheline syenite. Surrounding Campos Novos and Gavião intrusions we can find several phonolite dykes. The Pupunha, Piauí, Campos Novos and Gavião alkaline bodies intrude the Paleoproterozoic augen gneisses from Rio Urubu Intrusive Suite (Reis et al., 2004). The Queixada intrusion is a small and circular intrusion (700 m diameter) of sodalite nepheline syenite that is surrounded by phonolite dykes. This intrusion is emplaced into the contact between Paleoproterozoic augen gneiss from Rio Urubu Intrusive Suite and Mesoproterozoic rapakivi granite from Mucajaí Intrusive Suite (Reis et al., 2004).

Approximately 150 km south of those intrusions, there is only one alkaline intrusion which is known as Catrimâni. It corresponds to an elongated elevation (1.2 x 0.7 km) composed by nepheline syenite that is cut by phonolite dykes, which stands out in the flattened relief of an extensive sedimentary covering from Içá Formation (Reis et al., 2004). The access is very complicated and made only by inland waterway; for this reason, it is entirely dependent on the climatic conditions.

The alkaline intrusions occur following significant faults and shear zones into a structurally complex terrane of central Guyana Shield, northern Amazonian Craton. The main tectonic feature corresponds to the Paleoproterozoic Cauarane–Coeroni Belt (CCB), a sinuous NW–SE/NE–SW structure related to Trans Amazonian Orogeny, which includes amphibolite to granulite facies supracrustal rocks (Kroonemberg, 1976; Delor et al., 2003; Fraga et al., 2009). To the south of the belt, predominate granitoids, gneisses, charnockites and granulite (1.96-1.91 Ga) metamorphosed at 1.91 Ga (Gaudette et al., 1996; Fraga, 2002; Reis et al., 2003; Costa, 2005; Fraga et al., 2009). An anorthosite/gabbro-mangerite-granite rapakivi association (~1.5 Ga) is also described in this area (Fraga, 2002; Fraga et al., 2009; Heinonen et al., 2012). Moreover, this region was affected by the Mesoproterozoic K'Mudku event (1.49 and 1.15 Ga), a NE-SW shear belt that truncates the CCB and crosses the Guyana Shield from

Suriname to Brazil, in which mylonites of low metamorphic grade and intraplate magmatism were generated (Gibbs and Barron, 1993; Santos et al., 2000, 2006b; 2009; Fraga, 2002; Fraga et al., 2009; Cordani et al., 2010; Souza et al., 2015).

The emplacement of those alkaline rocks is related to reactivation of those Precambrian structures during the Equatorial Atlantic opening (Figueiredo et al., 2018). The reactivation event was responsible for the development of the Tacutu aulacogen, a half-graben which extend in NE-trending for 300 km between Brazil and Guyana (Crawford et al., 1985; Eiras and Kinoshita, 1988). The initial rift phase was marked by tholeiitic magmatism from the Central Atlantic Magmatic Province - CAMP at the beginning of the Triassic, with dykes around 200 Ma and volcanic floods between 153-135 Ma (Marzoli et al., 1999; Leal et al., 2000; Reis et al., 2006). The final sedimentation of Tacutu Basin occurred during the Early Cretaceous, at the same time as the emplacement of alkaline magmatism (Vaz et al., 2007; Figueiredo et al., 2018).

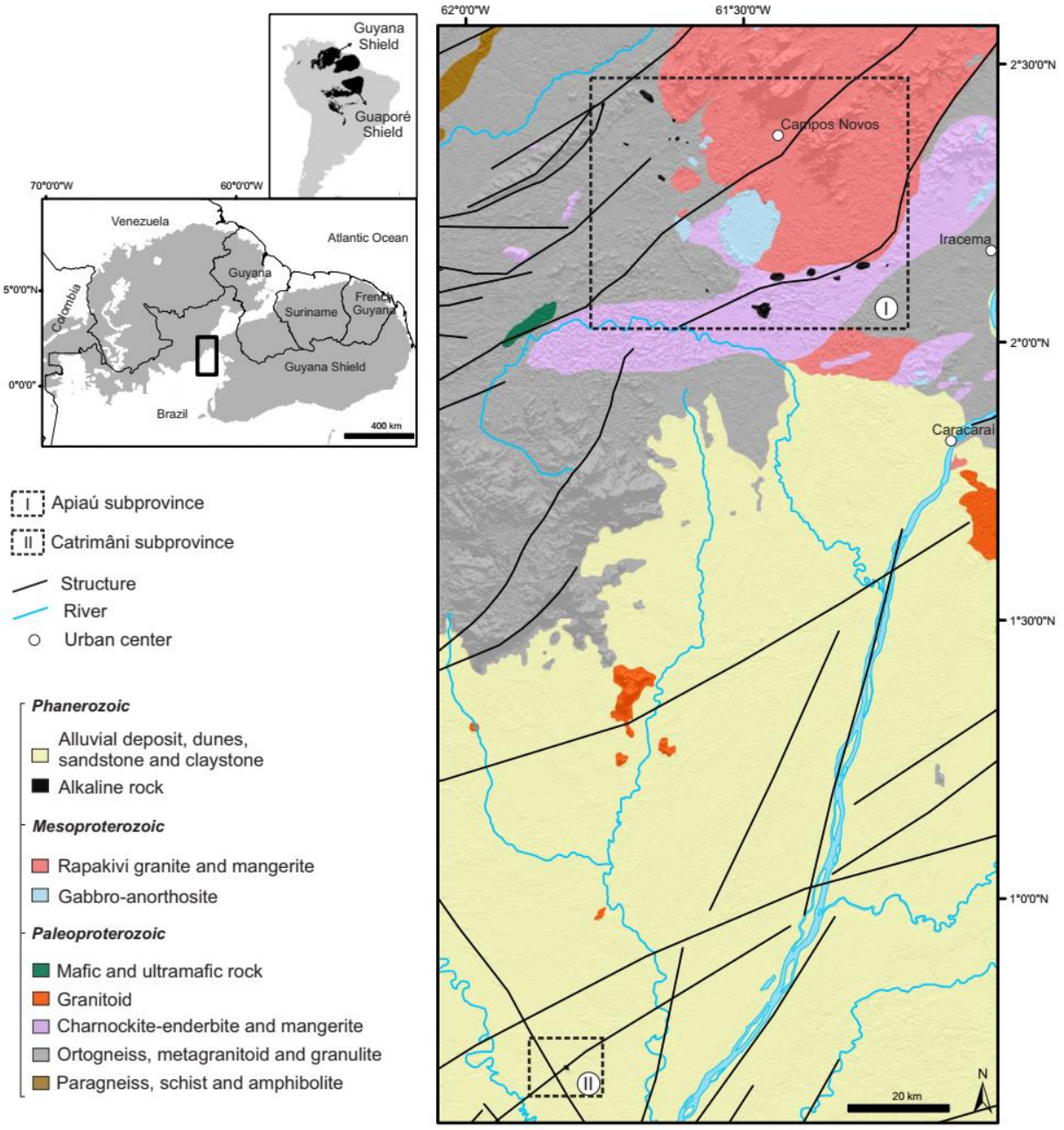

Figure 2.2: Simplified geological map of the Roraima Alkaline Province, modified from Reis et al. (2004) and Borges (1990). Alkaline rocks are represented by black polygons, showing a close relationship with the main faults in the region.

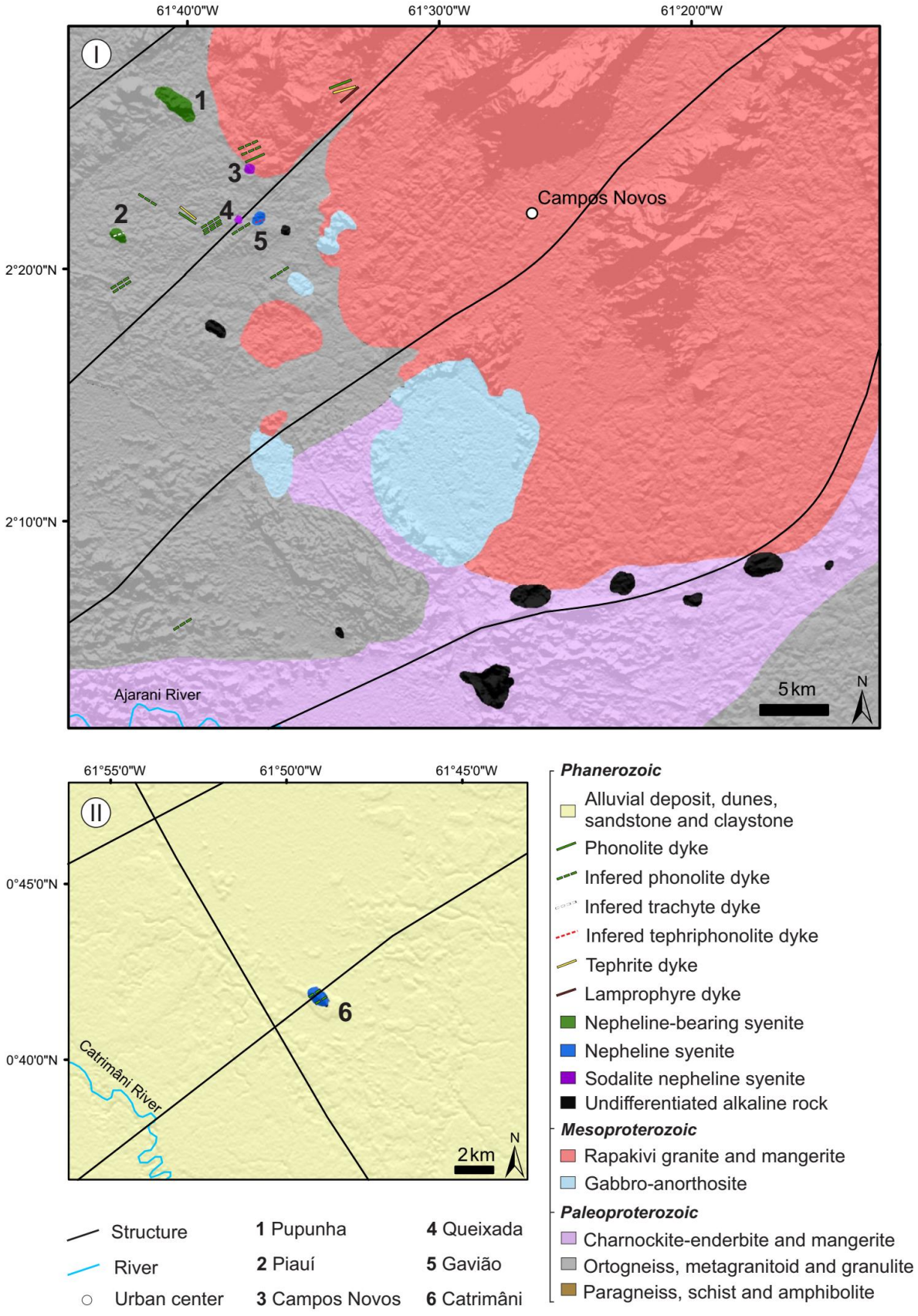

Figure 2.3: Detailed map of Apiaú (I) and Catrimâni (II) subprovinces. The numbers in map correspond to studied alkaline intrusions.

Table 2.2: Summary of geological features of studied alkaline intrusions from RAP.

Intrusion	Lithology	Emplacement	Main country rock	Latitude	Longitude
Pupunha	Nepheline- bearing syenite and nepheline-bearing alkali syenite	Stock	Augen gneiss	2°26'57" N	61°40'51" W
Piauí	Nepheline- bearing syenite and trachyte	Stock and dyke	Augen gneiss	2°21'24" N	61°42'44" W
Campos Novos	Nepheline syenite, phonolite and tephriphonolite	Stock and dyke	Augen gneiss	2°21'59" N	61°37'20" W
Queixada	Sodalite nepheline syenite with eudialyte, nepheline syenite and phonolite	Stock and dyke	Augen gneiss and rapakivi granite	2°22'03" N	61°37'58" W
Gavião	Sodalite nepheline syenite	Stock	Augen gneiss	2°22'04" N	61°37'57" W
Catrimâni	Nepheline syenite and melanite nepheline syenite	Stock and dyke	Sedimentary covering	0°41'53" N	61°49'12" W

4. Analytical techniques

4.1 Major and trace elements

Whole-rock samples were analysed for major and minor oxides by X-ray fluorescence (Philips, PW2404) according to the procedures outlined in Vendemiatto and Enzweiler (2001), using pressed pellets and glass disks. The trace elements were determined by an ICP-Q-MS equipped with a collision cell, following the protocols of Cotta and Enzweiler (2011). All the analyses were performed at the Analytical Geochemical Laboratory of the Institute of Geosciences of the University of Campinas.

4.2 Sr-Nd isotopic geochemistry

The Sr and Nd isotopic compositions of 13 samples were performed at the Geochronological Research Center of the Institute of Geosciences of the University of São Paulo. Technique details on chemical separation and measurement are described in Souza (2009) and Petronilho (2009). The Sr isotopic ratios were determined with a thermal ionisation mass spectrometry (TIMS – Thermo Triton), while the Nd isotopes were measured by ICP-MS Thermo-Neptune. The measured ratios were normalized to $^{86}Sr/^{88}Sr = 0.1194$ and $^{146}Nd/^{144}Nd = 0.7219$ and $^{143}Nd/^{144}Nd = 0.7219$. They were calculated using the NBS 987 Sr-isotope reference material (Mean: 0.710248 ± 0.000017; n = 100) and the JNDi-1 Nd-isotope reference material (Mean: 0.512100 ± 0.000005; n = 20). In addition, the $^{87}Sr/^{86}Sr_i$ and $^{143}Nd/^{144}Nd_i$ values are age-corrected isotopic data for 116 Ma.

4.3 U-Pb Geochronology

Five syenitic plutons from RAP were collected for zircon and baddeleyite U-Pb dating and are listed in Tables 2.8 and 2.9. Three of them was processed as normally done for zircon geochronology, using jaw crushers and disk mill, density techniques and Frantz isodynamic separator. Baddeleyite separation occurred in two samples which were performed according to the water-based procedures described by Söderlund and Johansson (2002). Zircon and baddeleyite crystals were picked out from the concentrated heavy minerals, mounted in epoxy resin and polished to obtain a flat surface. Baddeleyite crystals were carefully polished only to obtain an exposed surface. The internal structure of zircon grains was studied by cathodoluminescence (CL) imaging before analysis.

The ages were obtained at the Isotope Geology Laboratory of the University of Campinas by LA-SF-ICP-MS, in a Thermo Scientific Element XR coupled with an Excite

193 laser ablation system from Photon Machines (spot diameter 25 µm, 91500 zircon as reference material and Peixe zircon as internal standard; Phalaborwa baddeleyite as reference material and Kovdor baddeleyite as internal standard). Data reduction was performed using IOLITE software, and age calculations were performed with ISOPLOT (Ludwig, 1991).

5. Petrography

The RAP is constituted by foid-bearing and foid-syenite plutons, mafic and felsic dykes, being free of deformation. The plutons intrude metagranitoids/augen gneiss or rapakivi granites and may be crosscut by alkaline dikes. Furthermore, most alkaline dykes intrude the basement following important structures in that region. We analysed superficial samples which correspond to 6 foid-syenitic plutons and 15 dykes of varied composition. The province encompasses more nine plutons described in Borges (1990), but we were not able to access them. One sample from Queixada intrusion and several peralkaline phonolite dykes present rare mineralogy such as wohlerite and catapleiite.

Petrography was carried out using standard optical petrography, and selected samples were also analysed by EDS to confirm the identity of some minerals. Most collected samples are from Apiaú subprovince in which we analysed five plutons and 13 dykes. From Catrimâni subprovince we analysed one pluton of nepheline syenite and two dykes of phonolite. The main characteristics of the representative alkaline intrusions are described below, while their detailed mineralogy and features are summarised in Table 1.

5.1 Foid-bearing and foid-syenites

The plutons are within a range of syenitic varieties such as nepheline-bearing syenite, nepheline syenite and sodalite nepheline syenite. They have typically 500 - 5,000 m wide and are located at the intersection of important faults or shear zones. In some plutons, we could see field evidence of felsic and mafic xenoliths with an uncertain origin, as well as xenoliths of phonolite and trachyte. The foid and foid-bearing syenites are pale grey coarse-grained and rarely porphyritic, which may present exotic mineralogy. Their main petrographic feature is K-feldspar with mesoperthitic intergrowths that sometimes has been albitized (Fig. 2.4A). The nepheline generally shows partial or almost total alteration into cancrinite or carbonate.

The nepheline-bearing syenite found in Apiaú subprovince may contain abundant xenoliths (felsic and mafic) and feldspar cumulates. They consist of alkali feldspar, biotite, aegirine-augite, amphibole, plagioclase and nepheline as major minerals constituents. Biotite zoned is common, with colour orange to brown, sometimes with darkest rims. Titanite, zircon, and sodalite are accessory phases. The mafic xenoliths consist of biotite with interstitial feldspar and tiny apatite, while the felsic ones are constituted by alkali feldspar. Other xenoliths are the phonolite and trachyte described in the next section.

The nepheline syenites from Apiaú are hypidiomorphic medium-grained rocks constituted of alkali feldspar, nepheline and less amount of plagioclase. These rocks exhibit tightly packed elongate albite as cumulative texture with intercumulus of nepheline, feldspar and biotite. Moreover, we can find aplitic dyke with hypidiomorphic granular texture (Fig. 2.4C). The main mafic mineral is sodic clinopyroxene and/or calcic to sodic amphibole, while biotite is less common. These minerals are zoned in many rocks. Na amphibole rims in aegirine are observed. Nepheline is commonly altered into cancrinite and carbonate. Accessory phases are titanite, apatite, allanite, fluorite, opaque minerals, sodalite, and REE carbonate. There are samples from Campos Novos intrusions whose wohlerite (Fig. 2.4I) was observed.

The nepheline syenites from Catrimâni intrusion present some petrographic differences relative to rocks from Apiaú. Most of the intrusion are medium-grained nepheline syenite, but some portions are fine-grained and display flow texture. Pertitic alkali feldspar is very common and sometimes occurs as megacrysts with corroded and recrystallised rims (probable xenocrysts). Plagioclase occurs in minor quantity. Nepheline replaced by cancrinite is very common, but sometimes it is replaced by albite in the rims and cleavages. We can find melanite which occurs weakly zoned and associated with amphibole and titanite. Interstitial titanite is common, but sometimes it occurs as megacrysts. The amphibole is often bluish and can appear as megacrysts. Aegirine-augite occurs partial or totally replaced by amphibole and biotite. We can observe crystallisation/recrystallisation of intergrowth minerals of granular alkali pyroxene, feldspar, opaque minerals and sometimes epidote. Accessory minerals are fluorite, epidote, carbonate, allanite and apatite.

The sodalite nepheline syenites are found in Apiaú subprovince and exhibit xenomorphic texture and venules of sodic minerals. These rocks are composed mainly of perthitic alkali feldspar, sodalite, nepheline, amphibole and clinopyroxene. The clinopyroxene often present spongy texture. Nepheline has been altered into sericite and carbonate. Sodalite

is predominantly interstitial and sometimes occurs in venules with pyrite and albite. The main mafic is amphibole which occurs in the rims of augite. Aegirine-augite is less common and also occurs in rims of augite. Apatite and sphalerite are the main accessory phases. One sample exhibits a post magmatic assemblage of catapleiite and REE carbonate (Fig.2.4 J-K).

5.2 Mafic dykes

The mafic rocks are found in Apiaú subprovince and correspond to lamprophyre, tephrite and tephriphonolite (see item 6.1) as narrow dykes with less than a metre wide. They exhibit porphyritic and/or seriate texture with a fine-grained groundmass. Generally, they are olivine-poor to olivine-free rocks. The main macrocrysts are subhedral-anhedral clinopyroxene with oscillatory and step zoning (Fig. 2.4D). Macrocrysts of olivine are subordinate.

In lamprophyre, the macrocrysts are clinopyroxene and olivine which are usually surrounded by biotite and phlogopite corone reaction. These macrocrysts are embedded in a fine-grained groundmass of apatite, nepheline, feldspar, biotite/phlogopite, clinopyroxene and opaque minerals. The tephrite groundmass is rich of brown amphibole (kaersutite?), plagioclase, nepheline, clinopyroxene and opaque minerals with fluidal texture (Fig. 2.4E). Feldspar are present exclusively as groundmass phases.

The tephriphonolite dyke crosscut a nepheline syenite (paa15a). The dyke macrocrysts are zoned brown amphibole and nepheline whose is embedded in a groundmass of plagioclase, nepheline, alkali feldspar, brown amphibole and biotite (Fig. 2.4F). Titanite is the main accessory.

5.3 Phonolites and trachyte

Phonolite is the main petrographic type of the RAP in quantity, occurring either as narrow or large dykes. Because of the difficulties of access in that area, we cast doubt on the emplacement of some phonolites whose are so large that confuse about dyke or lava flow. There is no petrographic difference between phonolites from Apiaú and Catrimâni subprovinces. Most of them are agpaitic, showing minerals from wohlerite group identified by EDS analysis.

Phonolites are green to greenish-grey and typically exhibit porphyritic or glomeroporphyritic texture (Fig. 2.4G). Sometimes there are narrow hydrothermal or residual

venules. The macrocrysts are euhedral to subhedral alkali feldspar and nepheline, as well as, less common, zoned brown amphibole and clinopyroxene. The macrocrysts are usually surrounded by corone of aegirine. The groundmass is often fine-grained to aphanitic, principally formed by tabular alkaline feldspar and interstitial nepheline arranged in a trachytic texture. Amygdale filled by zeolite, aegirine and carbonate have been sporadically found (Fig. 2.4H). Small and variable amounts of sodalite, brown amphibole, zircon, titanite and opaque minerals are presented. Furthermore, associations of wohlerite, REE carbonate, titanite and zircon with ameboid habits is observed in groundmass (Fig. 2.4L). Cancrinite and carbonate are typical secondary minerals.

Trachyte is less common in RAP and is observed in only one dyke occurrence. The rock shows glomeroporphyritic and weak fluidal textures, with macrocrysts of alkali feldspar and clinopyroxene. The groundmass is fine-grained and includes alkali feldspar, clinopyroxene and biotite. Carbonate occurs as a secondary mineral. Titanite occurs as accessory phases.

Table 2.3: Summary of petrographic features of rocks from Apiaú subprovince. Afs-alkali feldspar; Agt-aegirine augite; Aln-alanite; Amp-amphibole; Ap-apatite; Bt-biotite; Cb-carbonate; Ccn-cancrinite; Cpx-clinopyroxene; Fl-fluorite; Nph-nepheline; Ol-olivine; Phl-phlogopite; Pl-plagioclase; Rbk-riebeckite; Sdl-sodalite; Ttn-titanite; Zrn-zircão.

Locality	Rocks	Intrusion	Mineral composition		Texture and notable features
			Early and main-stages	Late-stage	
Apiaú Subprovince	Nepheline-bearing syenite	Pupunha; Piauí	Afs, Bt, Agt, Aeg, Pl, Nph, Zrn.	Bt, Carbonate	Xenomorphic. Afs with mesoperthitic intergrowths. Felsic xenoliths and biotitite.
	Nepheline syenite	Campos Novos;	Afs, Nph, Aeg, Agt, Arf, Bt, Phl, brown Amp, Ttn, Ap, Aln, Zrn, Sdl.	Fl, Ccn, Na Amp, Ttn Wohlerite. Secondary cancrinite and carbonate in nepheline	Seriate and cumulative. Afs with mesoperthitic intergrowths. Cpx and Amp usually zoned. Lath-shaped feldspar albitized. Rarely fluidal structure and allotriomorphic-granular texture. Intergrowth of Bt and Aeg
	Peralkaline nepheline syenite	Campos Novos; Queixada	Afs, Nph, brown Amp, Arf, Bt, Sdl, Ttn, Aln, Rbk, Zrn.	Nph altered into cancrinite and clay minerals. Fl, Wohlerite, REE carbonate	Partly cumulative with Afs and Nph. Afs with mesoperthitic intergrowths. Intergrowth of Bt and Amp. Anhedral mafics. Agt with Aeg rims. Inclusions of Afs and Nph into Bt and Bt into Cpx. Skeletal Cpx with intergrowth of Bt, Afs and Nph.
	Sodalite nepheline syenite	Gavião	Afs, Nph, Aug.	Amp, Agt, Sdl is interstitial or may replace earlier Nph. Nph altered into sericite and cb.	Venulated rock. Venules of sodalite, albite, carbonate and pyrite. Augite with rims of amp and aegirine-augite. Spongy cpx.
	Peralkaline sodalite nepheline syenite	Queixada	Afs, Nph, Aug, Ap.	Interstitial carbonate or as a pseudomorph. Sdl, sericite, Aeg, catapleiite, REE carbonate and sphalerite.	Replacement textures. Nph with cpx corone. Tiny Aeg. Anhedral and subhedral Nph altered into Sdl, sericite and Cb. Subhedral lath-shaped Afs. Aug with Aeg rims.

	Lamprophyre	Dyke crosscut the basement	Cpx, Nph, Bt, Phl, Ol, Aug, Ap, Ep.	Bt and Phl	Seriate, porphyritic and cumulative. The macrocrysts are Cpx and rarely Ol. Aug macrocrysts often show step zoning. Poikilitic cpx. Bt and Phl corone formed around Aug macrocryst. The groundmass includes Nph, Bt, Phl and Cpx. Ap and epidote as accessory minerals.
	Tephrite	Dyke crosscut the basement	Aug, Aeg and Ol as macrocrysts. Groundmass includes brown Amp, Cpx, Pl and Nph. The main accessory phase is the tiny needle Ap.	Aug with rims of Na Cpx. Serpentine.	Porphyritic. Fluidal structure. Step and oscillatory zoning in cpx are common. Ol is rarer than in olivine nephelinite. Cpx cluster
	Tephriphonolite	Dyke crosscut Campos Novos	Amp. Bt, Kfs, Nph, Agt, Pl, Sdl, Ttn, Ap. Rare macrocrysts of Nph and Amp.	Amp rims in Agt	Seriate. Zoned brown Amp
	Phonolite	Queixada and dyke	Macrocrysts are usually Afs and nph, with amp and cpx less common, embedded in a fine-grained groundmass of afs, nph, aeg, amp, sdl and ccn. Ttn, fl, tiny needle ap and zrn as accessory phases.	Wohlerite and REE carbonate.	Fluidal and glomeroporphyritic or porphyritic. Amygdales infilled with zeolite are rare. The macrocrysts often exhibit reaction corona.
	Trachyte	Dyke crosscut Piauí	Macrocrysts of Cpx, Bt, Nph and Afs. Xenocrysts of Afs. The groundmass of Cpx, Afs and Nph. Epidote and titanite as accessory minerals.	Carbonates as secondary minerals.	Glomeroporphyritic. Weak fluidal structure.

Table 2.4: Summary of petrographic features of rocks from Catrimâni subprovince. Afs-alkali feldspar; Agt-aegirine augite; Aln-alanite; Amp-amphibole; Ap-apatite; Bt-biotite; Cb-carbonate; Ccn-cancrinite; Cpx-clinopyroxene; Fl-fluorite; Grt – garnet; Nph-nepheline; Pl-plagioclase; Sdl-sodalite; Ttn-titanite; Zrn-zircão.

Locality	Rocks	Intrusion	Mineral composition		Texture and notable features
			Early-stage	Late-stage	
Catrimâni Subprovince	Nepheline syenite	Catrimâni	Afs, Nph, Aeg, Agt, Bt, Grt, Amp, Pl, Ttn, Ap, Aln, Sdl, Fl.	Secondary cancrinite and carbonate in nepheline. Zircon	Afs with mesoperthitic intergrowths. Grt, Cpx and Amp usually zoned. Lath-shaped feldspar albitized. Fluidal and allotriomorphic-granular textures. Trachytic venules.
	Phonolite	Dyke crosscut Catrimâni	Macrocrysts are usually Afs and nph, with amp and cpx less common, embedded in a fine-grained groundmass of afs, nph, aeg, amp, sdl and ccn. Ttn, fl, tiny needle ap and zrn as accessory phases.	Wohlerite and REE carbonate.	Fluidal and glomeroporphyritic porphyritic. Amygdales infilled with zeolite are rare. The macrocrysts often exhibit reaction corona.

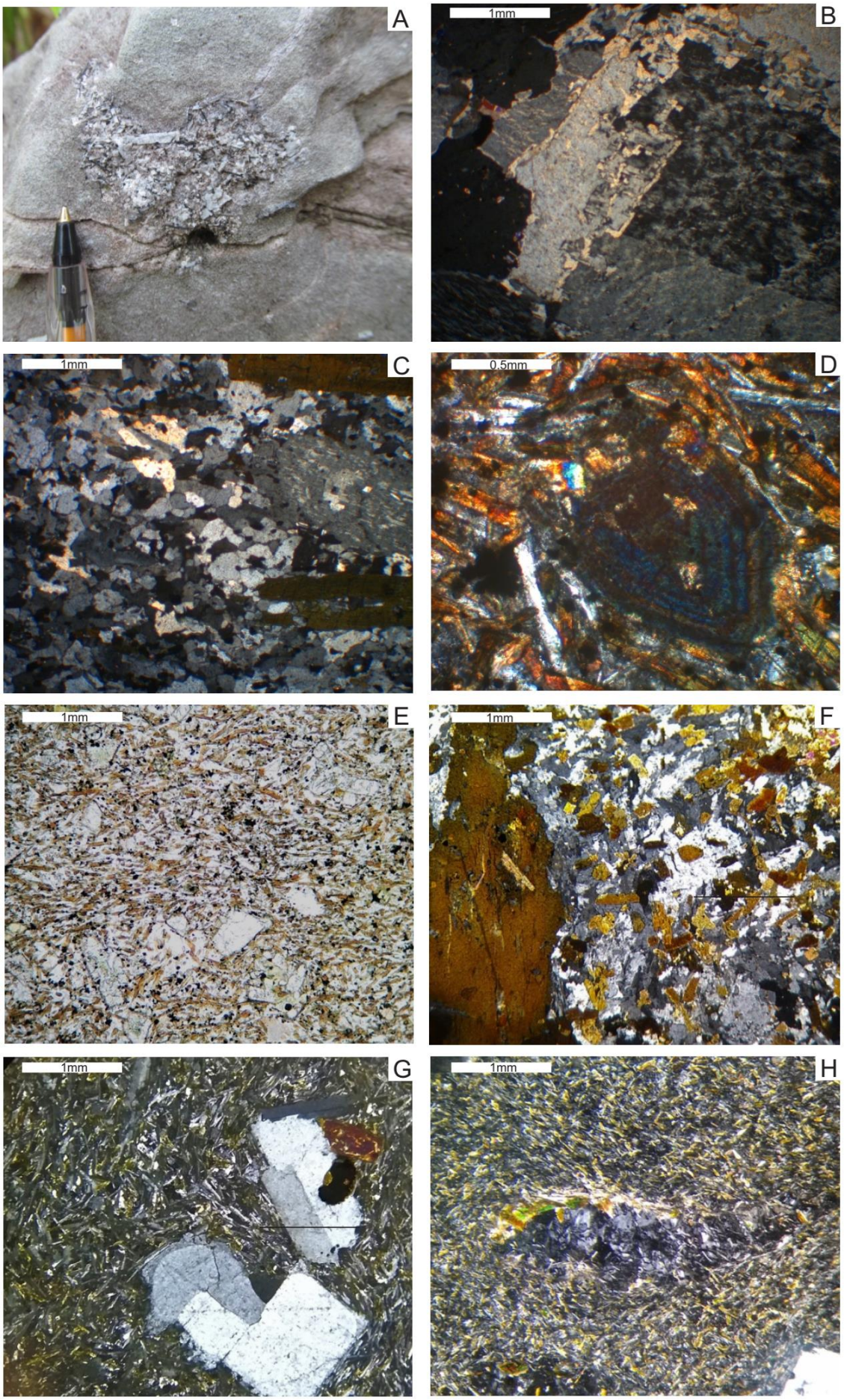
A
1mm
B
1mm
C
0.5mm
D
1mm
E
1mm
F
1mm
G
1mm
H

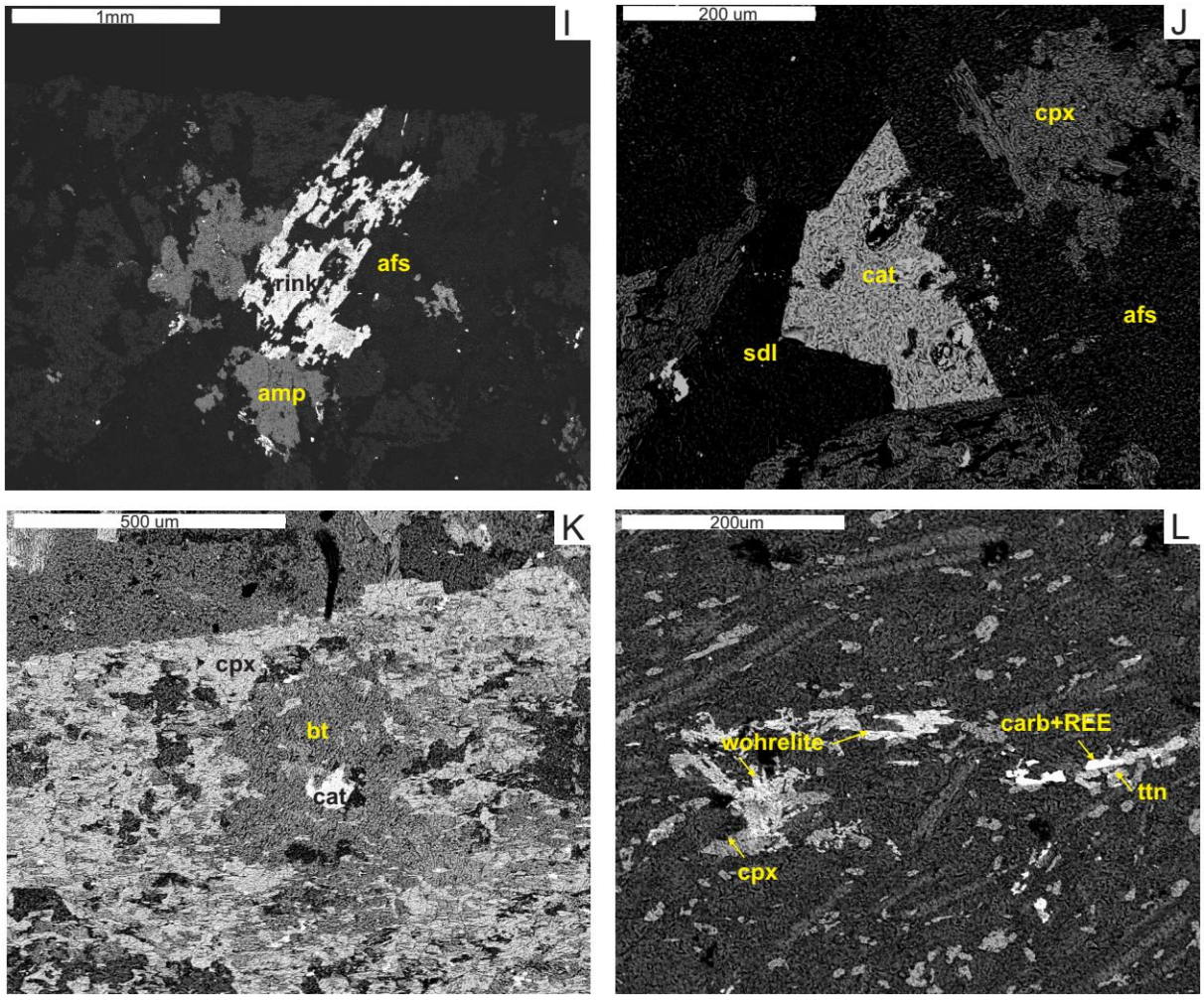

Figure 2.4: Field and thin section photographs of rocks from RAP. A) Cumulus of tightly packed elongate feldspar in phonolite. B) K-feldspar with mesoperthitic intergrowth and some crystals almost entirely albitized. C) Aplitic dyke with hypidiomorphic granular texture that crosscut a nepheline syenite. D) Crystal of cpx with oscillatory zoning in a lamprophyre. E) Macrocrysts of cpx and serpentinized olivine embedded in a fine groundmass with fluidal texture in a tephrite. F) Tephriphonolite sample with macrocryst of brown amphibole. G) Cluster of nepheline and feldspar embedded in a fine-grained groundmass in phonolite. H) Amidale filled with zeolite (?), carbonate and aegirine in a phonolitic sample. *SEM backscattering images of the agpaitic minerals:* I) Rinkite (?) in substitution of alkali feldspar. J) Catapleiite as pseudomorph in a sodalite nepheline syenite. K) Post magmatic catapleiite in a sodalite nepheline syenite. L) Aggregate of wohlerite and carbonate of REE and Si with titanite and cpx in a fine-grained groundmass of phonolite.

6. Geochemistry

The rocks of RAP have a wide compositional range with SiO_2 varying from 39.66 wt.% in a lamprophyre dyke to 62 wt.% in a nepheline-bearing syenite pluton (Tab.2.2). In terms of significant elements, the mafic dykes plot in the foidite, tephrite and tephriphonolite fields of TAS diagram, while the felsic one plot in phonolite and trachyte fields (Fig.2.5A). All of them are silica undersaturated with ne normative ranging from 0.9 to 34.2. These rocks are peralkaline and metaluminous, with some samples straddling the boundary to the peralkaline field (Fig. 2.5B). The agpaitic indices [A.I = (Na_2O + K_2O) / Al_2O_3] for many samples are ranging from 1 to 1.2, suggesting their agpaitic nature, which was confirmed by founding exotic mineralogy.

Harker diagrams are shown in Fig. 2.6. The mafic to intermediate dykes are characterised by high contents of MgO (3-10 wt.%), FeO (5-11 wt.%), TiO2 (1.1-1.7 wt.%) and CaO (5-16 wt.%), as well as low Na_2O (3-6 wt.%). Their concentrations of Al_2O_3 and K_2O increase systematically with increasing SiO_2 contents, whereas MgO and CaO contents decrease. The felsic dykes show low MgO (0.01-1.5 wt.%) contents and high Na_2O (7-11 wt.%) and K_2O (4-6 wt.%). Most syenitic samples lie within the range 52-62 wt.% SiO_2, with low MgO (0.1-2 wt.%) contents. However, among the felsic rocks, the behaviour of the major elements is more complicated. Notably, Na_2O values are distinctly higher in phonolite, while all felsic samples have overlapping K_2O contents. Moreover, phonolites are also enriched in Al_2O_3 relative to trachyte and syenites. Low MgO contents characterise all felsic samples.

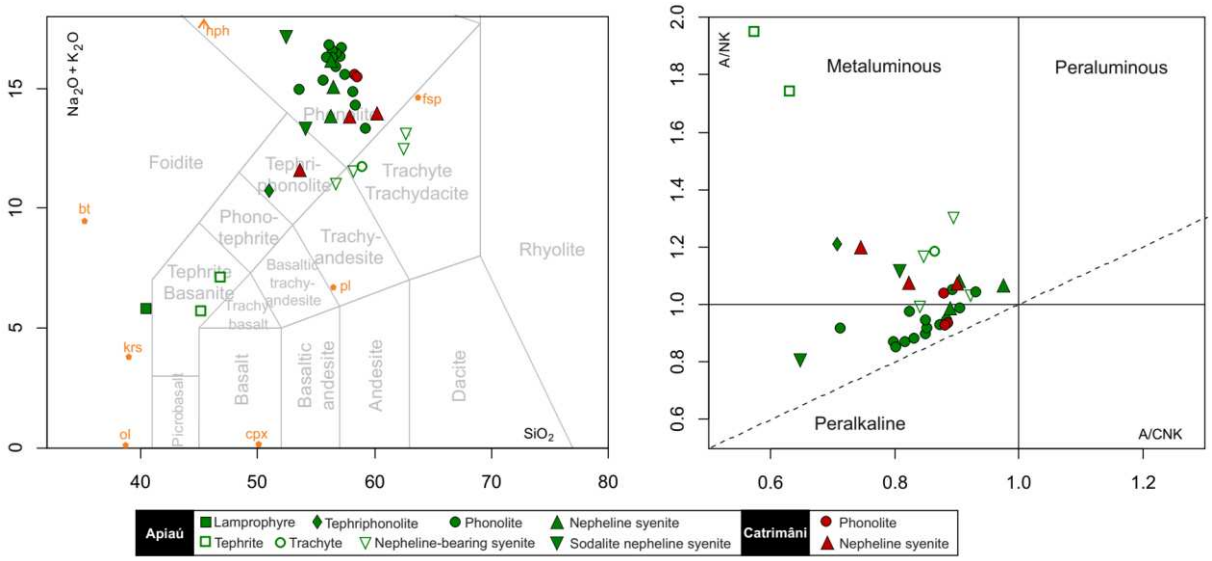

Figure 2.5: Major-element diagrams for the silica undersaturated rocks from RAP. A) The TAS diagram showing the composition of the subvolcanic and plutonic varieties. Note that most of the samples are felsic rocks. B) Alumina saturation diagram (Shand, 1943) showing a peralkaline tendency for the majority of the rocks.

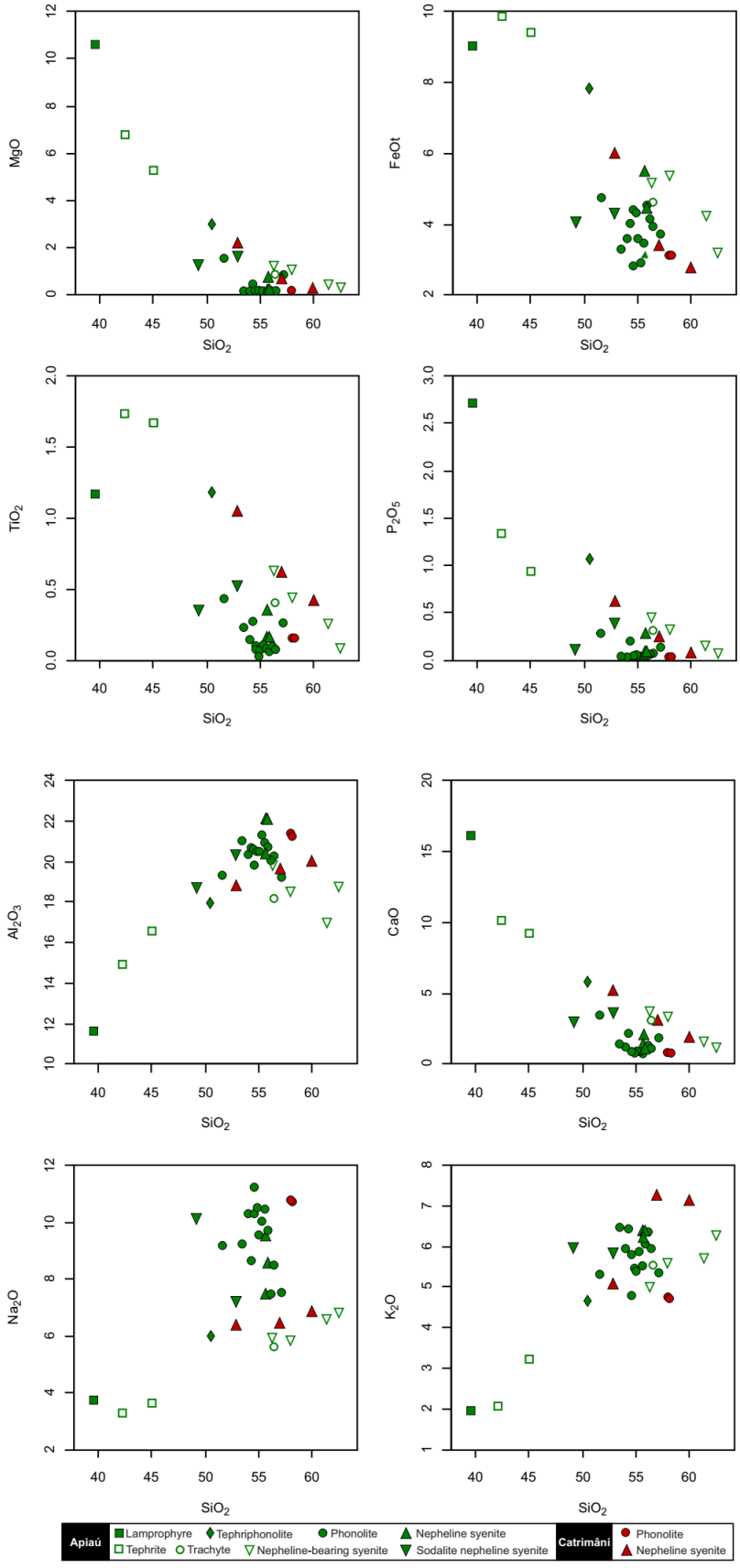

Figure 2.6: Whole-rock SiO_2, versus MgO, Al_2O_3, Na_2O, FeO, CaO, and K_2O concentration (mass %) in studied rocks of the RAP.

The syenites trace elements pattern (Fig. 2.7) varies substantially. All of them exhibit strong negative P and Ti anomalies, besides the patterns of Ba, Ta and Ce can vary strongly depending on the sample. Their contents of Pb and Sr vary weakly. The mafic dykes exhibit a smooth pattern, although the tephriphonolite is slightly enriched in U and Pb. The phonolites in general exhibit positive Pb and Zr anomalies and strong negative Ba, Sr, O and Ti anomalies. The Ta pattern can appear either as positive or negative anomalies. Trachyte exhibit positive anomaly of Ba and negative of P, Zr and Ti.

The syenitic rocks also vary the REE pattern, with absent or only slight negative Eu anomalies (Eu/Eu* = 0.27-1.24). The most hydrothermally altered syenite (Queixada intrusion - paa33) has the highest REE concentrations (∑REE = 2673.06), owing to the presence of REE carbonate. The mafic to intermediate dykes display similar LREE-enriched patterns with La_N/Sm_N from 5.24-6.44 and absent Eu anomalies. All phonolites have convex REE patterns coupled with MREE depletion, Eu anomaly and a slight positive anomaly of Gd. The trachyte is more LREE-enriched than phonolite and is absent of Eu anomaly.

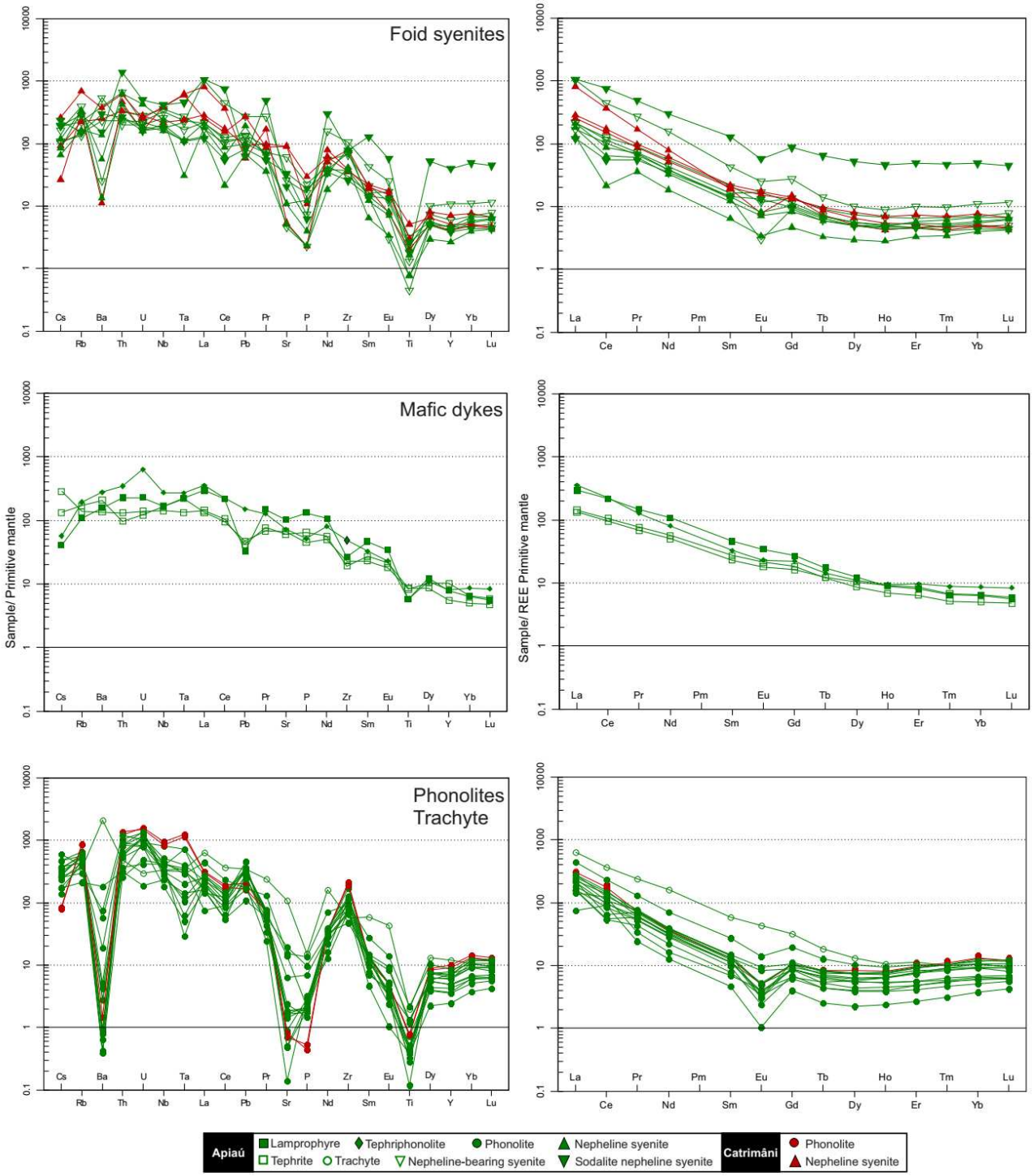

Figure 2.7: Primitive mantle-normalised incompatible trace element (left side) and REE patterns (right side) for the studied rocks from RAP. Normalizing values from McDonough and Sun (1995).

Table 2.5: Whole-rock composition of the rocks from the Apiaú Subprovince. LOI = Loss on ignition. DL= Detection limit. ne-ol=normative nepheline-olivine; A.I.= $(Na_2O + K_2O)/Al_2O_3$.

Rock	**Lamprophyre**	**Tephrite**		**Tephriphono**	**Trachyte**	**Phonolite**		
Latitude	2°27'28" N	2°27'28" N	2°22'05" N	2°21'54" N	2°21'18" N	2°21'54" N	2°19'30" N	2°19'29" N
Longitude	61°33'31" W	61°33'29" W	61°39'38" W	61°37'20" W	61°42'40" W	61°39'11" W	61°42'22" W	61°42'21" W
Intrusion	-	-	-	Campos Novos	Piauí	-	-	-
Sample	rep10	rep12	paa26b	paa15b	rep28	rrtj8	rrtj12	rrtj13
SiO_2 wt.%	39.66	45.06	42.29	50.5	56.42	54.53	56.41	56.13
TiO_2	1.16	1.67	1.73	1.18	0.40	0.10	0.08	0.09
Al_2O_3	11.64	16.57	14.93	17.95	18.18	20.58	20.29	20.02
Fe_2O_3 (t)	10.01	10.45	10.98	8.69	5.14	3.13	4.38	4.60
MnO	0.19	0.17	0.16	0.22	0.27	0.24	0.22	0.22
MgO	10.60	5.26	6.78	3.01	0.86	0.01	0.06	0.10
CaO	16.12	9.24	10.13	5.78	3.16	0.91	1.12	1.33
Na_2O	3.74	3.65	3.28	5.98	5.68	11.20	8.50	7.45
K_2O	1.95	3.23	2.08	4.66	5.53	4.78	5.95	6.35
P_2O_5	2.709	0.93	1.33	1.06	0.32	0.04	0.07	0.06
LOI	1.20	3.5	5.96	0.57	1.50	4.19	2.90	3.63
Li ppm	6.31	32.60	21.30	37.10	77.70	294	48.20	36
Be	2.21	1.51	2.20	3.90	4.32	13.30	7.33	6.62
Sc	23	13.20	13.47	4.98	2.82	1.62	0.92	0.86
V	144	148	177	98.20	13.10	2.44	1.25	1.14
Cr	115	74.80	78.90	20.20	3.52	5.21	4.27	3.81
Co	35.70	29.20	44.70	20.50	4.34	0.34	1.03	1.23
Ni	160	66.90	98.30	19.30	0.64	0.31	0.17	0.19
Cu	54.40	52.60	60.60	16.70	2.88	0.78	3.28	4.45
Zn	75.60	90.60	114	125	155	190	101	99.6
Ga	12.70	16.50	16.40	17.90	19.20	32.40	23.60	23
Rb	65.80	102	82.20	117	213	345	247	260
Sr	2049	1338	1215	1441	2145	32.70	2.79	17.70
Y	34	44.20	23.80	34.90	51.70	30.50	10.50	15.40
Zr	284	241	201	511	597	1218	774	708
Nb	111	110	93	181	225	543	273	273
Mo	0.92	1.43	1.46	6.93	25.60	9	6.10	4.12
Cd	0.34	0.28	0.30	0.57	0.19	0.44	0.21	0.19
Sn	1.32	1.15	0.84	1.50	1.74	3.04	2.47	2.50
Sb	0.02	0.06	0.13	0.11	0.44	1.09	0.37	0.38
Cs	0.86	2.82	6	1.20	5.48	9.86	3.70	8.10
Ba	1050	1383	893	1833	13964	18.30	2.61	27.70
La	193	86	92.70	230	414	91.80	49.40	104
Ce	366	159	179	377	620	205	151	144
Pr	37.80	17.20	19.70	32.70	61.90	8.69	6.17	13.20
Nd	135	62.90	70.80	102	205	20.50	16	35.10
Sm	18.80	9.38	11.10	13.30	24.20	2.83	1.92	3.92
Eu	5.28	2.78	3.29	3.53	6.63	0.63	0.16	0.37
Gd	14.70	8.85	9.92	12.14	17.50	3.50	2.18	3.75
Tb	1.72	1.21	1.21	1.43	1.82	0.54	0.25	0.44
Dy	8.25	7.01	5.85	7.31	8.85	3.86	1.51	2.58
Ho	1.34	1.35	1.03	1.41	1.61	0.96	0.35	0.58
Er	3.57	3.80	2.81	4.21	4.96	3.24	1.17	1.81
Tm	0.44	0.46	0.35	0.60	0.69	0.61	0.21	0.32
Yb	2.82	2.86	2.21	3.82	4.62	4.19	1.68	2.25
Lu	0.38	0.40	0.33	0.57	0.64	0.62	0.29	0.38
Hf	5.66	5.03	4.85	9.37	11	16.30	11.90	11.10
Ta	8.26	8.18	4.93	10	12.80	26.60	13.20	12.10
W	0.61	0.67	1.38	2.92	3.11	5.36	1.82	2.46
Pb	4.85	7.06	6.28	22.60	51.60	67.80	29.10	24.60
Bi	0.02	0.02	0.03	0.08	0.07	0.41	0.25	0.25
Th	18.10	7.77	10.50	27.80	39.10	25.70	20.50	29.50
U	4.57	2.42	2.78	12.70	5.99	18.40	9.77	8.27
Eu/Eu*	0.97	0.93	0.96	0.85	0.98	0.61	0.24	0.29
$(La/Sm)_{CN}$	6.44	5.76	5.24	10.82	10.71	20.37	16.13	16.55
∑REE	789.45	363.36	399.83	789.05	1372.36	346.98	232.16	311.90
ne	1.70	0.92	4.32	13.30	4.20	29.09	19.90	15.98
ol	18.50	9.18	7.72	2.70	0.12	-	-	-
A.I.	0.71	0.57	0.51	0.83	0.84	1.15	1.01	0.96

Table 2.5: Continued

Rock	**Phonolite**							
Latitude	2°20’02” N	2°05’49” N	2°22’04” N	2°21’58” N	2°22’06” N	2°22’44” N	2°22’20” N	2°22’05” N
Longitude	61°36’28” W	61°40’13” W	61°38’34” W	61°38’34” W	61°37’37” W	61°41’22” W	61°39’59” W	61°39’40” W
Sample	rrtj18	rrtj30b	paa2	paa6	paa8a	paa22	paa25	paa26d
SiO_2 wt.%	53.95	57.09	55.26	55.57	55.90	53.52	54.52	54.81
TiO_2	0.14	0.26	0.10	0.08	0.06	0.23	0.08	0.02
Al_2O_3	20.38	19.22	21.31	20.95	20.72	20.99	19.85	20.49
Fe_2O_3 (t)	4.01	4.12	3.25	3.86	5.03	3.68	4.88	4.80
MnO	0.22	0.15	0.16	0.21	0.25	0.19	0.31	0.28
MgO	0.04	0.85	0.05	0.03	0.02	0.14	0.05	0.02
CaO	1.21	1.84	0.89	0.80	1.01	1.42	0.89	0.83
Na_2O	10.31	7.53	10.03	10.48	9.71	9.22	10.30	10.50
K_2O	5.94	5.37	5.87	5.55	6.06	6.46	5.79	5.46
P_2O_5	0.03	0.14	0.04	0.04	0.04	0.04	0.04	0.05
LOI	3.84	3.40	2.88	2.21	0.97	3.91	3.10	2.33
Li (ppm)	47.80	65.10	26.50	22.30	25.60	61.80	118	56.80
Be	9.95	10.10	7.72	11.90	9.23	8.65	11.80	11.30
Sc	1.19	2.39	<DL	<DL	<DL	<DL	<DL	<DL
V	1.42	14.60	4.37	2.44	3.21	10.40	2.54	2.08
Cr	3.11	12.60	2.95	2.19	6.92	3.02	2.37	3.15
Co	1.07	4.81	1.07	0.83	0.99	1.69	1.25	0.72
Ni	0.25	12	0.11	0.03	0.21	0.83	0.07	0.17
Cu	4.42	6.19	2.65	1.7	1.51	2.36	2.27	2.12
Zn	161	106	108	144	162	121	162	193
Ga	29.20	23.90	23.30	26.70	25.50	24.80	28.50	26.40
Rb	331	237	308	338	297	268	359	328
Sr	48	126	37	9.70	36.40	275	33.15	9.79
Y	18.40	21.40	15.70	26.10	26	27	30.20	30.50
Zr	998	745	811	1252	826	972	1338	1222
Nb	343	214	120	199	180	267	216	206
Mo	10.50	6.76	5.40	5.74	2.35	12	4.26	10.24
Cd	0.28	0.20	0.85	1.20	1.01	0.94	1.56	1.27
Sn	2.41	2.99	1.49	2.71	1.96	1.01	2.89	3.21
Sb	0.61	0.53	0.19	0.23	0.16	0.34	0.23	0.42
Cs	7.84	12.70	6.68	5.72	2.93	4.93	7.25	6.09
Ba	18	125	5.17	2.56	4.19	373	6.35	2.80
La	149	120	101	140	182	142	158	166
Ce	231	165	90.30	162	214	108	184	249
Pr	16.10	13.90	11.10	15.60	18.70	17.90	19.20	19.60
Nd	40.60	36.10	27.70	38.50	46.30	48.20	48.30	49.80
Sm	4.58	4.66	3.19	4.65	5.43	6.14	5.82	5.90
Eu	0.80	0.60	0.51	0.55	0.82	1.43	0.77	0.48
Gd	4.72	4.80	3.36	4.74	5.66	5.86	5.80	6.22
Tb	0.52	0.62	0.43	0.66	0.71	0.81	0.80	0.82
Dy	2.94	3.70	2.68	4.18	4.32	4.96	5.03	5.05
Ho	0.67	0.80	0.59	0.96	0.98	1.08	1.15	1.14
Er	2.09	2.44	2.08	3.46	3.34	3.63	4.09	3.99
Tm	0.38	0.43	0.37	0.62	0.57	0.59	0.70	0.69
Yb	2.61	2.93	2.72	4.67	4.07	4.02	5.26	5.14
Lu	0.42	0.47	0.42	0.72	0.63	0.54	0.80	0.84
Hf	14.20	12	12.20	19.50	11.50	13.90	20	19.20
Ta	14.90	11.80	1.88	3.85	4.57	1.08	2.35	7.40
W	3.75	5.69	6.81	4.75	2.41	6.4	4.95	8.51
Pb	50.20	41.40	41.80	56.30	46.90	36.30	50.50	49.40
Bi	0.31	0.40	0.28	0.35	0.26	0.28	0.30	0.29
Th	43.70	67.20	42.50	67.20	65.50	73.60	48.20	50.80
U	22.80	16	16.10	27.80	23.40	16.20	21.19	22.10
Eu/Eu*	0.52	0.38	0.47	0.36	0.45	0.73	0.41	0.24
$(La/Sm)_{CN}$	20.40	16.11	19.88	18.84	20.99	14.53	16.98	17.57
∑REE	456.20	356.54	246.79	380.89	486.8	345.61	439.37	514.25
ne	30.49	12.70	29.19	29.29	26.81	29.67	28.74	29.36
ol	-	0.20	-	-	-	-	-	-
A.I.	1.15	0.95	1.07	1.11	1.09	1.06	1.17	1.13

Table 2.5: Continued

Rock	**Phonolite**		**Nepheline-bearing syenite**				**Nepheline syenite**	
Latitude	2°24'11" N	2°27'37" N	2°27'00" N	2°26'55" N	2°26'55" N	2°21'30" N	2°22'03" N	2°21'54" N
Longitude	61°37'33" W	61°33'45" W	61°40'56" W	61°40'52" W	61°40'48" W	61°42'55" W	61°37'20" W	61°37'20" W
Intrusion	paa38	rep17	Pupunha	Pupunha	Pupunha	Piauí	Campos Novos	Campos Novos
Sample	54.35	54.97	rrtj21	rrtj22	rrtj23	rep24	paa12	paa15a
SiO_2 wt.%	0.27	0.06	56.25	62.50	57.95	61.37	55.85	55.64
TiO_2	20.63	20.46	0.64	0.09	0.45	0.26	0.16	0.33
Al_2O_3	4.46	4.00	19.85	18.77	18.57	17.01	21.97	20.27
Fe_2O_3 (t)	0.18	0.26	5.75	3.60	5.99	4.75	4.87	6.07
MnO	0.47	0.06	0.12	0.20	0.22	0.24	0.15	0.23
MgO	2.17	0.93	1.24	0.16	1.16	0.40	0.10	0.66
CaO	8.62	9.54	3.86	1.25	3.36	1.73	0.97	1.93
Na_2O	6.43	5.39	5.94	6.85	5.91	6.61	8.45	7.42
K_2O	0.20	0.04	5.01	6.30	5.64	5.73	6.34	6.20
P_2O_5	1.58	4.40	0.46	0.05	0.34	0.15	0.05	0.25
LOI	43.20	88.80	0.46	0.46	0.62	1.18	1.28	0.69
Li ppm	5.50	14.20	34.90	32.60	34.80	91.80	16.30	30.50
Be	<DL	0.42	2.93	4.54	3.01	4.38	4.28	4.21
Sc	11.90	1.27	1.87	1.04	2.25	1.79	<DL	<DL
V	3.55	1.24	40.60	2.05	36.90	6.08	5.97	18.40
Cr	1.59	0.87	6.65	7.52	7.61	2.20	3.33	7.76
Co	0.58	<DL	9.71	1.34	7.42	2.09	1.23	3.07
Ni	4.68	3.61	4.25	1.01	1.30	0.30	0.14	1.72
Cu	28	192	8.62	1.49	5.21	<DL	5.46	3.87
Zn	18.50	30	66.4	67.1	95.8	72.4	46.70	56.70
Ga	128	403	17.50	19.60	18	17.10	19.60	17.60
Rb	386	28.30	80.8	236	89	135	195	100
Sr	20.50	34	1206	90.40	518	645	102	218
Y	502	1814	19.70	17.30	25.90	46.50	11.40	19.40
Zr	152	255	315	748	697	1104	433	395
Nb	14.90	14.40	170	237	215	115	106	132
Mo	0.48	1.39	3.22	2.66	2.06	12.40	5.63	2.26
Cd	1.46	6.34	0.11	0.17	0.15	0.78	0.47	0.56
Sn	0.18	0.92	1.26	1.64	1.83	0.86	1.52	1.70
Sb	3.57	9.87	0.14	0.41	0.23	0.43	0.11	0.11
Cs	1204	34	2.30	3.46	2.17	3.98	1.79	1.39
Ba	106	180	3580	167	1525	2608	90.10	898
La	94.10	260	142	110	137	675	84.90	138
Ce	14.90	17.60	194	170	212	742	36.20	145
Pr	41	44	18.80	16.90	23.20	69.10	9.20	17.90
Nd	5.27	5.06	55	47.50	68.80	199	23.20	48.80
Sm	1.28	0.47	6.66	5.52	8.61	17.40	2.60	5.85
Eu	4.89	5.08	2.63	0.46	1.82	3.86	0.52	1.26
Gd	0.65	0.74	6.26	4.93	7.38	14.90	2.53	5.64
Tb	3.76	4.94	0.72	0.59	0.89	1.41	0.33	0.68
Dy	0.78	1.08	3.75	3.34	4.94	6.77	1.99	3.76
Ho	2.48	4.01	0.74	0.70	1	1.32	0.42	0.76
Er	0.40	0.7	2.06	2.07	2.86	4.37	1.45	2.40
Tm	2.84	5.59	0.32	0.34	0.45	0.67	0.23	0.36
Yb	0.43	0.81	2.10	2.38	3.09	4.86	1.75	2.53
Lu	8.93	27.5	0.34	0.42	0.53	0.79	0.29	0.43
Hf	5.28	27.2	5.34	12.30	11.50	18.70	8.46	8.35
Ta	11.80	6.24	6.13	10	8.76	8.13	4.17	4.19
W	16.10	51.90	1.93	3.22	1.77	6.91	4.73	1.71
Pb	0.18	0.30	17.10	19.50	20.60	41.30	10.20	15.10
Bi	25.50	82.80	0.05	0.13	0.11	0.02	0.06	0.16
Th	3.74	27	16	26	19	53.50	21	33.95
U	0.77	0.28	4.01	5.70	4.53	4.35	3.76	3.22
Eu/Eu*	12.59	22.32	1.24	0.27	0.7	0.73	0.62	0.67
$(La/Sm)_{CN}$	278.67	530.11	13.37	12.53	9.98	24.26	20.44	14.73
∑REE	26.58	24.72	435.7	365.66	473.33	1740.36	165.59	373.10
Ne	-	-	5.22	3.97	4.89	1.37	22.92	17.27
Ol	1.03	1.05	1.75	-	0.44	-	-	0.15
A.I.			0.77	0.96	0.85	1	0.95	0.93

Table 2.5: Continued

Rock	**Nepheline syenite**		**Sodalite nepheline syenite**	
Latitude	2°22'17" N	2°23'59" N	2°22'04" N	2°23'58" N
Longitude	61°37'04" W	61°37'34" W	61°37'57" W	61°37'30" W
Intrusion	Campos Novos	Queixada	Gavião	Queixada
Sample	paa20	paa36	paa32	paa33
SiO_2 wt.%	55.65	51.68	52.86	49.20
TiO_2	0.15	0.44	0.53	0.37
Al_2O_3	22.11	19.28	20.38	18.72
Fe_2O_3 (t)	3.47	5.27	4.84	4.53
MnO	0.18	0.22	0.12	0.29
MgO	0.17	1.55	1.69	1.35
CaO	1.26	3.44	3.83	3.18
Na_2O	9.55	9.20	7.25	10.18
K_2O	6.34	5.32	5.85	5.95
P_2O_5	0.08	0.28	0.40	0.13
LOI	0.92	2.83	1.85	4.63
Li ppm	32.70	69.40	37.10	179
Be	6.84	9.95	3.41	22.40
Sc	<DL	1.09	1.22	<DL
V	5.23	49	53.50	41.80
Cr	2.19	32.90	33.80	35.40
Co	1.28	7.75	6.62	4.58
Ni	0.20	23.30	19.30	23.30
Cu	0.64	3.83	9.98	5.73
Zn	55.80	147	51.50	61.20
Ga	21.10	26.30	16.10	26.60
Rb	203	178	92.40	171
Sr	215	305	668	411
Y	20	37.20	16.60	173
Zr	859	973	269	812
Nb	158	294	117	274
Mo	5.36	1.86	3.35	1.87
Cd	0.87	1.04	0.39	0.75
Sn	1.04	1.91	0.53	1.43
Sb	0.12	0.21	0.15	0.48
Cs	2.51	5.30	4.98	4.08
Ba	374	505	1963	1015
La	116	287	78.60	689
Ce	107	390	91.90	1277
Pr	15.40	32.90	13.90	124.60
Nd	41.50	90	43.30	375
Sm	4.94	11.10	5.93	52.40
Eu	1.09	2.19	2.04	8.95
Gd	4.55	10.80	5.36	47.60
Tb	0.59	1.28	0.65	6.37
Dy	3.46	6.97	3.38	35
Ho	0.71	1.39	0.66	6.88
Er	2.50	4.50	2.01	21.70
Tm	0.41	0.68	0.28	3.21
Yb	2.98	4.61	1.92	21.5
Lu	0.46	0.67	0.30	3.03
Hf	14.10	15.40	5.17	13.70
Ta	1.14	10.80	4.06	16.80
W	3.69	3.72	8.24	8.33
Pb	28.60	26.10	12.30	9.45
Bi	0.23	0.23	0.45	0.05
Th	51.50	96.30	21.50	113
U	8.61	20.40	3.22	10.20
Eu/Eu*	0.43	0.61	1.10	0.55
$(La/Sm)_{CN}$	24.35	16.23	8.31	8.24
∑REE	632.94	843.24	250.23	2673.06
ne	29.67	30.44	21.82	34.22
ol	-	-	0.61	-
A.I.	1.02	1.08	0.90	1.24

Table 2.6: Whole-rock composition of the rocks from the Catrimâni Subprovince. LOI=Loss on ignition. DL= Detection limit;ne-ol=normative nepheline-olivine;A.I.=$(Na_2O+K_2O)/Al_2O_3$.

Rock	**Phonolite**		**Nepheline syenite**		
Latitude	0°41'46" N	0°41'57" N	0°41'37" N	0°41'50" N	0°41'53" N
Longitude	61°49'11" W	61°49'08" W	61°48'54" W	61°49'14" W	61°49'12" W
Sample	cat6a	cat39	cat03	cat35	cat37
SiO_2 wt.%	57.93	58.06	59.92	52.91	56.96
TiO_2	0.16	0.16	0.41	1.03	0.60
Al_2O_3	21.37	21.26	19.94	18.72	19.54
Fe_2O_3 (t)	3.49	3.49	3.04	6.62	3.68
MnO	0.23	0.25	0.17	0.19	0.18
MgO	0.01	<0.017	0.20	2.10	0.66
CaO	0.79	0.8	1.86	5.14	3.00
Na_2O	10.80	10.73	6.74	6.28	6.38
K_2O	4.74	4.70	7.09	5.04	7.19
P_2O_5	0.01	0.01	0.05	0.62	0.23
LOI	0.42	1.09	0.70	0.93	1.14
Li ppm	17.30	16.70	10.30	49.30	71.50
Be	12.60	13.30	2.37	2.98	7.11
Sc	0.42	0.49	0.20	3.78	1.09
V	2.03	2.03	8.17	66.10	33.30
Cr	2.99	3.44	1.79	13.30	2.92
Co	0.59	0.61	0.68	10.60	3.16
Ni	<DL	<DL	<DL	9.81	4.80
Cu	<DL	<DL	<DL	4.22	8.95
Zn	152	170	32.20	91.80	115.40
Ga	40.40	43.70	18	18.80	19.30
Rb	518	529	180	137	413
Sr	16.40	14.10	109	1830	1814
Y	38.70	42.40	17.70	21.60	30.60
Zr	2046	2249	407	383	829
Nb	551	622	255	146	255
Mo	0.12	0.16	1.92	10.20	4.35
Cd	1.73	1.88	0.30	0.14	0.63
Sn	4.04	4.17	1.59	1.55	2.52
Sb	0.08	0.11	0.03	0.08	0.11
Cs	1.78	1.71	0.56	1.93	5.5
Ba	9.49	5.56	74.8	1663	2469
La	203	208	530	186	165
Ce	293	329	615	290	258
Pr	18.70	18.70	43.60	25.10	22.10
Nd	45.40	44.40	98.80	76.90	64.50
Sm	5.41	5.36	7.77	8.95	8.14
Eu	0.76	0.76	1.21	2.68	2.37
Gd	5.62	5.59	8.15	7.61	7.15
Tb	0.83	0.86	0.73	0.89	0.95
Dy	5.64	5.93	3.49	4.46	5.41
Ho	1.21	1.30	0.64	0.80	1.03
Er	4.24	4.73	2.06	2.31	3.24
Tm	0.75	0.83	0.29	0.32	0.48
Yb	5.76	6.38	2.12	2.23	3.39
Lu	0.82	0.88	0.31	0.32	0.46
Hf	32.20	34.80	8.57	7.83	13.10
Ta	42.30	47.20	23.10	8.98	22.40
W	1.10	0.97	1.22	5.32	2.96
Pb	25.10	31.30	8.67	13.90	41.20
Bi	0.32	0.38	0.02	0.03	0.14
Th	110	98.10	37.20	26.70	49.80
U	30.40	32.50	3.230	5.65	5.15
Eu/Eu*	0.42	0.99	0.47	0.42	0.95
$(La/Sm)_{CN}$	23.46	12.99	42.72	23.46	12.71
∑REE	590.97	607.92	1313.63	590.97	542.37
ne	26.09	27.2	10.83	9.37	14.16
ol	-	2.46	-	3.67	-
A.I.	1.07	1.07	0.94	0.84	0.94

7. Sr-Nd Isotopes

Results of Sr and Nd isotopic composition of 13 samples of wide compositions from RAP are given in Table 3. We analyzed samples of tephrite, tephriphonolite, phonolite, trachyte, nepheline-bearing, nepheline and sodalite nepheline syenite, which were calculated for an emplacement age of 116 Ma. Besides, two samples from the Precambrian basement were analyzed for Sr-Nd isotopes plus one granite sample compilated from Fraga (2002), all of them were recalculated to 116 Ma. The data are plotted on a Nd_i vs Sr_i (Fig. 2.8A) for comparison with granitic basement and alkaline rocks.

The studied alkaline rocks have $^{143}Nd/^{144}Nd_i$ ranging from 0.51229 to 0.51248 (ε_{Nd} values of -4 to -0.1) and $^{87}Sr/^{86}Sr_i$ ranging from 0.7029 to 0.7069, except one phonolite sample from Catrimâni intrusion (cat39) with the value of 0.6664 that is not plotted on the graph. The other lowest radiogenic Sr values are related to an agpaitic nepheline syenite from Campos Novos (paa20) and a nepheline syenite from Catrimâni (cat03), with $^{87}Sr/^{86}Sr_i$ of 0.7029 and 0.7032, respectively. The agpaitic sodalite nepheline syenite from Queixada has the highest $^{87}Sr/^{86}Sr_i$ and lowest $^{143}Nd/^{144}Nd_i$ values. The most basic rock from RAP (tephrite – rep12) corresponds to one of the samples more radiogenic in ^{87}Sr ($^{87}Sr/^{86}Sr_i = 0.7066$). The ages of Nd model (T_{DM}) vary from 548 to 657, except for one sample from Queixada (paa33) with 825 Ma.

The analyzed host rocks present granitic compositions. One sample corresponds to Paleoproterozoic augen gneiss (paa26a) and another to Mesoproterozoic rapakivi granite (paa08b). The Precambrian basement exhibits lower $^{143}Nd/^{144}Nd_i$ (0.51162 – 0.51175) and higher $^{87}Sr/^{86}Sr_i$ (0.7993 – 0.7484) than alkaline rocks.

In the Nd_i-Sr_i diagram, the RAP samples rocks plot close to the Bulk Silicate Earth field (Fig. 2.8B). For comparison, the data compiled for Central Atlantic Magmatic Province – CAMP, Amazonian Craton and Southern South America were plotted. Most isotope composition obtained for RAP is typical of the CAMP, including dykes from Surinam and French Guyana (Deckart et al., 2005). Furthermore, some samples of RAP plot within the field of data available for the other alkaline rocks from Amazonian Craton (Seis Lagos carbonatite and Velasco-Candelaria Provinces) and south of South America.

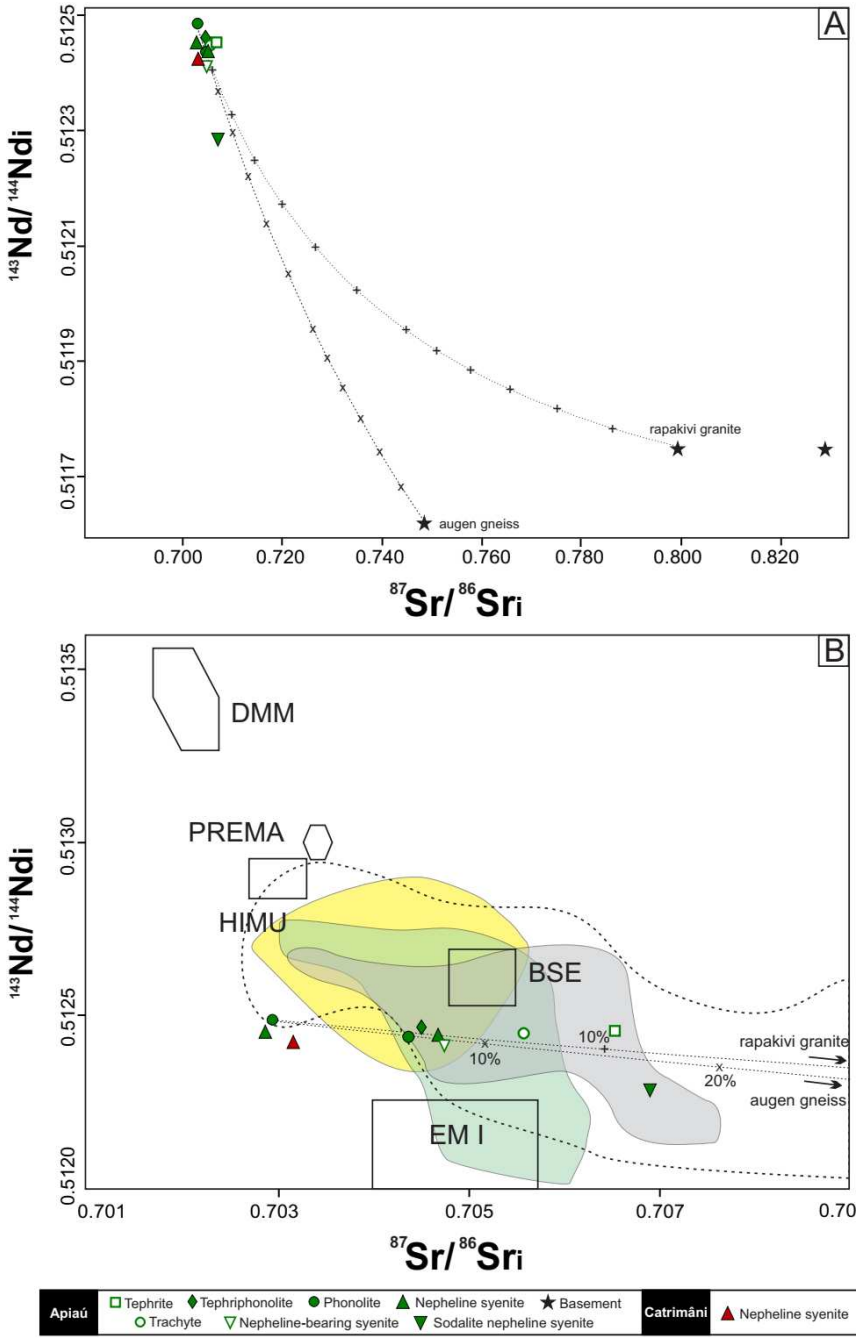

Figure 2.8: Diagrams of Sr-Nd isotopic compositions for representative lithologies from the RAP and the granitic basement. A) Variations of $^{87}Sr/^{86}Sr_i$ versus $^{143}Nd/^{144}Nd_i$ for the rocks from the RAP and for three samples from the granitic basement. The black stars are samples paa08B paa26A and one sample compiled from Fraga (2002). B) Zoom of (A) diagram with DMM, HIMU, PREMA, BSE and EMI reservoirs fields. Gray field = tholeiitic rocks from CAMP; green field = Mesozoic alkaline rocks from south of South America; yellow field = alkaline rocks from Amazonian Craton. The complete database of Sr-Nd isotope analyses is available on Geofacets Elsevier repository (www.geofacets.com).

Table 2.7: Rb-Sr and Sm-Nd concentrations and isotopic ratios for samples from the RAP and Precambrian basement.

Sample	Rock type	Coordinates	Rb (ppm)	Sr (ppm)	$^{87}Rb/^{86}Sr$	$^{87}Sr/^{86}Sr_m$	2σ	$^{87}Sr/^{86}Sr_i$	Sm (ppm)	Nd (ppm)	$^{147}Sm/^{144}Nd$	$^{143}Nd/^{144}Nd_m$	2σ	$^{143}Nd/^{144}Nd_i$	ε_{Nd}	T_{DM}
Apiaú Subprovince																
rep-12	Tephrite	2°27'28" N 61°33'29" W	102	1338	0.2206	0.70696	0.000020	0.70659808	9.38	62.9	0.0902	0.512521	0.000005	0.51245214	-0.7	657
paa-15b	Tephri phonolite	2°21'54" N 61°37'20" W	117	1441	0.2349	0.704947	0.000022	0.704559514	13.3	102	0.0788	0.512522	0.000004	0.51246204	-0.5	602
rep-28	Trachyte	2°21'18" N 61°42'40" W	213	2145	0.2873	0.706103	0.000023	0.705629041	24.2	205	0.0714	0.512503	0.000004	0.5124492	-0.8	590
paa-22	Phonolite	2°22'44" N 61°41'22" W	268	275	2.8205	0.707640	0.000015	0.702989895	6.14	48.2	0.0770	0.512543	0.000005	0.51248496	-0.1	571
paa-38	Phonolite	2°24'11" N 61°37'33" W	128	386	0.9596	0.706001	0.000048	0.704419095	5.27	41	0.0777	0.512495	0.000007	0.51243638	-1.0	626
rrtj-21	Nph bearing syenite	2°27'00" N 61°40'56" W	80.8	1206	0.1939	0.705118	0.000018	0.704798719	6.66	55	0.0732	0.512468	0.000004	0.51241283	-1.5	635
paa-12	Nph syenite	2°22'03" N 61°37'20" W	195	102	5.5363	0.713857	0.000018	0.704729827	2.6	23.2	0.0678	0.512493	0.000005	0.51244118	-0.9	587
paa-20	Nph syenite	2°22'17" N 61°37'04" W	203	215	2.7326	0.707418	0.000039	0.702912953	4.94	41.5	0.0720	0.512505	0.000010	0.51245072	-0.7	591
paa-33	Sdl nph syenite	2°23'58" N 61°37'30" W	171	411	1.2043	0.708960	0.000017	0.706975135	52.4	375	0.0845	0.512350	0.000003	0.51228572	-4	825
Catrimâni Subprovince																
cat-39	Phonolite	0°41'57" N 61°49'08" W	529	14.1	110.0843	0.847963	0.000018	0.666482908	5.36	44.4	0.0730	0.512490	0.000005	0.51243469	-1.05	611
cat-03	Nph syenite	0°41'37" N 61°48'54" W	180	109	4.7810	0.711093	0.000018	0.703211655	7.77	98.8	0.0476	0.512459	0.000005	0.51242247	-1.3	548
Precambrian basement – Apiaú Subprovince																
paa-08b	Granite	2°22'06" N 61°37'37" W	138	91.6	4.4027	0.806548	0.000044	0.799290119	10.6	54.1	0.1185	0.511842	0.000005	0.51175227	-14.4	1922
paa-26a	Augen gneiss	2°22'05" N 61°39'38" W	84	125	1.9510	0.751578	0.000009	0.748361745	7.18	33.2	0.1308	0.511719	0.000004	0.51162023	-16.9	2446

8. Geochronology

One sample of zircon and two of baddeleyite from foid syenite have been analysed for U-Pb age determination. Zircon sample is from Piauí intrusion (rep24), while baddeleyite samples are from Campos Novos (paa12) and Gavião (paa32), all of them are from Apiaú Subprovince. We also analysed zircon grains from Queixada and Catrimâni intrusions. Sample from Queixada intrusion (paa33) has only inherent zircon from Meso and Paleoproterozoic basement, no one recent zircon was found. The zircon crystals from Catrimâni have extremely low uranium contents, with radiogenic lead contents below detection limits, and were rejected from data processing.

All zircon crystals hand-picked from Piauí intrusion are colourless to very pale red with euhedral-subhedral shape. They are 100 - 250 μm in the longest dimension, with width/length ratios of about 1: 1-2. Inclusions are typical and were avoided by a critical analysis from transmitted light and CL images. The Fig.2.9 shows the CL images of zircon crystals with analytical spots. The image reveals faint and broad zoning with an almost homogeneous texture and reaction rims surrounding all zircon crystals. From a total of 33 measured spots in sample rep24, seventeen of them are concordant and yield a concordia age of 114 ± 0.5 Ma, with an MSWD of 3.2 (Fig 2.10). Data with less than 98% concordance were rejected. The U contents of these zircons range from 406 to 1932 ppm, Th contents varied from 481 to 3310 ppm and Th/U ratios from 0.94 to 1.91.

Zircon grains from Queixada are pale red to colourless with euhedral to subhedral shape. One zircon is brown. Size and width/length ratios vary considerably, 100 to 250 μm and 1:1-5 or 2:5, respectively. CL images reveal faint and broad zoning texture (Fig. 2.11), however any reaction rims, similar to sample from Piauí (rep24), is observed in zircon grains from paa33. All analytical spots are inherent from the granitic basement. Concordia diagram exhibit two populations of zircon (Fig. 2.12). One population presents weighted mean $^{206}Pb/^{238}U$ ages of 1556 ± 13 Ma and is referent to Mesoproterozoic rapakivi granites. Another population presents weighted mean $^{206}Pb/^{238}U$ ages of 1948 ± 14 Ma, which is referent to Paleoproterozoic orthogneisses and metagranites from the basement. It is worth to note the sample from Queixada is an agpaitic sodalite nepheline syenite that intrudes in the contact of rapakivi granites and metagranites, indicating reactive assimilation of the granitic basement by alkaline magma.

Zircon crystals hand-picked from Catrimâni intrusion (cat38) are very heterogeneous, with different colours and a wide range of size. Inclusions are typical in all of them. The biggest crystals (150-450 µm) are anhedral to subhedral, often present milk-white colour (few grains are milk-pale yellow), and width/length ratios of 1:1-5. The smallest zircon crystals are rounded colourless and transparent, but few of them are milk-white colour and subhedral. The size ranges from 50 µm to 150 µm, and width/length ratios are 1:1-2. The CL image exhibits complex texture in many grains, suggesting the dissolution of those zircon crystals (Fig. 2.13). Few zircons present faint and broad zoning with an almost homogeneous texture, without dissolution texture. Regardless of morphological aspects, all analysed crystals have extremely low U and Pb contents, below detection limits, impossible to obtain any analytical data.

Zircon from alkaline intrusions from RAP often present texture of dissolution and precipitation, mainly as reaction rims. This feature is also observed in CL of some grain of Pupunha intrusion (rrtj21, Figueiredo et al., 2018). The solubility of Zr increases in alkaline fluids at high pH, which may result in alterations and dissolution-precipitation of Zr minerals (Ayers et al., 2012; Wilke et al., 2012). In addition, the intensive albitization in the most sample from RAP suggests that Na-rich fluid likely played an important role in the genesis of those rocks.

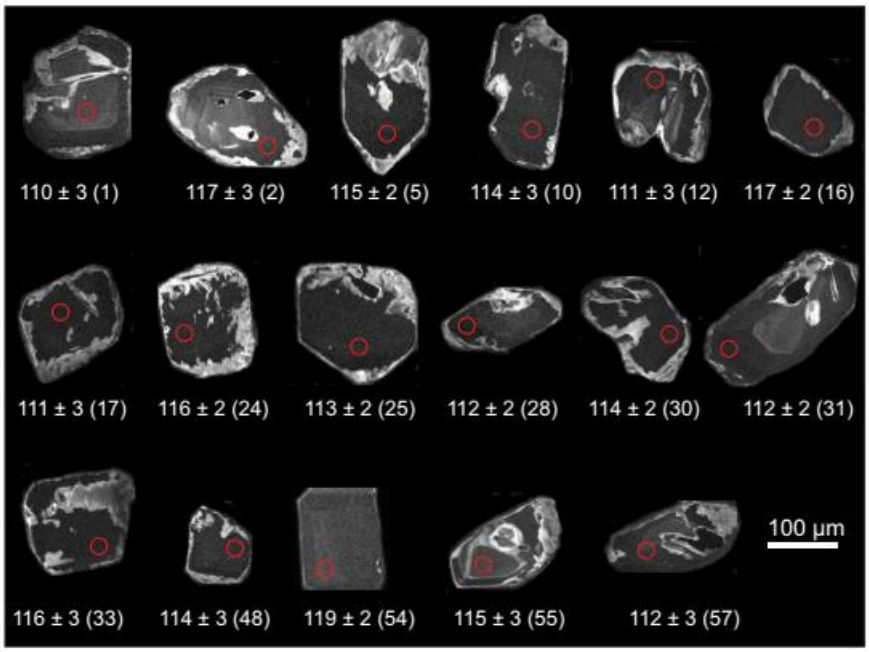

Figure 2.9: Cathodoluminescence images of zircon crystals from Piauí intrusion. Values in parenthesis are the zircon numbers.

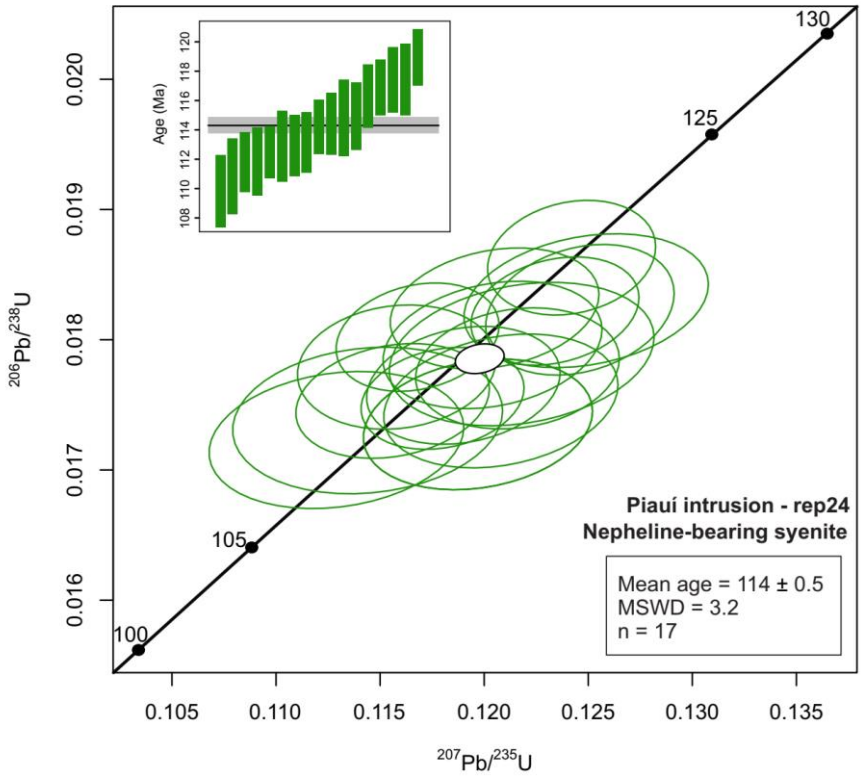

Figure 2.10: Concordia diagram of zircon U–Pb data for Piauí intrusion

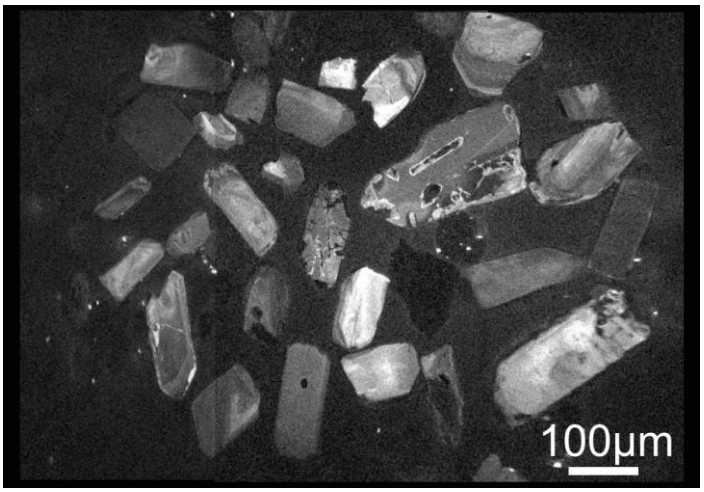

Figure 2.11: Cathodoluminescence image of zircon grains from Queixada intrusion.

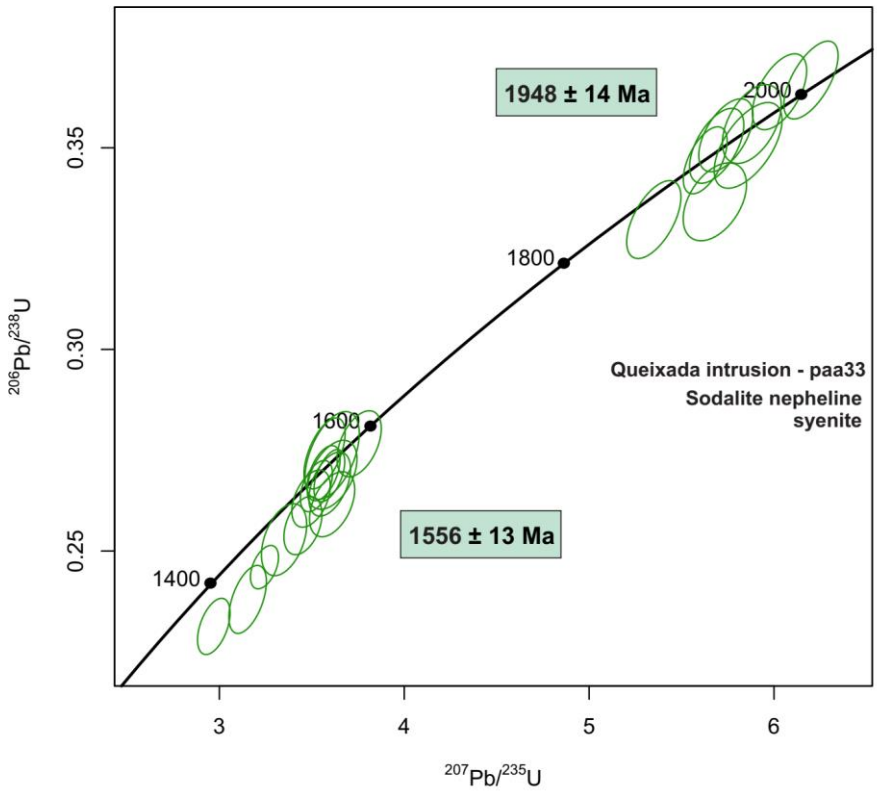

Figure 2.12: Concordia diagram of zircon U–Pb data for Queixada intrusion.

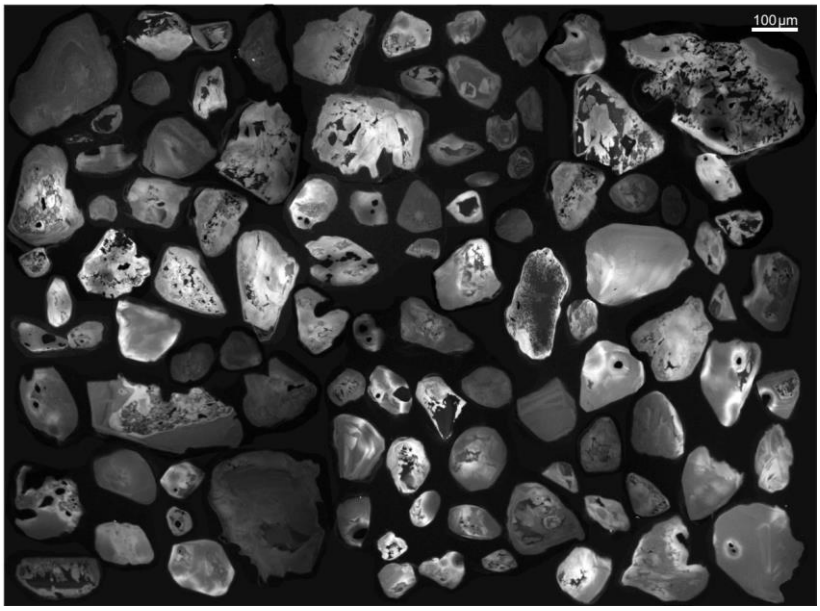

Figure 2.13: Cathodoluminescence image of zircon grains from Catrimâni.

Baddeleyite crystals hand-picked are slightly brown and most of them are extremely small (< 40 μm). The concentration of U in analysed crystals vary significantly, ranging from 195 to 6420 ppm. A total of 9 baddeleyite grains were analysed from sample paa12. The results are discordant (3-33%) and the $^{206}Pb/^{238}U$ ages have a wide dispersion. One younger fraction presents ages between 78 and 88 Ma, another fraction between 92 and 103 Ma, and an older one between 123-142 Ma. The results are plotted in Tera-Wasserburg concordia diagrams in Fig. 2.14. Excluding four spots with low U contents and/or high common-Pb (bd1, 3, 6 and 7), the remaining analyses define a regression line on the Tera-Wasserburg plot, anchored to the initial Pb isotopic composition of $^{207}Pb/^{206}Pb$ ratio of 0.86 (Stacey and Kramers, 1975) and a lower intercept date of 91.7 ± 2.5 Ma (MSWD = 23). A total of four baddeleyite grains were analysed from sample PAA32. All baddeleyite yield discordant results ranging from 27 to 75%. The analyses yield $^{206}Pb/^{238}U$ ages are 103 ± 2 (bd1), 118 ± 5 (bd2), 91 ± 3 (bd3) and 119 ± 6 (bd4). The older ages (bd2 and bd4) correspond to spots with the highest common-Pb (up to 78%).

Baddeleyite analyses give imprecise ages, with a wide data spread and often younger than previously published for baddeleyite from Apiaú Subprovince (~116 Ma, Figueiredo et al., 2018). The analyses do not yield concordant ages, possibly due to Pb loss (Fig. 2.14 and 2.15). Baddeleyite analyses may present too low U–Pb ages due to the loss of Pb from the outer rims of the crystals (Svensen et al., 2012; Corfu et al., 2013). Thus, the Pb loss of analysed baddeleyite may be a consequence of the tiny shape of the crystals and, therefore, younger ages than previously published. A similar situation is reported for Ponta Grossa Arch, in which younger baddeleyite and zircon ages are a consequence of Pb loss (Almeida et al., 2017).

Although baddeleyite ages do not help to constrain the emplacement ages of Campos Novos and Gavião intrusions, they are in good agreement with the timing of magmatism in RAP. One possible scenario is that alkaline magmatism in central Guyana Shield took place in multiple episodes, beginning with less undersaturated magma and evolving to more undersaturated – agpaitic magmatism.

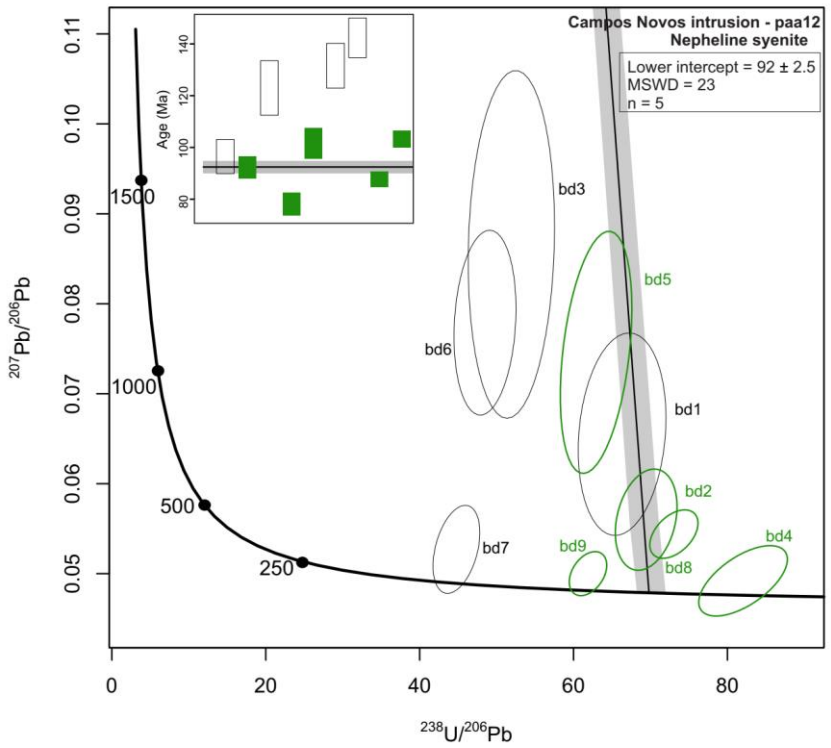

Figure 2.14: Concordia diagram of baddeleyite U–Pb data for Campos Novos intrusion.

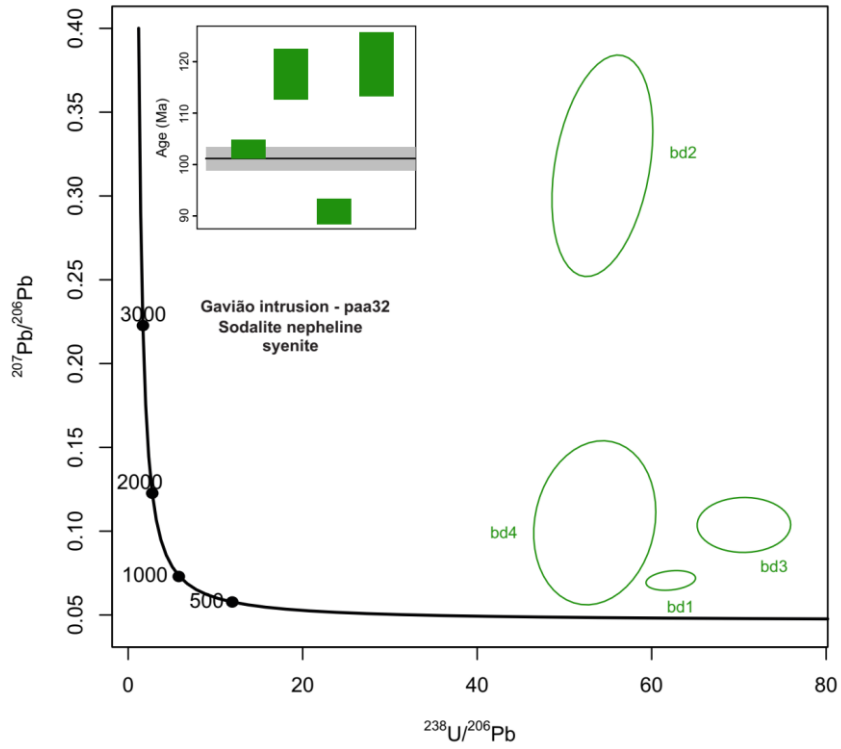

Figure 2.15: Concordia diagram of baddeleyite U–Pb data for Gavião intrusion.

Table 2.8: LA-ICPMS zircon U–Pb dating results for a miaskitic nepheline-bearing syenite (rep24) and sodalite nepheline syenite (paa33) from the Apiaú Subprovince.

Zircon	*f*206 (%)	U (µg.g^{-1})	Th (µg.g^{-1})	Pb (µg.g^{-1})	Th/U calculated	$^{206}Pb/^{204}Pb$	$^{207}Pb/^{235}U$	2s	$^{206}Pb/^{238}U$	2s	Rho	$^{207}Pb/^{206}Pb$ (Age Ma)	2s	$^{206}Pb/^{238}U$ (Age Ma)	2s	$^{207}Pb/^{235}U$ (Age Ma)	2s	% conc[2]
Piauí intrusion - rep24 – Nepheline-bearing syenite (coordinates: 2°21'30" N, 61°42'55" W)																		
1	0.65	406	520	28	1.28	2885	0.1129	0.005	0.0172	0.0004	0.19	671	50	110.1	2.7	108.2	4.6	102
2	0.38	670	697	41.9	1.04	4960	0.1249	0.0048	0.0183	0.0004	0.24	584	38	117	2.7	118.7	4.3	99
5	0.20	1343	2560	137.2	1.91	9380	0.1168	0.0032	0.0180	0.0003	0.22	411	29	115.1	2.1	112.3	2.9	102
10	0.30	912	856	47.9	0.94	6220	0.1158	0.0039	0.0178	0.0004	0.12	497	33	113.6	2.5	111.1	3.5	102
12	0.62	458	481	25.3	1.05	3035	0.1144	0.0053	0.0174	0.0005	0.13	683	47	111	2.9	109.2	4.8	102
16	0.32	902	930	51.1	1.03	5935	0.1205	0.0041	0.0182	0.0004	0.23	443	34	116.5	2.4	115	3.7	101
17	0.39	771	799	45.1	1.04	4820	0.1197	0.0045	0.0174	0.0004	0.20	578	37	110.8	2.6	114.1	4.1	97
24	0.18	1689	1883	108.6	1.11	10315	0.1234	0.0033	0.0182	0.0003	0.25	411	29	116.4	2.2	117.8	3	99
25	0.28	1109	1096	59.5	0.99	6575	0.119	0.0038	0.0177	0.0004	0.21	506	35	112.7	2.4	114.7	3.5	98
28	0.30	1153	2281	123.1	1.98	6185	0.1156	0.0038	0.0175	0.0004	0.21	519	39	112	2.3	110.5	3.4	101
30	0.31	1140	1363	73	1.20	6085	0.1216	0.004	0.0178	0.0004	0.16	527	34	113.5	2.4	116.8	3.6	97
31	0.21	1702	3310	181	1.94	9025	0.118	0.0032	0.0176	0.0003	0.21	395	28	112.1	2	113	2.9	99
33	0.25	1359	1336	73.7	0.98	7340	0.1246	0.0037	0.0182	0.0004	0.25	487	37	116.4	2.6	118.9	3.3	98
48	0.46	792	734	42.3	0.93	4025	0.1218	0.0052	0.0179	0.0005	0.23	588	41	114.2	2.9	116.6	4.6	98
54	0.19	1932	2016	124.7	1.04	10030	0.1242	0.0033	0.0186	0.0004	0.19	431	30	119	2.3	119	3	100
55	0.40	921	1299	69.7	1.41	4620	0.1204	0.0043	0.0180	0.0004	0.24	571	38	114.7	2.5	114.7	3.8	100
57	0.47	783	1017	55.1	1.30	3950	0.1208	0.0046	0.0175	0.0004	0.24	613	42	112	2.7	114.8	4.2	98

Table 2.8: Continued.

Zircon	$f206$ (%)	U ($\mu g.g^{-1}$)	Th ($\mu g.g^{-1}$)	Pb ($\mu g.g^{-1}$)	Th/U calculated	$^{206}Pb/^{204}Pb$	$^{207}Pb/^{235}U$	2s	$^{206}Pb/^{238}U$	2s	Rho	$^{207}Pb/^{206}Pb$ (Age Ma)	2s	$^{206}Pb/^{238}U$ (Age Ma)	2s	$^{207}Pb/^{235}U$ (Age Ma)	2s	% conc[2]
Queixada intrusion - paa33 – Sodalite nepheline syenite (coordinates: 2°23'58" N, 61°37'30" W)																		
1	0.09	226	59	65	0.26	21650	5.860	0.150	0.3506	0.0087	0.59	1980	22	1926	41	1950	21	97
3	0.13	135	44	48	0.32	14300	5.880	0.130	0.3559	0.0080	0.48	1969	23	1955	37	1957	20	99
7	0.08	251	78	79	0.31	24550	5.350	0.120	0.3322	0.0079	0.58	1888	22	1846	38	1871	19	98
9	0.06	279	156	182	0.56	31250	6.200	0.120	0.3668	0.0079	0.63	1993	18	2018	37	2004	18	101
10	0.20	94	35	38	0.38	9355	5.680	0.140	0.3366	0.0079	0.44	2014	27	1862	38	1922	21	92
12	0.12	149	66	77	0.44	15800	6.030	0.120	0.3639	0.0077	0.56	1968	20	1993	36	1981	17	101
13	0.04	491	252	230	0.51	48450	5.628	0.097	0.3469	0.0068	0.57	1940	17	1915	32	1918	15	99
16	0.11	157	52	57	0.33	16650	5.740	0.120	0.3531	0.0074	0.55	1932	21	1945	36	1932	17	101
20	0.06	267	73	75	0.27	30150	5.690	0.120	0.3505	0.0076	0.56	1926	20	1930	36	1924	18	100
2	0.05	459	100	82	0.22	35150	3.595	0.068	0.2687	0.0053	0.53	1572	20	1531	27	1547	15	97
4	0.19	127	60	52	0.47	9850	3.756	0.098	0.2766	0.0067	0.46	1622	27	1572	34	1568	21	97
5	0.19	130	60	53	0.46	9770	3.496	0.085	0.2630	0.0058	0.44	1588	25	1499	30	1521	19	94
6	0.15	163	89	74	0.54	12735	3.525	0.071	0.2661	0.0052	0.49	1566	24	1516	26	1534	16	97
8	0.33	74	33	28	0.44	5715	3.610	0.110	0.2689	0.0070	0.46	1641	31	1528	35	1544	23	93
11	0.11	258	118	86	0.46	17350	3.153	0.083	0.2380	0.0069	0.52	1601	28	1376	36	1447	20	86
14	0.38	61	23	21	0.38	4865	3.610	0.100	0.2616	0.0066	0.45	1675	31	1495	34	1541	23	89
15	0.07	327	176	154	0.54	26400	3.569	0.091	0.2742	0.0072	0.57	1559	28	1555	36	1542	20	100
17	0.17	147	107	66	0.73	10850	2.970	0.072	0.2313	0.0057	0.48	1543	28	1335	29	1399	19	87
18	0.13	182	84	51	0.46	13930	3.244	0.062	0.2460	0.0044	0.46	1556	21	1418	23	1465	15	91
19	0.26	87	70	34	0.80	7255	3.350	0.100	0.2528	0.0073	0.42	1559	37	1450	37	1482	24	93
21	0.23	99	33	25	0.33	8190	3.610	0.120	0.2737	0.0089	0.50	1613	38	1553	45	1534	26	96
22	0.27	84	40	35	0.47	6890	3.597	0.092	0.2666	0.0065	0.47	1650	31	1518	33	1542	20	92
23	0.12	189	77	62	0.41	16200	3.564	0.073	0.2693	0.0056	0.51	1560	23	1531	28	1533	16	98
24	0.20	113	53	42	0.47	9330	3.452	0.084	0.2563	0.0059	0.39	1615	31	1475	30	1510	19	91

Table 2.9: LA-ICPMS baddeleyite U–Pb dating results for a miaskitic nepheline syenite (paa12) and sodalite nepheline syenite (paa32) from the Apiaú Subprovince.

Baddeleyite	f206 (%)	U (µg.g^{-1})	$^{206}Pb/^{204}Pb$	$^{238}U/^{206}Pb$	1s	$^{207}Pb/^{206}Pb$	1s	$^{207}Pb/^{235}U$	2s	$^{206}Pb/^{238}U$	2s	Rho	$^{207}Pb/^{206}Pb$ (Age Ma)	2s	$^{206}Pb/^{238}U$ (Age Ma)	2s	$^{207}Pb/^{235}U$ (Age Ma)	2s	% conc[2]
Campos Novos intrusion - paa12 – Nepheline syenite (coordinates: 2°22'03" N, 61°37'20" W)																			
bd1	0.53	499	3545	66.313	2.330	0.0655	0.005	0.130	0.009	0.0151	0.0005	0.16	1059	79	96	3	122	8	79
bd2	0.27	931	7000	69.444	1.639	0.0560	0.002	0.110	0.004	0.0144	0.0003	0.26	667	44	92	2	106	4	87
bd3	0.93	195	2015	51.921	2.291	0.0866	0.008	0.203	0.015	0.0193	0.0009	0.10	1427	96	123	5	183	13	67
bd4	0.10	4082	19650	82.034	2.355	0.0492	0.001	0.083	0.003	0.0122	0.0004	0.61	385	33	78	2	81	3	97
bd5	0.22	1090	8600	62.932	1.901	0.0746	0.005	0.140	0.007	0.0159	0.0005	0.36	965	67	102	3	131	6	77
bd6	0.31	621	6030	48.496	1.646	0.0779	0.004	0.214	0.011	0.0206	0.0007	0.15	1159	70	132	5	193	9	68
bd7	0.21	891	8870	44.782	1.243	0.0527	0.002	0.160	0.006	0.0223	0.0006	0.38	539	40	142	4	151	6	94
bd8	0.05	6420	40400	73.046	1.280	0.0544	0.001	0.102	0.002	0.0137	0.0002	0.45	445	23	88	2	99	2	89
bd9	0.06	4530	30900	61.881	0.995	0.0500	0.001	0.111	0.002	0.0162	0.0003	0.38	303	20	103	2	107	2	97
Gavião intrusion - paa32 – Sodalite nepheline syenite (coordinates: 2°22'04" N, 61°37'57" W)																			
bd1	0.12	3500	15700	62.189	1.160	0.0706	0.002	0.156	0.005	0.0161	0.0003	0.23	913	45	103	2	147	4	70
bd2	1.13	298	1655	54.348	2.363	0.3180	0.027	0.626	0.034	0.0184	0.0008	0.31	3238	67	118	5	475	21	25
bd3	0.95	429	1970	70.572	2.191	0.1037	0.007	0.186	0.010	0.0142	0.0004	0.01	1630	77	91	3	169	8	54
bd4	78.67	245	24	53.476	2.859	0.1050	0.020	0.181	0.015	0.0187	0.0010	0.13	1380	110	119	6	163	12	73

9. Discussion

9.1 The proposition of the Roraima Alkaline Province (RAP)

The term 'igneous province' is usually employed to group rocks and is described all over the world. It refers to cotemporal and cospatial magmatism which covers since a few plugs to enormous magma volume, where the ages of the spatially associated rocks fall within a narrow range (Rock, 1981). Thus, this term points out a broad area with similar rocks that have been formed during the same period of igneous activity (Bates and Jackson, 1987). Therefore, the term province is a very useful concept of indicating the broad-scale association between extrusive and intrusive rocks that are linked to a specific tectonothermal event or series of related events (Gillespie et al., 2008).

Many Meso-Cenozoic alkaline provinces are described to the Brazilian platform in which are associated with the Atlantic opening. The 15 provinces within central-southeastern Brazil are closely related to reactivations of crustal discontinuities along the borders of sedimentary basins (Ulbrich and Gomes, 1981; Almeida, 1986; Riccomini et al., 2005). Although the structural control is clear, the trigger for alkaline magmatism in South America is very debatable. Gibson et al. (1995, 1999) argue that the Late Cretaceous alkaline magmatism in southeastern Brazil is owing to a plume underneath the subcontinental lithosphere. In contrast, other authors hold that magmas are derived from a sublithospheric mantle source, without interaction with a convective mantle (Riccomini et al., 2005; Gomes et al., 2011; Guarino et al., 2013).

Only two alkaline provinces, Velasco and Candelaria, are proposed to Amazonian Craton, both in Central Brazil Shield (Fletcher and Beddoe-Stephens, 1987; Comin-Chiaramonti et al., 2005). So far, there was no alkaline province described in Guyana Shield. On the other hand, several alkaline complexes, structurally controlled and from different ages, have been reported by many authors (Table 2.1). Rossoni et al. (2017) described that the emplacement of the Mesoproterozoic Seis Lagos Alkaline Complex was controlled by an E-W lineament, but NE-SW and WNW-ESE structures are also found nearby. Moreover, the Neoproterozoic Maicuru Complex seems to have been emplaced in the Guyana Shield along with major NE-SW and NW-SE fault systems that cross the region (Ulbrich and Gomes, 1981; Gomes et al., 1990; Costa et al., 1991).

In this context, we have introduced the RAP in order to designate the broad region of occurrence of clusters of alkaline bodies with specific ages and petrological relationships. All the rock types are associated in time and over a relatively restricted area, with petrological affinities, and must, therefore, be considered as an igneous province. It is the first proposition of an alkaline province in Guyana Shield. Besides, two spatial subprovinces exist within the RAP: the Apiaú subprovince, situated into the northern area, that encompasses most alkaline bodies of the province; and the Catrimâni subprovince, in the south, that include one intrusion with the same name (Fig. 2.2).

Rocks of the RAP can be classified into two groups: (i) evolved phonolite, trachyte and foid syenite found as large or small plutons and dykes; and (ii) basic alkaline magmas, such as lamprophyre, tephrite and tephriphonolite, all of them found as dykes. These rocks are located over 200 km in length, emplaced into main faults and shear zones of central Guyana Shield. U-Pb ages obtained for Piauí, Gavião and Campos Novos intrusions range from ~100 to 114 Ma, which is in good agreement with previous data of 111-116 Ma for Pupunha intrusion and 100 Ma (Rb-Sr) for Catrimâni (Figueiredo et al., 2018; Montalvão et al., 1975). Despite the Pb loss of baddeleyite from Gavião and Campos Novos, resulting in inaccurate U-Pb ages around 100 Ma, those data show that alkaline magmatic activity in central Guyana Shield was a short-lived event.

The RAP is noteworthy structurally controlled by significant Proterozoic faults. The alkaline rocks occur following significant faults and shear zones mainly by the NE-trending. The importance of the NE-SW lineaments in that region is presented by several authors and correlated to the Paleoproterozoic Trans Amazonian Orogeny and the Mesoproterozoic K'Mudku event (Santos et al., 2000, 2006b; 2009; Fraga et al., 2009; Cordani et al., 2010). Nevertheless, most plutons are located into the intersection of faults. We can find many NW-SE alkaline dykes, the same trend of the foliation of the Paleoproterozoic gneiss, also suggesting the importance of NW-SE structures to the emplacement of RAP.

Figueiredo et al. (2018) highlight the relationship between the emplacement of the alkaline rocks from Apiaú subprovince and the reactivation of main shear zones in Guyana Shield during the Equatorial Atlantic opening. The reactivation event was responsible for the development of the Tacutu aulacogen, a half-graben which extend in NE-trending for 300 km between Brazil and Guyana (Crawford et al., 1985; Eiras and Kinoshita, 1988). Although the rift-related tectonic setting is well known, it is unclear whether the RAP is related to a passive rifting caused by an extension, or active rifting, induced by a mantle plume. The RAP is

associated with the final sedimentation of Tacutu Basin (Vaz et al., 2007; Figueiredo et al., 2018). The initial rift phase was marked by tholeiitic magmatism from CAMP, which occurs ~200 Ma around the Atlantic margins (Marzoli et al., 1999). The long timing of the CAMP magmatism, as well as the width of the rift system and the role of preexisting weak zones, are consistent with rifting initiated by lithospheric extension with mantle uplift and magma production (Lamotte et al., 2015).

Therefore, the model of passive rift is more likely to Tacutu basin, which triggers the mantle metasomatism and generated alkaline and enriched tholeiitic magmatism. The absence of both time progression and radial structures, as well as repeated magmatic activity along same lineaments and the lack of widespread flood basalts throughout the peri-Atlantic zone, are in favour of alkaline magmatism related to asthenospheric upwelling and controlled by lithospheric fracturing (Matton and Jébrak, 2009).

9.2 Possible magmatic linkages of the bimodal magma-types from RAP

Bimodal magmatism has been reported for many alkaline provinces and complexes, such as Serra do Mar (Brazil; Gomes et al., 2017), Rarotonga (Southern Pacific; Thompson et al., 2001) and Saghro (West Africa; Berger et al., 2009). Several mechanisms have been suggested to link the bimodal magma-types in the same context. Petrological studies have often demonstrated that felsic magma evolved by fractional crystallization of basic parental magma (Macciotta et al., 1990; Berger et al., 2014), which may be associated with crustal assimilation processes (Marsh et al., 2010; Ackerman et al., 2015). Alternatively, partial melting of basic material in the lower crust-upper mantle (Bailey, 1987), as partial melting of underplated basanites (Legendre et al., 2005), could explain bimodal chemical composition.

The spatial and temporal distribution of the basic and felsic studied rocks suggest a genetic relationship. They are silica undersaturated, with a variable degree of saturation (ne-normative = 0.9 to 34.2), from metaluminous to peralkaline affinities and with mineralogy that varies from miaskitic to agpaitic. The similar evolutionary trends observed in the TAS (Fig.2.5) and Harker diagrams (Fig.2.6) for all rock-types seem that these tend to be controlled mainly by fractional crystallization processes. The geochemical patterns of alkaline rocks from Apiaú and Catrimâni subprovince are very similar. The evolutionary trends of these melts indicate a progressive reduction of MgO, FeO, CaO, and an increase in Al_2O_3 and

alkalis (Tab.2.3). They suggest that the early-crystallized phases are olivine, spinel, plagioclase and apatite, as observed in the most primitive rocks, whereas alkali feldspar represent late fractionated phase. Phosphorous contents are very low in evolved rocks, reflecting apatite fractionation. In addition, the low Sr and Ba contents suggest plagioclase fractionation, supported by negative Eu anomalies.

The mafic dykes and most foid syenites are metaluminous varieties, while most phonolites and the agpaitic syenites from Campos Novos and Queixada (paa20 and paa33) are peralkaline types. The presence of wohlerite and titanite marks the miaskitic to agpaitic transition in peralkaline phonolites. According to Marks and Markl (2017), the term "transitional agpaitic" is more appropriated if the rock contains HFSEs that are typical of agpaitic and miaskitic rocks, such as titanite and eudialyte. The peralkaline character of RAP is interpreted as evidence of extensive fractionation of feldspar, which is corroborated by very lower Sr and Ba contents in the most evolved phonolites. Fractionation of feldspar as a cause for the increase in peralkalinity is also suggested for Pilanesberg Complex in Africa (Elburg and Cawthorn, 2017). In addition to peralkaline character, some trace elements, such as Zr, Nb and Th display behaviour of very incompatible elements, reaching extreme concentration in most differentiated phonolites (>2000, 600 and 1000 ppm, respectively).

Marks and Markl (2017) hold that alkali basaltic, basanitic, and nephelinitic compositions are likely to represent the most important types of parental melts for peralkaline rocks. Moreover, Kramm and Kogarko (1994) discussed the origin of nepheline syenites in the Kola Province as a differentiation product from a variety of nepheline-normative parental melts, such as olivine nephelinites, melilitic basalts and alkali basalts. Fractional crystallization from a parental magma of basanitic composition has been proposed as the main evolution process for many alkaline occurrences from southern Brazil (Brotzu et al. 1992; Beccaluva et al. 1992; Azzone et al. 2016) and may be an alternative for rocks from RAP.

The most primitive rock from the RAP is represented by a lamprophyre dyke (rep10) from Apiaú subprovince, showing MgO = 10.6%, Co = 35.7 and Ni = 160 ppm. However, this rock is very porphyritic and may not represent the primary liquid composition. Thus, the most primitive melt composition of this series is best represented by the tephrite rock-types (rep12 and rep26B). The geochemical trend of the series also indicates that olivine nephelinite or basanite melts could have evolved mainly from fractional crystallization, reaching tephrite-phonolite and even more extreme phonolite compositions.

We used the MELTS thermodynamic models of fractional crystallization (Asimow and Ghiorso, 1998; Ghiorso and Sack, 1995) to test the possible relationship between basic and felsic rocks from RAP by fractional crystallization processes (Fig.2.16). The selected initial liquid composition corresponds to the least porphyritic tephrite (rep12). Models variable include two oxygen buffers, FMQ (M1) and FMQ+1 (M2), with an initial temperature of 1141°C and 1177°C, respectively, and P of 1 kbar. Both models provided olivine, clinopyroxene and spinel as early-crystallized minerals, while feldspar and biotite occur as other fractionated phases. These models suggest that some phonolites and syenites may be the result of 51–68% crystallization of an assemblage of 1-3% olivine, 23% clinopyroxene, 1–1.08% apatite, 8–10% spinel, 11–21% feldspar, and 0.6-2% biotite from tephrite.

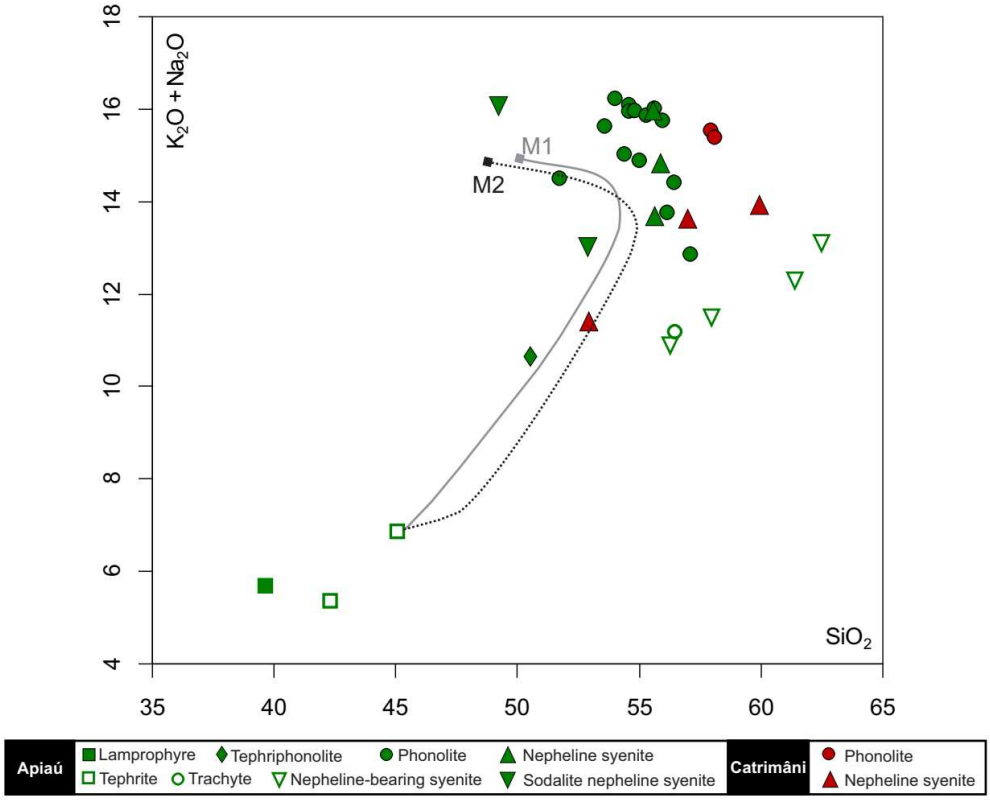

Figure 2.16: Variation of SiO_2 vs. $K_2O + Na_2O$ for rocks from RAP. The lines correspond to liquid evolution trends acquired by models of fractional crystallization using the MELTS algorithm. Tephrite from Apiaú subprovince (rep12) was considered the initial liquid composition. M1is the model for FMQ and M2 for FMQ+1.

Compatible with the modelled evolutionary trend, in the normative Qz-Ne-Ks petrogeny residual diagram (Fig. 2.17), the most evolved rocks from RAP plot toward the phonolitic minimum. This behaviour suggests that these rocks could be linked by extensive fractional crystallization processes, from a similar mafic parental magma, evolving firstly to undersaturated syenitic types (some of these indicating some degree of accumulation of alkali feldspar) and, after fractionation, evolving to agpaitic types. The main nepheline syenites of RAP with cumulatic character plot in the petrogeny residual diagram closer to the Ab-Or boundary, and do not present the Eu anomaly registered for the phonolites.

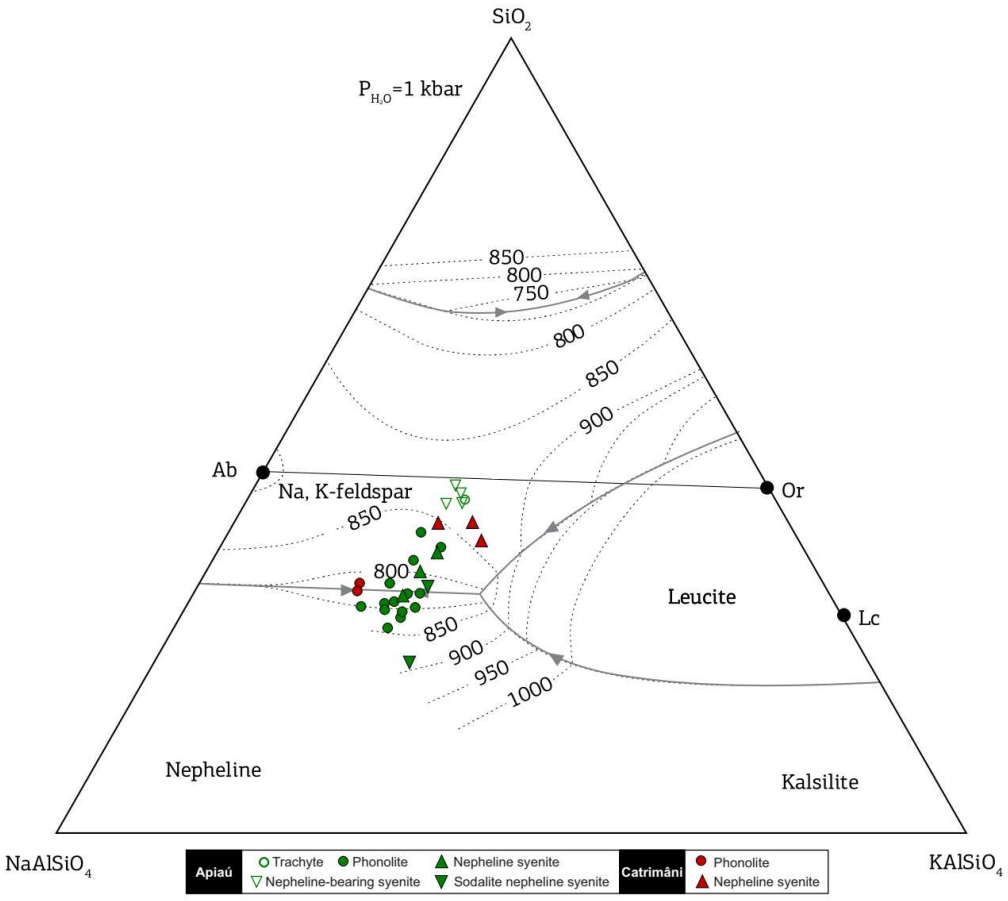

Figure 2.17: The RAP differentiated rocks plotted into the normative Qz-Ne-Ks Petrogeny's Residual System (after Hamilton and MacKenzie 1965). Phase boundaries are for P_{H20}=1 kbar. Isotherms and cotectic lines after Hall (1987).

9.3 Evidence of crustal contribution processes on RAP

The petrographic, geochemical, isotopic, and geochronological features allow us to assign that crustal assimilation process played a role in the genesis of rocks from RAP. The effect of assimilation of wall rocks is evident in petrography of most studied rocks, such as reaction rims (biotite corona), zoned clinopyroxene and spongy texture, suggesting open system conditions (Streck, 2008). Furthermore, xenocrysts and xenoliths are observed in some intrusions. Regarding the geochemical data, high values of Sr, Rb and Ba, as well the absence of Eu anomaly in some samples, may provide a clue of crustal contribution by the granitic basement.

The studied rocks exhibit significant variations in the Sr isotopic ratios, which initial $^{87}Sr/^{86}Sr$ ranges mainly from 0.7029 to 0.7069. Wide range of Sr isotopic ratios (0.7024 to 0.7057) is also described for Fortaleza alkaline rocks (Macciotta et al., 1990), in northern Brazil, which is associated with significant crustal contamination processes. In Queixada intrusion, which presents the most radiogenic signature of the entire province (paa33), we found many inherent zircon grains from 1948 Ma and 1556 Ma that correspond to augen gneiss and rapakivi granite, respectively (Fig. 2.12). In addition, this intrusion exhibits disequilibrium textures, such as zoned clinopyroxene and spongy texture. Figueiredo et al. (2018) have also described inherent zircon grains in Pupunha intrusion.

Mixing-model isotope curves were developed to evaluate the crustal assimilation hypothesis. For modelling, we considered the least radiogenic phonolite (paa22) as the most representative of the liquids, whereas augen gneiss and rapakivi granite were used as crustal contaminants. The samples are plotted along the mixing lines (Fig. 2.8), suggesting a magma mixing process between alkaline magma and the country rocks, as supported by petrographic, geochemical and geochronological data.

In addition to features cited above, the crustal contamination influences the Nd isotopic ratios, which varies from 0.51229 to 0.51248. Consequently, the interval of model ages also varies. A similar scenario is described for the wide T_{DM} intervals of Ponte Nova alkaline massif (Azzone et al., 2020) in southern Brazil, attributed to crustal contribution. The most contaminated sample of RAP (paa33) corresponds to the older T_{DM} age (825 Ma) which is an outline relative to the slight variation in model ages (548-657 Ma) for most studied rocks. This older age indicates that T_{DM} values cannot be explained only by the mantle metasomatism event. Considering the older model ages for the granitic basement (2446 and

1922 Ma) in which the alkaline rocks intrude, we assumed that crustal contamination processes played an important role in model ages for RAP.

9.4 Clues of mantle signatures of RAP

Regarding crustal contamination affecting most rocks from RAP, the discussions about mantle signature take account only the least contaminated samples. The isotopic signatures of the least radiogenic rocks suggest that two main mantle components could have been responsible for generating the alkaline magmatism, probable a mixture of depleted and enriched mantle source (Fig. 2.8B). The isotopic ratios are probably linked to HIMU and EMI mantle components. Lustrino and Wilson (2007) argue that this mixture of components could represent the sub-lithospheric mantle locally contaminated with recycled crustal lithologies. Furthermore, the studied alkaline rocks have isotope compositions similar to those of basalts from CAMP, which has been attributed to heterogeneities of mantle source and magma - upper crust interaction (Deckart et al., 2005; De Min et al., 2003), as well as alkaline rocks from northern Brazil, suggesting less radiogenic mantle sources in the Atlantic Equatorial region (Macciotta et al., 1990).

Depleted-mantle model ages (T_{DM}) of the Apiaú subprovince (571-657 Ma) is the same as the Catrimâni subprovince (548-611 Ma). The least radiogenic rocks of the entire province present short interval of model ages, between 548 to 591 Ma. The T_{DM} of alkaline and carbonatitic rocks is usually explained by metasomatic mantle events. Model ages of the Paraná - Etendeka Igneous Province and Ponta Grossa Arch have been attributed to metasomatic events in the lithospheric mantle source as precursors to the alkaline and tholeiitic magmas (Comin-Chiaramonti et al., 1999; Gomes et al., 2011).

Besides, the interval of T_{DM} obtained for RAP coincides with the least contaminated tholeiites of CAMP in French Guyana/Surinam (575-812 Ma, Deckart et al., 2005), suggesting the same metasomatic event for Mesozoic alkaline and tholeiite magmatism in Guyana Shield. The geochemical signature of CAMP basalts that occur along the margins of the Tacutu rift is interpreted as the product of an enriched sub-continental lithospheric mantle source affected by metasomatism (Pinto et al., 2017). Thus, these basalts generation are in good agreement with a passive rift model, in which the MORB-type melts became enriched through interaction with an enriched sub-continental lithospheric mantle (Dunworth, 2001; Wilson and Downes, 1991, 1992).

There was no geotectonic event earlier to rifting that could be correlated to lithospheric enrichment, since the younger event, after Mesozoic magmatism, is dated of ~1.2 Ga (K'Mudku event). Thus, the mantle metasomatism was triggered by a single event regarding the Tacutu rift and the Atlantic opening. Rifting may localize mantle degassing, which would metasomatise the subcontinental lithospheric mantle and cause partial melting (Bailey, 1987).

Table 2.10: Summary of MELTS results of fractional crystallization modelling fo M1. The start composition is found under condition of 1 kbar and with fO2 equal to the QFM buffer.

Steps	1	2	3	4	5	6	7	8	9	10	11	12	13	14	15	16	17
T °C	1141	1121	1101	1081	1061	1041	1021	1001	981	961	941	921	901	881	861	841	821
Solid fractionation f (%)	0	1.4	2.6	6.2	15	20.9	25.7	29.4	33.4	38.4	42.5	47.3	51.4	54.9	58.2	62.4	75.2
MELTS composition																	
SiO_2	45.58	45.67	45.75	46.42	47.46	48.25	49.1	49.87	50.67	51.57	52.31	53.08	53.67	54.05	54.21	53.97	50.27
TiO_2	1.69	1.72	1.74	1.54	1.15	0.88	0.68	0.53	0.42	0.35	0.29	0.25	0.22	0.19	0.17	0.16	0.17
Al_2O_3	16.77	16.99	17.21	17.64	18.65	19.45	20.21	20.85	21.13	20.96	20.78	20.46	20.18	19.92	19.68	19.51	19.83
Fe_2O_3	1.8	1.81	1.82	1.71	1.5	1.33	1.18	1.05	0.93	0.81	0.71	0.63	0.56	0.49	0.42	0.37	0.35
FeO	7.89	7.76	7.62	6.9	5.9	5.1	4.42	3.84	3.3	2.77	2.32	1.96	1.65	1.37	1.13	0.92	0.82
MnO	0.17	0.17	0.17	0.18	0.19	0.21	0.22	0.23	0.25	0.27	0.29	0.31	0.34	0.36	0.39	0.44	0.66
MgO	5.31	4.81	4.35	3.85	3.05	2.45	1.95	1.56	1.29	1.18	1.1	0.82	0.59	0.42	0.3	0.21	0.16
CaO	9.35	9.47	9.58	9.59	8.67	7.93	7.13	6.41	5.71	4.95	4.32	3.76	3.3	2.93	2.66	2.48	2.9
Na_2O	3.69	3.74	3.79	3.93	4.32	4.63	4.92	5.16	5.42	5.71	5.95	6.22	6.43	6.57	6.65	6.75	8.06
K_2O	3.27	3.31	3.36	3.48	3.84	4.13	4.39	4.62	4.89	5.28	5.64	5.99	6.36	6.74	7.15	7.54	6.86
P_2O_5	0.94	0.95	0.97	1	1.11	1.19	1.13	1.04	0.99	0.98	0.98	0.99	1.01	1.07	1.16	1.28	1.77
H_2O	3.04	3.08	3.12	3.23	3.57	3.83	4	4.13	4.25	4.35	4.45	4.56	4.67	4.77	4.87	5.02	6.12
CO_2	0.51	0.51	0.52	0.54	0.59	0.64	0.68	0.72	0.76	0.82	0.88	0.96	1.04	1.12	1.21	1.34	2.03
K_2O+Na_2O	6.96	7.05	7.15	7.41	8.16	8.76	9.31	9.78	10.31	10.99	11.59	12.21	12.79	13.31	13.8	14.29	14.92
Solid Phases (in equilibrium with each step)																	
olivine	0.04	1.34	1.25	0.85													
clinopyroxene				1.43	7.09	4.79	3.7	2.76	1.79	0.86	0.55						
apatite							0.24	0.25	0.19	0.14	0.09	0.11	0.07	0.03			0.1
spinel				1.26	1.79	1.15	0.85	0.63	0.64	0.71	0.55	0.48	0.37	0.29	0.23	0.2	0.24
feldspar									1.34	3.18	2.77	3.48	3.11	2.84	2.74	3.7	12.07
biotite												0.62	0.48	0.32	0.22	0.15	0.13
Summary of accumulated fractionated phases from anterior steps																	
olivine		0.04	1.37	2.62	3.46	3.46	3.46	3.46	3.46	3.46	3.46	3.46	3.46	3.46	3.46	3.46	3.46
clinopyroxene					1.43	8.51	13.3	17	19.75	21.54	22.4	22.95	22.95	22.95	22.95	22.95	22.95
apatite								0.23	0.48	0.66	0.79	0.88	0.98	1.05	1.08	1.08	1.08
spinel					1.25	3.04	4.19	5.04	5.67	6.31	7.01	7.56	8.04	8.4	8.69	8.91	9.11
feldspar										1.33	4.51	7.28	10.75	13.86	16.7	19.44	23.12
biotite												0.62	1.09	1.41	1.62	1.77	0.62

Table 2.11: Summary of MELTS results of fractional crystallization modelling fo M2. The start composition is found under condition of 1 kbar and with fO2 equal to the QFM+1 buffer.

Steps	1	2	3	4	5	6	7	8	9	10	11	12	13	14	15	16	17	18	19
T °C	1177	1157	1137	1117	1097	1077	1057	1037	1017	997	977	957	937	917	897	877	857	837	817
Solid fractionation f (%)	0	0.3	2.3	4.2	6.9	15	20.9	25.3	28.9	31.7	35.4	39.6	44.4	49	52.9	56.5	59.9	68.4	79.5
MELTS composition																			
SiO_2	45.54	45.68	46.57	47.37	48.09	48.94	49.61	50.2	50.88	51.48	52.15	52.84	53.57	54.18	54.6	54.81	54.81	53.38	48.88
TiO_2	1.69	1.67	1.52	1.39	1.3	1.11	0.94	0.8	0.68	0.57	0.5	0.45	0.44	0.44	0.44	0.45	0.45	0.4	0.3
Al_2O_3	16.75	16.77	16.93	17.12	17.45	18.45	19.26	19.94	20.56	21.07	21.19	21	20.65	20.33	20.04	19.77	19.54	19.51	19.89
Fe_2O_3	2.53	2.52	2.27	2.05	1.83	1.54	1.32	1.15	1	0.89	0.78	0.67	0.59	0.53	0.46	0.4	0.35	0.32	0.34
FeO	7.22	7.06	6.12	5.29	4.55	3.73	3.13	2.67	2.29	1.99	1.7	1.42	1.2	1.02	0.86	0.71	0.58	0.5	0.49
MnO	0.17	0.17	0.18	0.18	0.18	0.2	0.22	0.23	0.24	0.25	0.26	0.28	0.31	0.33	0.36	0.39	0.42	0.53	0.79
MgO	5.32	5.3	5.18	4.94	4.47	3.63	2.97	2.42	1.98	1.63	1.42	1.33	1.1	0.8	0.58	0.42	0.3	0.22	0.16
CaO	9.34	9.37	9.55	9.74	9.88	8.99	8.21	7.52	6.75	6.07	5.37	4.68	4.1	3.57	3.14	2.81	2.57	2.64	3.29
Na_2O	3.69	3.7	3.77	3.85	3.95	4.32	4.62	4.88	5.12	5.31	5.54	5.77	6.01	6.23	6.38	6.47	6.49	6.86	8.12
K_2O	3.26	3.27	3.34	3.4	3.5	3.83	4.11	4.36	4.58	4.77	5.03	5.37	5.7	6.04	6.4	6.79	7.23	7.36	6.66
P_2O_5	0.94	0.95	0.96	0.98	1.01	1.11	1.19	1.26	1.18	1.09	1.04	1.03	1.02	1.03	1.07	1.14	1.24	1.53	2.21
H_2O	3.03	3.04	3.1	3.16	3.25	3.56	3.78	3.91	4.04	4.14	4.24	4.33	4.42	4.51	4.6	4.68	4.77	5.15	6.4
CO_2	0.51	0.51	0.52	0.53	0.54	0.59	0.64	0.67	0.71	0.74	0.78	0.83	0.91	0.99	1.07	1.16	1.25	1.6	2.46
K_2O+Na_2O	6.95	6.97	7.11	7.25	7.45	8.15	8.73	9.24	9.7	10.08	10.57	11.14	11.71	12.27	12.78	13.26	13.72	14.22	14.78
Solid Phases (in equilibrium with each step)																			
olivine				0.3	0.8														
clinopyroxene					0.49	6.81	4.97	3.84	2.96	2.29	1.42	0.72	0.04						
apatite																			
spinel		0.31	1.97	1.65	1.35	1.39	0.84	0.55	0.38	0.28	0.34	0.38	0.35	0.27	0.21	0.17	0.14	0.09	0.04
feldspar											1.64	2.89	3.62	3.5	3.14	2.96	2.96	7.96	10.48
biotite													0.57	0.66	0.44	0.3	0.2	0.15	0.1
rhm-oxide																		0.11	0.14
Summary of accumulated fractionated phases from anterior steps																			
olivine					0.3	1.1	1.1	1.1	1.1	1.1	1.1	1.1	1.1	1.1	1.1	1.1	1.1	1.1	1.1
clinopyroxene						0.49	7.3	12.26	16.1	19.05	21.35	22.77	23.49	23.52	23.52	23.52	23.52	23.52	23.52
apatite										0.24	0.46	0.63	0.75	0.87	0.97	1.03	1.04	1.04	1.07
spinel			0.31	2.28	3.94	5.28	6.67	7.51	8.05	8.44	8.71	9.05	9.43	9.78	10.05	10.26	10.43	10.56	10.65
feldspar												1.64	4.53	8.15	11.65	14.78	17.73	20.69	28.64
biotite														0.57	1.22	1.66	1.95	2.15	2.3
rhm-oxide																			0.1

10. Conclusions

We have introduced the Roraima Alkaline Province - RAP in order to designate the broad region of occurrence of clusters of alkaline bodies in northern Amazonian Craton, which present petrological relationships and the ages fall within a narrow range. This province encompasses two subprovinces: Apiaú, in the north, and Catrimâni, in the southern area. The studied rocks can be classified into two groups: (i) evolved phonolite, trachyte and foid syenite found as large or small plutons and dykes, which predominate within the province; and (ii) basic alkaline magmas, such as lamprophyre, tephrite and tephriphonolite, all of them confined to scarce dykes. These rocks occur over 200 km in length, following significant faults and shear zones into a structurally complex terrane of central Guyana Shield. The U-Pb ages obtained for RAP range from ~100 to 116 Ma, indicating that alkaline magmatic activity in central Guyana Shield was a short-lived event.

The studied rocks are nepheline-normative, from metaluminous to peralkaline affinity and with mineralogy that varies from miaskitic to agpaitic. The geochemical patterns of alkaline rocks from Apiaú and Catrimâni subprovinces are very similar. They indicate that the rock-types seem to be controlled mainly by fractional crystallization, with olivine, spinel, plagioclase and apatite as early-crystallized phases and alkali feldspar as late fractionated phase. The extensive fractionation of feldspar is interpreted as a cause for the increase in peralkalinity conditions. In order to test the possible relationship between basic and felsic rocks from RAP by fractional crystallization processes, we used the MELTS thermodynamic models of fractional crystallization. The models suggest that some phonolites and syenites may be the result of 51–68% crystallization of a tephritic magma, with olivine, clinopyroxene and spinel as early-crystallized minerals, while apatite, feldspar and biotite as other fractionated phases.

The geochemical, isotopic, geochronological and petrographic features demonstrate that crustal assimilation process played a role in the genesis of rocks from RAP. In addition to significant variation in Sr-Nd isotope signature, we found inherent zircon grains from the Precambrian basement, xenoliths and disequilibrium textures, such as reaction rims, zoned clinopyroxene and spongy texture. In the mixing-model isotope curves, the samples are plotted along the mixing lines, suggesting a magma mixing process between alkaline magma and the country rocks.

The Sr-Nd isotopic signatures of the least contaminated samples suggest that two main mantle components could have been responsible for generating those rocks, probable a mixture of depleted and enriched mantle source. The studied alkaline rocks have isotope compositions similar to those of basalts from CAMP, which have been attributed to heterogeneities of mantle source and magma - crust interaction. Depleted-mantle model ages for RAP coincides with model ages for tholeiites of CAMP in Guyana Shield, suggesting the same metasomatic event for Mesozoic alkaline and tholeiite magmatism. Therefore, the lithospheric mantle metasomatism took place shortly before magmatism, and was triggered by a single event regarding to the Tacutu rift and the Atlantic opening.

References

Aarden, H.M., Holm, V., Iturralde de Arozena, J.M., Moticska, P., Navarro, J., Pasquali, Z.J., Sifontes, R.S., 1973, Aspectos geoeconomicos del Cerro Impacto: Congreso Latinoamericano de Geologia, 2nd, Caracas, Venezuela, Memoria; Ministerio de Energia y Minas, Dirección de Geologia Boletin de Geologia Publicación Especial 7, v. 5, pp. 3901-3902.

Ackerman, L., Ulrych, J., Řanda, Z., Erban, V., Hegner, E., Magna, T., Balogh, K., Frána, J., Lang, M., Novák, J. K. 2015. Geochemical characteristics and petrogenesis of phonolites and trachytic rocks from the České Středohoří Volcanic Complex, the Ohře Rift, Bohemian Massif. Lithos, 224–225(January), 256–271.

Almeida,F. F. M., 1983. Relações toctônicas das rochas alcalinas mesozoicas da região meridional da plataforma sul-americana. Revista Brasileira de Geociências 13,139-158.

Almeida, F.F.M., 1986. Distribuição regional e relações tectônicas do magmatismo pós-paleozóico no Brasil. Revista Brasileira de Geociências 16, 325-349.

Almeida, M. E., 2006. Evolução geológica da porção centro-sul do Escudo das Guianas com base no estudo Geoquímico, Geocronológico e Isotópico dos granitoides paleoproterozóicos do sudeste de Roraima, Brasil. PhD thesis, Federal University of Pará, 227 pp.

Almeida, M.E., Macambira, M.J.B., Valente, S. de C., 2008. New geological and single-zircon Pb evaporation data from the Central Guyana Domain, southeastern Roraima, Brazil: Tectonic implications for the central region of the Guyana Shield. Journal of South America Earth Science 26, 318–328.

Almeida, V. V., Janasi, V. A., Heaman, L. M., Shaulis, B. J., Hollanda, M. H. B. M., Renne, P. R. 2017. Contemporaneous alkaline and tholeiitic magmatism in the Ponta Grossa Arch, Paraná-Etendeka Magmatic Province: Constraints from U–Pb zircon/baddeleyite and 40Ar/39Ar phlogopite dating of the José Fernandes Gabbro and mafic dykes. Journal of Volcanology and Geothermal Research.

Angélica, R. S., Costa, M. L. 1993. Geochemistry of rare-earth elements in surface lateritic rocks and soils from the Maicuru complex, Para, Brazil. Journal of Geochemical Exploration, 47(1–3), 165–182.

Asimow, P.D., Ghiorso, M.S., 1998. Algorithmic modifications extending MELTS to calculate subsolidus phase relations. American Mineralogist 83, 1127–1131.

Azzone, R. G., Montecinos Munoz, P., Enrich, G. E. R., Alves, A., Ruberti, E., Gomes, C. B. 2016. Petrographic, geochemical and isotopic evidence of crustal assimilation processes in the Ponte Nova alkaline mafic-ultramafic massif, SE Brazil. Lithos, 260, 58–75.

Azzone, R. G., Chmyz, L., Guarino, V., Alves, A., Gomes, C. de B., Ruberti, E. 2020. Isotopic clues tracking the open-system evolution of the Ponte Nova mafic-ultramafic alkaline massif, SE Brazil: The contribution of Pb isotopes. Chemie Der Erde, April, 125648.

Bates, R.L., Jackson, J.A. 1987. Glossary of Geology. 3rd Edition, American Geological Institute, Alexandria, 788 p.

Baker, B.H. 1987. Outline of the petrology of the Kenya rift alkaline province. In: Fitton, J.G., Upton, B.G.J. (Eds.) Alkaline igneous rocks. Geological Society Special Publication 30, 293-311.

Barros, A.M., Alves, E.D.O., Araujo, J.F.V., Lima, M.I.C., Fernandes, C.S.C. 1977. Projeto Radam Brasil: Folha SB/SC18 Javari/Contama. DNPM, Rio de Janeiro, pp 161.

Beccaluva, L., Born, H., Brotzu, P., Coltorti, M., Conte, A.M., Garbarino, C., Gomes, C.B., Loss, E.L., Macciotta, G., Morbidelli, L., Ruberti, E., Siena, F., Traversa, G. 1992. Fractional crystallization and liquid immiscibility processes in the alkaline-carbonatite complex of Juquiá (São Paulo State, Brazil). Journal of Petrology, 33:1371-1404.

Bell, K., Simonetti, A. 1996. Carbonatite magmatism and plume activity: Implications from the Nd, Pb and Sr isotope systematics of Oldoinyo Lengai. Journal of Petrology, 37(6), 1321–1339.

Berger, J., Ennih, N., Mercier, J.-C. C., LiéGeois, J.P., Demaiffe, D. 2009. The role of fractional crystallization and late-stage peralkaline melt segregation in the mineralogical evolution of Cenozoic nephelinites/phonolites from Saghro (SE Morocco). Mineralogical Magazine, 73(1), 59–82.

Berger, J., Ennih, N., Ligeois, J. P. 2014. Extreme trace elements fractionation in Cenozoic nephelinites and phonolites from the Moroccan Anti-Atlas (Eastern Saghro). Lithos, 210, 69–88.

Borges, F.R., 1990. Projeto Serra do Repartimento. Technical report, CPRM, 30 pp.

Brandão, R.L., Freitas, A.F.F., 1994. Serra do Ajarani: Folha NA.20-X- C- VI. Technical report, CPRM, 153 pp.

Brooks, E.W., Orris, G.J., Wynn, J.C. 1983. Deposits formed in supracrustal rocks and epizonal plutons: carbonatite deposits. In: Wynn, J.C., Gray, F., Page, N.J. (Eds), Geology and mineral resource assessment of the Venezuelan Guayana Shield, USGS, pp.73-74.

Brotzu, P., Barbieri, M., Beccaluva, L., Garbarino, C., Gomes, C.B., Macciotta, G., Melluso, L., Morbidelli, L., Ruberti, E., Sígolo, J.B. 1992. Petrology and geochemistry of the Passa Quatro alkaline complex, MG-RJ-SP, Brazil. Journal of South American Earth Sciences, 6:237-252.

Comin-Chiaramonti, P. et al. 1999. Early Cretaceous-Tertiary Magmatism in Eastern Paraguay (Western Parana Basin): Geological, Geophysical and Geochemical Relationships. Journal of Geodynamics 28(4–5): 375–91.

Comin-Chiaramonti, P., Gomes, C.B., Velázquez, V.F., Censi, P., Antonini, P., Comin-Chiaramonti, F., Punturo., R. 2005. Alkaline complexes from southeastern Bolivia. In: Comin-Chiaramonti, P., Gomes, C.B. (Eds.), Mesozoic to Cenozoic Alkaline Magmatism in the Brazilian Platform. Edusp/Fapesp, São Paulo, pp. 159 - 212.

Comin-Chiaramonti, P., De Min, A., Girardi, V.A.V., Ruberti, E., 2011. Post-Paleozoic magmatism in Angola and Namibia: a review. Geological Society of America (GSA) Special Paper 478, 223–247.

Cordani, U.G., Fraga, L.M., Tassinari, C.C.G., Brito-Neves, B.B., 2010. On the origin and tectonic significance of the intra-plate events of Grenvillian-type age in South America: A discussion. Journal of South American Earth Science 29, 143-159.

Corfu, F., Polteau, S., Planke, S., Faleide, J. I., Svensen, H., Zayoncheck, A., Stolbov, N. 2013. U-Pb geochronology of cretaceous magmatism on svalbard and franz josef land, barents sea large igneous province. Geological Magazine, 150(6), 1127–1135.

Costa, J.B.S., Pinheiro, R.V.L., Reis, N.J., Pessoa, M.R., Pinheiro, S.S., 1991. O hemigraben do Tacutu: uma estrutura controlada pela geometria do Cinturão de Cisalhamento Guiana Central. Geociências 10, 119-130.

Costa, M. L., Fonseca, L. R., Angélica, R. S., Lemos, V. P., Lemos, R. L. 1991. Geochemical exploration of the Maicuru alkaline-ultramafic-carbonatite complex, northern Brazil. Journal of Geochemical Exploration, 40(1–3), 193–204.

Costa, S.S., 2005. Delimitação do arcabouço tectônico do Cinturão Guiana Central, estado de Roraima, com base na análise integrada dos dados geofísicos, geológicos, isotópicos e imagens de satélite. PhD thesis, University of Campinas, 189 pp.

Cotta, A.J.B., Enzweiler, J., 2011. Classical and new procedures of whole rock dissolution for Trace Element determination by ICP-MS. Geostandards and Geoanalytical Research, 1-24.

Deckart, K., Bertrand, H., Liégeois, J. P. 2005. Geochemistry and Sr, Nd, Pb isotopic composition of the Central Atlantic Magmatic Province (CAMP) in Guyana and Guinea. Lithos, 82(3-4 SPEC. ISS.), 289–314.

Downes, Hilary et al. 2005. "Petrogenetic Processes in the Ultramafic, Alkaline and Carbonatitic Magmatism in the Kola Alkaline Province: A Review." Lithos 85(1-4 SPEC. ISS.): 48–75.

Dunworth, E. A. 2001. "The Turiy Massif, Kola Peninsula, Russia: Isotopic and Geochemical Evidence for Multi-Source Evolution." Journal of Petrology 42(2): 377–405.

Eiras, J.F., Kinoshita, E.M., 1988. Evidências de movimentos transcorrentes na Bacia do Tacutu. Boletim de Geociências da Petrobras 2, 193-208.

Eiras, J.F., Kinoshita E.M., 1990. Geologia e perspectivas petrolíferas da Bacia do Tacutu. In: Gabaglia, G.P.R, Milani, E.J (Eds), Origem e Evolução de Bacias Sedimentares. Petrobras, Rio de Janeiro, pp 197-220.

Elburg, M. A., Cawthorn, R. G. 2017. Source and evolution of the alkaline Pilanesberg Complex, South Africa. Chemical Geology, 455, 148–165.

Figueiredo, R.F., 2016. Contexto tectônico do Complexo Alcalino Apiaú– Roraima: Aerogeofísica, petrologia e geocronologia U-Pb. M.S. thesis, University of Campinas, 102 pp.

Figueiredo, R. F. de, Santos, T. J. S. dos, Tonetto, E. M. 2018. Petrology, geochemistry and U-Pb zircon and baddeleyite ages of the alkaline rocks from the central-southern Guyana Shield, northern Amazonian Craton. Journal of South American Earth Sciences, 86, 461–474.

Fitton, J.G., Upton, B.G.J., 1987.Alkaline igneous rocks. Geological Society of London, London, 568 pp.

Fletcher, C.J.N., Beddoe-Stephens, B. 1987. The petrology, chemistry and crystallization history of the Velasco alkaline province, eastern Bolivia. In: Fitton, J.G., Upton, B.G.J. (Eds.) Alkaline igneous rocks. Geological Society Special Publication 30, 403-413.

Fraga, L.M.B., Almeida, M.E., Macambira, M.J.B., 1997. First lead-lead zircon ages of charnockitic rocks from Central Guiana Belt (CGB) in the state of Roraima, Brazil, in: South American Symposium on Isotope Geology, Campos do Jordão, SP, 115-117.

Fraga, L.M.B., 2002. A associação anortosito-mangerito-granito rapakivi (AMG) do Cinturão Guiana Central, Roraima, e suas encaixantes paleoproterozóicas: evolução estrutural, geocronologia e petrologia. PhD thesis, Federal University of Pará, 351 pp.

Fraga, L.M., Dall'Agnol, R., Costa, J.B.S., Macambira, M.J.B., 2009. The Mesoproterozoic Mucajaí anorthosite-mangerite-rapakivi granite complex, Amazonian Craton, Brazil. The Canadian Mineralogist 47, 1469-1492.

Gaudette, H. E., Olszewski Jr., W. J., Santos, J.O.S., 1996. Geochronology of Precambrian rocks from the northern part of Guiana Shield, State of Roraima, Brazil. Journal of South American Earth Sciences 9, 183- 195.

Guarino, V., Wu, F. Y., Lustrino, M., Melluso, L., Brotzu, P., Gomes, C. de B., Svisero, D. P. 2013. U-Pb ages, Sr-Nd- isotope geochemistry, and petrogenesis of kimberlites, kamafugites and phlogopite-picrites of the Alto Paranaíba Igneous Province, Brazil. Chemical Geology, 353, 65–82.

Gibson, S.A., Thompson, R.N., Leonardos, O.H., Dickin, A.P., Mitchell, J.G., 1995. The Late Cretaceous impact of the Trindade mantle plume: Evidence from large-volume, mafc potassic magmatism in SE Brazil. Journal of Petrology 36, 189-229.

Gibson, S.A., Thompson, R.N., Leonardos, O.H., Dickin, A.P., Mitchell, J.G., 1999. The limited extent of plume-lithosphere interactions during continental flood-basalt genesis: Geochemical evidence from Cretaceous magmatism in southern Brazil. Contributions to Mineralogy and Petrology 137, 147-169.

Gibson, S. A., R. N. Thompson, and J. A. Day. 2006. "Timescales and Mechanisms of Plume-Lithosphere Interactions: 40Ar/39Ar Geochronology and Geochemistry of Alkaline Igneous Rocks from the Paraná-Etendeka Large Igneous Province." Earth and Planetary Science Letters 251(1–2): 1–17.

Ghiorso, M.S., Sack, R.O., 1995. Chemical mass transfer in magmatic processes. IV. A revised and internally consistent thermodynamic model for the interpolation and extrapolation of liquid–solid equilibria in magmatic systems at elevated temperatures and pressures. Contributions to Mineralogy and Petrology 119, 197–212.

Gillespie, M.R., Stephenson, D., Millward, D. 2008. BGS classification of lithodemic unit: Proposals for classifying units of intrusive rocks. *British Geological Survey Research Report RR/08/05*.

Gomes, C.B., Ruberti, E., Morbidelli, L., 1990. Carbonatite complexes from Brazil: A review. Journal of South American Earth Sciences 3, 51-63.

Gomes, C. B., E. Ruberti, P. Comin-Chiaramonti, and R. G. Azzone. 2011. "Alkaline Magmatism in the Ponta Grossa Arch, SE Brazil: A Review." Journal of South American Earth Sciences 32(2): 152–68.

Gomes, C.B., Comin-Chiaramonti, P., 2005. An introduction to the alkaline and alkaline-carbonatitic magmatism in and around the Paraná Basin. In: Comin-Chiaramonti, P., Gomes, C.B. (Eds.), Mesozoic to Cenozoic Alkaline Magmatism in the Brazilian Platform. Edusp/Fapesp, São Paulo, pp. 21-29.

Hall, A. 1987. Igneous petrology. Longman Scientific Technical, 573 p.

Hamilton, D.L., MacKenzie, W.S. 1965. Phase equilibrium studies in the system NaAlSiO4 (nepheline)-KAlSiO4 (kalsilite)-SiO2-H2O. Mineralogical Magazine, 34:214-231.

Heaman, L.M., LeCheminant, A.N., 1993. Paragenesis and U-Pb systematics of baddeleyite (ZrO2). Chemical Geology 110, 95–126.

Heaman, L.M., 2009. The application of U–Pb geochronology to mafic, ultramafic and alkaline rocks: an evaluation of three mineral standards. Chemical Geology 261, 43–52.

Heinonen, A.P., Fraga, L.M., Rämö, O.T., Dall'Agnol, R., Mänttäri, I., Andersen, T., 2012. Petrogenesis of the igneous Mucajaí AMG complex, northern Amazonian craton - Geochemical, U-Pb geochronological, and Nd-Hf-O isotopic constraints. Lithos 151, 17–34.

Issler, R. S., 1974. Projeto Radam Brasil: Folha SA.22- Belém. DNPM, Rio de Janeiro, 503 pp.

Issler, R.S., Lima, R.M.G., Montalvao, G.G. 1975. Magmatismo alcalino no craton Guianense, in: Anais Décima Conferência Geológica Interguianas, Belém, Brazil, pp 103–122.

Issler, R.S., Silva, G.G., 1980. The Seis Lagos carbonatite complex. In: Congresso Brasileiro de Geologia 31, Camboriu, vol. 3, pp. 1564-1572.

Iwanuch, W. 1976. Idades Rb-Sr das alcalinas do "Domo do Sucunduri", AM. In: Congresso Brasileiro de Geologia XXIX, anais, p. 196.

Iwanuch, W. 1981. Geologia da região do domo do Sucunduri. Master thesis, University of São Paulo, pp 151.

Justo, L.J.E.C., Souza, M.M., 1986. Jazida de Niobio do Morro dos Seis Lagos, Amazonas. In: Schobbenhaus, C., Coelho, C.E.S. (Eds.), Principais Depositos Minerais do Brasil. Departamento Nacional de Produção Mineral, Brasília, pp. 463-468.

Kogarko, L.N. 1987. Alkaline rocks of the eastern part of the Baltic Shield (Kola Peninsula). In: Fitton, J.G., Upton, B.G.J. (Eds.) Alkaline igneous rocks. Geological Society Special Publication 30, 293-311.

Kramm, U., Kogarko, L. N. 1994. Nd and Sr isotope signatures of the Khibina and Lovozero agpaitic centres, Kola Alkaline province, Russia. Lithos, 32(3–4), 225–242.

Kroonenberg, S. B., De Roever, E. W. F., Fraga, L. M., Reis, N. J., Faraco, T., Lafon, J. M., Wong, T. E. 2016. Paleoproterozoic evolution of the Guiana Shield in Suriname: A revised model. Geologie En Mijnbouw/Netherlands Journal of Geosciences, 95(4), 491–522.

Lamotte, F. D., Fourdan, B., Leleu, S., Leparmentier, F., and De Clarens, P. 2015. Style of rifting and the stages of Pangea breakup. Tectonics, 34(5), 1009–1029.

Leal, A.B.M., Girardi, V.A.V., Leal, L.R.B., 2000. Petrologia e geoquímica do magmatismo básico mesozoico da Suíte Básica Apoteri, estado de Roraima. Geochimica Brasiliensis 14, 155-174.

Leal, J.W.L., Silva, G.H., Santos, D.B., Teixeira, W., Fernandes, C.A.C., Pinto, A.C. 1978. Projeto Radam Brasil: Folha SC.20 Porto Velho. DNPM, Rio de Janeiro, 403 pp.

Legendre, C., Maury, R.C., Caroff, M., Guillou, H., Cotton, J., Chauvel, C., Bollinger, C., Hémond, C., Guille, G., Blais, S., Rossi, P., Savanier, D. 2005. Origin of exceptionally abundant phonolites on Ua Pou Island (Marquesas, French Polynesia): partial melting of basanites followed by crustal contamination. Journal of Petrology, 46:1925-1962.

Lemos, V. P., Costa, M. L., 1987. Partição das terras raras nos lateritos fosfáticos de Maicuru, PA. Anais, Congresso Brasileiro de Geoquímica, Porto Alegre 1, 83-102.

Le Maitre, R. W., 2002. Igneous Rocks: A classification and glossary of terms. Cambridge University Press, New York, 236 pp.

Litherland, M., Annels, R.N., Appleton, J.D., Berrange, J.P., Bloomfield, K., Burton, C.C., Darbyshire, D.P.F., Fletcher, C.J.N., Hawkins, M.P., Klink, B.A., Llanos, A., Mitchell, W.I., O'Connor, E.A., Pitfield, P.E., Power, G.,Webb, B.C. 1986. The geology and mineral resources of the Bolivian Precambrian Shield. Keyworth Overseas Memoir 9, British Geological Survey, 153p.

Ludwig, K.R. 1991. ISOPLOT; a plotting and regression program for radiogenic-isotope data; version 2.53. USGS Open-File Report 91-445.

Lustrino, M., Wilson, M. 2007. "The Circum-Mediterranean Anorogenic Cenozoic Igneous Province." Earth-Science Reviews 81(1–2): 1–65.

Macciotta, G., Almeida, A., Barbieri, M., Beccaluva, L., Brotzu, P., Coltorti, M., Conte, A., Garbarino, C., Gomes, C. B., Morbidelli, L., Ruberti, E., Siena, F., & Traversa, G. 1990. Petrology of the tephrite-phonolite suite and cognate xenoliths of the Fortaleza district (Ceará, Brazil). European Journal of Mineralogy, 2(5), 687–710.

Markl, G., Marks, M.W., Schwinn, G., Sommer, H., 2001. Phase equilibrium constraints on intensive crystallization parameters of the Ilímaussaq Complex, South Greenland. Journal of Petrology 42, 2231–2257.

Marks, M. A. W., Hettmann, K., Schilling, J., Frost, B. R., Markl, G., 2011. The mineralogical diversity of alkaline igneous rocks: Critical factors for the transition from miaskitic to agpaitic phase assemblages. Journal of Petrology 52, 439–455.

Marks, M. A. W., Markl, G. 2017. A global review on agpaitic rocks. Earth-Science Reviews, 173(July), 229–258.

Marsh, J. S. 2010. The geochemistry and evolution of Palaeogene phonolites, central Namibia. Lithos, 117(1–4), 149–160.

Marzoli A., Renne P.R., Piccirillo E.M., Ernesto M., Bellieni G., De Min A. 1999. Extensive 200-Million-Year-Old Continental Flood Basalts of the Central Atlantic Magmatic Province. Science 284, 616–618.

Matton, G. and Jébrak, M. 2009. The Cretaceous Peri-Atlantic Alkaline Pulse (PAAP): Deep mantle plume origin or shallow lithospheric break-up? Tectonophysics, 469(1–4), 1–12.

McDonough, W.F., Sun, S., 1995. The composition of the Earth. Chemical Geology 120, 223-253.

Middlemost, E.A.K., 1975. The basalt clan. Earth Science Reviews 11, 337-364.

Montalvão, R. M.G., Muniz, M. C., Issler R. S., Dall'Agnol R., Lima M. I. C., Fernandes P. E. C. A, Silva G. G. 1975. Projeto Radam Brasil 8v: Folha NA.20- Boa Vista e parte das folhas NA.21 - Tumucumaque, NB.20 – Roraima e NB.21. DNPM, Rio de Janeiro, 403 pp.

Morbidelli, L., Gomes, C.B., Beccaluva, L., Brotzu, P., Conte, A.M., Ruberti, E., Traversa, G., 1995. Mineralogical, petrological and geochemical aspects of alkaline and alkaline carbonatite associations from Brazil. Earth Sciences Review 39, 135-168.

Navarro, M.S., Tonetto, E.M., Oliveira, E.P., 2015. LA-SF-ICP-MS U-Pb zircon dating at University of Campinas, Brazi. In: IAG, Geoanalysis 2015. Leoben, CD-ROM.

Oliveira, A.S., Fernandes, C.A.C., Issler, R.S., Abreu, A.S., Montalvão., R.M.G., Teixeira, W. 1975. Projeto Radam Brasil: Folha NA.21- Tumucumaque e parte da folha NB.21. DNPM, Rio de Janeiro, pp 361.

Peate, D.W. 1997. The Paraná-Etendeka Province. In: Mahoney, J.J. & Coffin, M.F. (eds.) Large igneous provinces: continental, oceanic and planetary flood volcanism. Geophysical Monograph, AGU 100, 217-246.

Petronilho L.A. 2009. Método Sm-Nd no CPGeo-IGc-USP: procedimentos analíticos atualmente em rotina. In: Simpósio 45 anos de Geocronologia no Brasil, Boletim de Resumos Expandidos, 116-118.

Pinto, V. M., Santos, J. O. S., Ronchi, L. H., Hartmann, L. A., Bicudo, C. A., de Souza, V. 2017. Field and geochemical constraints on the relationship between the Apoteri basalts (northern Brazil, southwestern Guyana) and the Central Atlantic Magmatic Province. Journal of South American Earth Sciences, 79, 384–393 https://doi.org/10.1016/j.jsames.2017.08.015.

Pirajno, F., 2015. Intracontinental anorogenic alkaline magmatism and carbonatites, associated mineral systems and the mantle plume connection. Gondwana Research 27, 1181–1216.

Premoli, C., Kroonenberg, S. B. 1984. Radioactive Mineral Potential of Carbonatites in Western Parts of the South American Shields. Geology and Metallogenesis of Uranium Deposits in South America: Proceedings of Working Group Meeting, San Luis, Argentina, pp 245-268.

Reis, N. J., Fraga, L.M., Faria, M.S.G., Almeida, M. E., 2003. A geologia de Roraima. Géologie de la France 2-3-4, 121-134.

Reis N.J., Faria M.S.G., Almeida M.E., Oliveira M.A. 2004. Folhas NA.20-Boa Vista e NB.20-Roraima. In: Schobbenhaus, C., Gonçalves, J.H., Santos, J.O.S., Abram, M.B., Leão Neto, R., Matos, G.M.M., Vidotti, R.M., Ramos, M.A.B., Jesus, J.D.A.de. (Eds.) Carta Geológica do Brasil ao Milionésimo, Sistema de Informações Geográficas-SIG, Programa Geologia do Brasil. CPRM, Brasília, CD-ROM.

Reis, N.J, Szatmari, P, Wanderley Filho, J.R, York, D, Evensen, N.M, Smith, P.E., 2006. Dois eventos de magmatismo máfico mesozóico na fronteira Brasil-Guiana, Escudo das Guianas: enfoque à região do rifte Tacutu-North Savannas, in: 43º Congresso Brasileiro de Geologia, Aracaju, 459–46.

Riccomini, C., Velázquez, V.F., Gomes, C.B., 2005. Tectonic controls of the Mesozoic and Cenozoic alkaline magmatism in Central-Southeastern Brazilian Platform. In: Comin-Chiaramonti, P., Gomes, C.B. (Eds.), Mesozoic to Cenozoic Alkaline Magmatism in the Brazilian Platform. Edusp/Fapesp, São Paulo, pp. 31 - 55.

Rock, N. M.S. 1981. “How Should Igneous Rocks Be Grouped?” Geological Magazine 118(5): 449–61.

Rooney, T. O. 2017. The Cenozoic magmatism of East-Africa: Part I — Flood basalts and pulsed magmatism. Lithos, 286–287, 264–301.

Rossoni, M. B., Bastos Neto, A. C., Souza, V. S., Marques, J. C., Dantas, E., Botelho, N. F., Pereira, V. P. 2017. U-Pb zircon geochronologycal investigation on the Morro dos Seis Lagos Carbonatite Complex and associated Nb deposit (Amazonas, Brazil). Journal of South American Earth Sciences, 80, 1–17.

Salas, N. J., Santos, J. O. S., 1974. Determinações geocronológicas pelo método da birrefringência em phonolite na área do Projeto Norte da Amazônia, in: 28º Congresso Brasileiro de Geologia, Porto Alegre, 221-224.

Santos, J. O. S., Hartmann, L. A., Gaudette, H. E., Groves, D. I., Mcnaughton, N. J., Fletcher, I. R., 2000. A new understanding of the Provinces of the Amazon Craton based on integration of field mapping and U-Pb and Sm-Nd Geochronology. Gondwana Research 3, 453-488.

Santos, J.O.S., Hartmann, L.A., Faria, M.S.G., Riker, S.R.L., Souza, M.M., Almeida, M.E., McNaughton, N.J., 2006a. A compartimentação do Cráton Amazonas em Províncias: Avanços ocorridos no período 2000-2006, in: 9º Simpósio de Geologia da Amazônia, Belém, CD-ROM.

Santos, J.O.S., Faria, M.S.G., Riker, S.R., Souza, M.M., Hartmann, L.A., Almeida, M.E., McNaughton, N.J., Fletcher, I.R., 2006b. A faixa colisional K'Mudku (idade Greenvilliana) no norte do Cráton Amazonas: reflexo intracontinental do orógeno Sunsás na margem ocidental do Cráton, in: 9º Simpósio de Geologia da Amazônia, Belém, CD-ROM.

Shand, S. J., 1943. Eruptive rocks: Their genesis, composition, classification, and their relation to ore-deposits with a chapter on Meteorite. John Wiley & Sons, New York, 488 pp.

Silva, H.G., Leal, J.W.L., Salum, O.A.L., Dall'Agnol, R., Basei, M.A.S. 1974. Esboço Geológico de parte da Folha SC21 Juruena. In: XXVIII Congresso Brasileiro de Geologia, v.4, pp 309-320.

Soares, M.A., 1985, Estudio petrografico de la estructura alcalina La Churuata, Territorio Federal Amazonas: Congreso Geologico Venezolano, 6th, Caracas, Memoria, v. 4, pp. 2117-2158.

Söderlund, U., Johansson, L., 2002. A simple way to extract baddeleyite (ZrO2). Geochemistry, Geophysics and Geosystems 3, 1-7.

Souza S.L. 2009. Métodos radiométricos Rb-Sr e Sm-Nd no CPGeoIGc-USP. In: Simpósio 45 anos de Geocronologia no Brasil, Boletim de Resumos Expandidos, 137-139.

Souza, V. D. S., Souza, A. G. H., Dantas, E. L., Valério, C. D. S., 2015. K'Mudku A-type magmatism in the southernmost Guyana shield, central-north Amazon Craton (Brazil): The case of Pedra do Gavião syenogranite. Brazilian Journal of Geology 45, 293–306.

Streck, M.J., 2008. Mineral textures and zoning as evidence for open system processes. Reviews in Mineralogy and Geochemistry 69, 595–622

Tassinari, C.C.G. 1996. O mapa geocronológico do Cráton Amazônico no Brasil: revisão dos dados isotópicos. Habilitation thesis, University of São Paulo, 139 pp.

Tassinari, C. C. G., Macambira, M. J. B., 1999. Geochronological Provinces of the Amazonian Craton. Episodes 22, 174-182.

Tassinari, C. C. G.; Bettencourt, J. S.; Geraldes,M. C.; Macambira, M. J. B.; Lafon, J. M. 2000. The Amazonian cráton. In: Cordani, U. G.; Milani,E. J.; Thomaz Filho, A.; Campos, D. A. (Eds.)Tectonic evolution of South America. Rio de Janei-ro, s.n. p. 41-95.

Tassinari, C.C.G., Macambira M.J.B., 2004. A evolução tectônica do Cráton Amazônico. In: Neto, V. M.; Bartorelli, A.; Carneiro, C.D.R.; Neves, B.B.B. (Eds.), Geologia do Continente Sul-Americano: Evolução da obra de Fernando Flávio Marques de Almeida. Beca, São Paulo, 471-485.

Teixeira, W., 1978. Significação tectônica do magmatismo anorogênico básico e alcalino na região amazônica. M.S thesis, University of São Paulo, 99 p.

Teixeira, W., Tassinari, C.C.G., Cordani, U.G., Kawashita, K. 1989. "A Review of the Geochronology of the Amazonian Craton: Tectonic Implications." Precambrian Research 42(3–4): 213–27.

Torsvik, Trond H., Mark A. Smethurst, Kevin Burke, and Bernhard Steinberger. 2008. "Long Term Stability in Deep Mantle Structure: Evidence from the ~ 300 Ma Skagerrak-Centered Large Igneous Province (the SCLIP)." Earth and Planetary Science Letters 267(3–4): 444–52.

Ulbrich, H.H.G.J, Gomes, C.B., 1981. Alkaline rocks from continental Brazil. Earth-Science Reviews 17, 135–154.

Souza, V. D. S., De Souza, A. G. H., Dantas, E. L., Valério, C. D. S. 2015. K'Mudku A-type magmatism in the southernmost Guyana shield, central-north Amazon Craton (Brazil): The case of Pedra do Gavião syenogranite. Brazilian Journal of Geology, 45(2), 293–306.

Svensen, H., Corfu, F., Polteau, S., Hammer, Ø., Planke, S. 2012. Rapid magma emplacement in the Karoo Large Igneous Province. Earth and Planetary Science Letters, 325–326, 1–9.

Thompson, G.M., Smith, I.E.M., Maipas, J.G. 2001. Origin of oceanic phonolites by crystal fractionation and the problem of the Daly gap: an example from Rarotonga. Contributions to Mineralogy and Petrology, 142:336-346.

Vaz, P.T., Wanderley Filho, J.R., Bueno, G.V. 2007. Bacia do Tacutu. Boletim de Geociências da Petrobras 15, 289–297.

Vendemiatto, M.A., Enzweiler, J., 2001. Routine control of accuracy in silicate rock analysis by X-Ray Fluorescence Spectrometry. Geostandards and Geoanalytical Research. 25, 283-291.

Wilson, M., and Downes, H. 1991. "Tertiary - Quaternary Extension-Related Alkaline Magmatism in Western and Central Europe." Journal of Petrology 32(4): 811–49.

Wilson, Marjorie, and Hilary Downes. 1992. "Mafic Alkaline Magmatism Associated with the European Cenozoic Rift System." Tectonophysics 208(1–3): 173–82.

Wohlgemuth-Ueberwasser, C.C., Söderlund, U., Pease, V., Nilsson, M.K.M., 2015. Quadrupole LA-ICP-MS U/Pb geochronology of baddeleyite single crystals. Journal of Analytical Atomic Spectrometry 30, 1191-1196.

Woolley, A.R. 1987. Alkaline rocks and carbonatites of the World. Part I: North and South America. London: British Museum (Natural History), 216p.

CAPÍTULO 3 - GEOPHYSICAL SIGNATURE OF THE RORAIMA ALKALINE PROVINCE, CENTRAL-SOUTHERN OF GUYANA SHIELD

Abstract

The Roraima Alkaline Province (RAP) is rift-related magmatism emplaced in the central-southern Guyana Shield that associates with reactivation of Precambrian structural zones during Mesozoic rifting. Most area of the province have very limited access owing to the dense rainforest and Cenozoic sedimentary covering. We analysed airborne radiometric and magnetometric data covering seven foid and foid-bearing syenites from RAP. Alkaline dykes are also associated with those rocks, but they are too narrow to be representative in the airborne data. The rocks are represented by high concentrations of eU, eTh and K contents about their host. Moreover, gamma-ray spectrometry data allowed us to delineate favourable areas of unknown alkaline bodies occur. The studied rocks exhibit mostly low to intermediate amplitude in the Analytic Signal Amplitude (ASA) image. Nevertheless, the high values probably reflect the presence of magnetized structures in where the alkaline rocks are emplaced or pre-existing highly magnetized rocks such as Precambrian gabbros. The major deformational events in the central Guyana Shield, such as Paleoproterozoic Cauarane-Coeroeni Belt, Mesoproterozoic K'Mudku and Mesozoic reactivation, provides a framework from which we can derive the magnetic framework of the area and insights over its structures, as well as understand their relationships with the alkaline magmatism. Alkaline magmatism often associates with reactivations of Paleo and Mesoproterozoic NE and NW-trending structures and, subsequently, E-W strike-slip faults during early rifting stage in the Equatorial Atlantic Ocean. Thus, interpretations of gamma-ray spectrometry and magnetic data constrained by field observations proved to be efficient in prospecting alkaline rocks and deciphering the regional structures in remote regions and areas of the limited outcrop.

Keywords: alkaline rocks; gamma-ray spectrometry; magnetometry; Tacutu rift; Guyana Shield.

1. Introduction

The geological setting of alkaline provinces shows that their location is controlled by structural weaknesses in the lithosphere, particularly in rift setting (Black et al., 1985; Fitton et al., 1986). According to Pirajno (2015), lower rates of rift extension in intra-continental setting, results in lower degrees of partial melting and more alkalic and silica-undersaturated magmas. Matton and Jébrak (2009) propose that the periodic reactivation of deep-seated pre-existing zones of structural weakness during the Atlantic Ocean tectonic evolution, combined with coeval asthenospheric upwelling, enhanced the ascent of alkaline magmas. The control of deep lithospheric structure on magma emplacement is not confined to large-scale structures but extends to the smaller ones (Begg et al. 2009).

In South American Platform, most alkaline–carbonatite provinces occur along with fault zones and flexural arcs areas around the Phanerozoic Paraná, Parnaíba and Amazonas basins over Precambrian basement (Almeida, 1983; Almeida, 1986). Riccomini et al. (2005) highlight that changes in the stress fields and reactivations of regional structures have generated a wide range of structural discontinuities along which alkaline magmas are emplaced. The relationship between the pre-exist structures framework and the Meso-Cenozoic alkaline magmatism in Brazilian Platform have been investigated by airborne geophysics (Dutra et al., 2012; Maragoni and Mantovani, 2013; Rocha et al., 2014). Likewise, alkaline bodies, without outcropping evidence, were proposed by using airborne magnetic data (Louro et al., 2019).

Geophysical methods are prospective tools for detecting the location of alkaline rocks and the structural context that controls their emplacement, particularly in remote regions and areas of the limited outcrop. Airborne gamma-ray data have been used to identify nepheline syenites suitable as possible sources for K-fertiliser in Malawi (Chiwona et al., 2020). Moreover, aeromagnetometry has been applied to recognize regional structures in sedimentary basins (Pinto and Vidotti, 2019), orogens (Spampinato et al., 2015; Kwayisi et al., 2020) and modern rift system (Katumwehe et al., 2015). Faults and shear zones can be recognised from aeromagnetic data by displacement or dislocation of magnetic features, juxtaposed domains with different magnetic character, or by a magnetic signature where the structure has undergone magnetite production or depletion as a result of igneous and metamorphic processes or fluid flow (Isles and Rankin, 2003).

The Roraima Alkaline Province (RAP) is rift-related magmatism associated with the reactivation of Precambrian faults and shear zones from Amazonian Craton during the

Equatorial Atlantic opening (Figueiredo et al., 2018). The RAP encompasses silica-undersaturated rocks of wide range compositions, mostly felsic types, with ages ranging from 100 to 116 Ma (Salas and Santos, 1974; Montalvão et al., 1975; Borges, 1990; Brandão and Freitas, 1994; Figueiredo et al. 2018), being the only Cretaceous alkaline magmatism in the Guyana Shield. The province is divided into two subprovinces: Apiaú, in the north, and Catrimâni, in the south. Most area of RAP is covered by dense rainforest and Cenozoic sediments, where geological mapping is very regional owing to limited access.

In this context, airborne geophysical data have become an indispensable tool for mapping alkaline rocks from the RAP and to investigate the spatial and timing relationships between tectonic and magmatic processes during Cretaceous. In this paper, we analysed the available regional aerogeophysical data to characterize the structural context and relevant features associated to foid and foid-bearing syenites from the RAP and to understand their tectonic context. Particularly we document the association of the syenites with structural features. More widely, we intend to demonstrate that airborne geophysical gamma-ray data coupled with regional geophysical-geological interpretation can be used to identify and map alkaline rocks in Guyana Shield within a structural context derived from indirect geophysical observation and limited surface information.

2. Geological setting

The Guyana Shield represents the northernmost part of the Amazonian Craton and is separated from the southern Central Brazil Shield or Guaporé Shield (Almeida, 1976) by the Phanerozoic Amazonas and Solimões basins. The Guyana Shield is situated in the northern part of the craton and covers Brazil, Colombia, Venezuela, Guyana, Suriname, and French Guyana. Cretaceous alkaline rocks from Roraima Alkaline Province (RAP, Figueiredo et al. in prep) exist in the central-southern part of Guyana Shield. The province is divided into two subprovinces: Apiaú, in the north, and Catrimâni, in the south (Figure 3.1B). Such rocks encompass monzonite, syenite, nepheline-bearing syenite and nepheline syenite plutons, plus nephelinite, lamprophyre tephrite, tephriphonolite, trachytes and phonolites dykes and its southern part is extensively covered by the Cenozoic sediments (Salas and Santos, 1974; Montalvão et al., 1975; Borges, 1990; Brandão and Freitas, 1994; Reis et al., 2004; Figueiredo, 2016; Figueiredo et al. 2018). The RAP presents U-Pb zircon and baddeleyite ages from 111-116 Ma (Figueiredo et al., 2018) and Rb-Sr age of 100 Ma (Montalvão et al., 1975).

The RAP occurs along with fault and shear zones forming a complex framewotk of Guyana Shield. The main Paleoproterozoic tectonic feature of the central part of the shield corresponds to the Cauarane–Coeroni Belt, associated with the Transamazonian Orogeny, in which is given by a sinuous NW–SE/NE–SW structures (Fig. 3.1), including amphibolite to granulite facies supracrustal rocks (Kroonemberg, 1976; Delor et al., 2003; Fraga et al., 2009). Immediately to the south of the Cauarane-Coeroeni Belt, Orosirian granitoids (1.96-1.91 Ga) and gneisses with A-type and high-K calc-alkaline affinities metamorphosed at 1.91 Ga are predominant (Gaudette et al., 1996; Fraga, 2002; Reis et al., 2003; Costa, 2005; Fraga et al., 2009). Charnockites and granulite lens also crop out at south, recording emplacement and crystallization/ recrystallization at deeper crustal levels (Fraga et al. 2009). Also at the south of Cauarane-Coeroeni belt, an anorthosite/gabbro-mangerite-granite rapakivi association dating ca. 1.5 Ga is described (Gaudette et al., 1996; Fraga, 2002; Reis et al., 2003; Fraga et al., 2009; Heinonen et al., 2012).

The evolution of the Cauarane-Coeroeni Belt is poorly understood. One line of thought suggests that it formed during the closing of orogenic basins ca. 2.00 Ga, during the collision of 2.04-2.03 magmatic arcs with Rhyacian blocks (Fraga et al., 2009, 2017), the belt is the result of the closing of orogenic basins ca. 2.00 Ga, during the collision of the 2.04-2.03 magmatic arcs with Rhyacian blocks. Alternatively, Kroonenberg et al. (2016) suggest two possible scenarios: 1) the belt evolved through rift-type basin formation, volcanism and sedimentation, followed by high-grade metamorphism at 2.07-2.05 Ga and 1.99-1.95 Ga, during the Transamazonian orogeny; 2) the belt records northwards subduction along an active continental margin and final collision around 2.03–2.00 Ga and post-orogenic magmatism ca. 1.98 Ga.

The central Guyana Shield was affected by the K'Mudku event during the Mesoproterozoic (1.49 and 1.15 Ga), which is characterized by NE-SW shear belt that truncates the Cauarane-Coeroeni Belt and crosses the Guyana Shield from Suriname to Brazil (Fig. 3.1A; Gibbs and Barron, 1993; Santos et al., 2000, 2006). The whole basement was affected by ductile shearing along NE-SW fault zones. This deformation has been interpreted as a tectonic flexure at medium to high-grade metamorphic conditions as a response to Sunsás collision in the southwestern Amazonian craton (Santos et al., 2000, 2006). In contrast, Fraga (2002) and Fraga et al. (2009) argue that K´Mudku event produced a set of brittle-ductile shear zones, with partial to total obliteration of Paleo to Mesoproterozoic pre-existing structures, developed by a transpression mechanism at the low-grade metamorphic conditions.

The emplacement of the RAP over this complex framework relates to the reactivation of those structural zones during the Mesozoic, regarding the Equatorial Atlantic opening (Figueiredo et al., 2018). The reactivation event was responsible for the development of the Tacutu aulacogen (Crawford et al., 1985; Eiras and Kinoshita, 1988), a half-graben which extend in NE-trending for 300 km between Brazil and Guyana. The initial rift phase was marked by tholeiitic dykes emplacement ca. 200 Ma and volcanic flooding between 153-135 Ma from the Central Atlantic Magmatic Province - CAMP at the beginning of the Triassic (Marzoli et al., 1999; Leal et al., 2000; Reis et al., 2006). The final sedimentation of Tacutu Basin occurred during the Early Cretaceous (Vaz et al., 2007), synchronous to alkaline magmatism (Montalvão et al., 1975; Figueiredo et al., 2018).

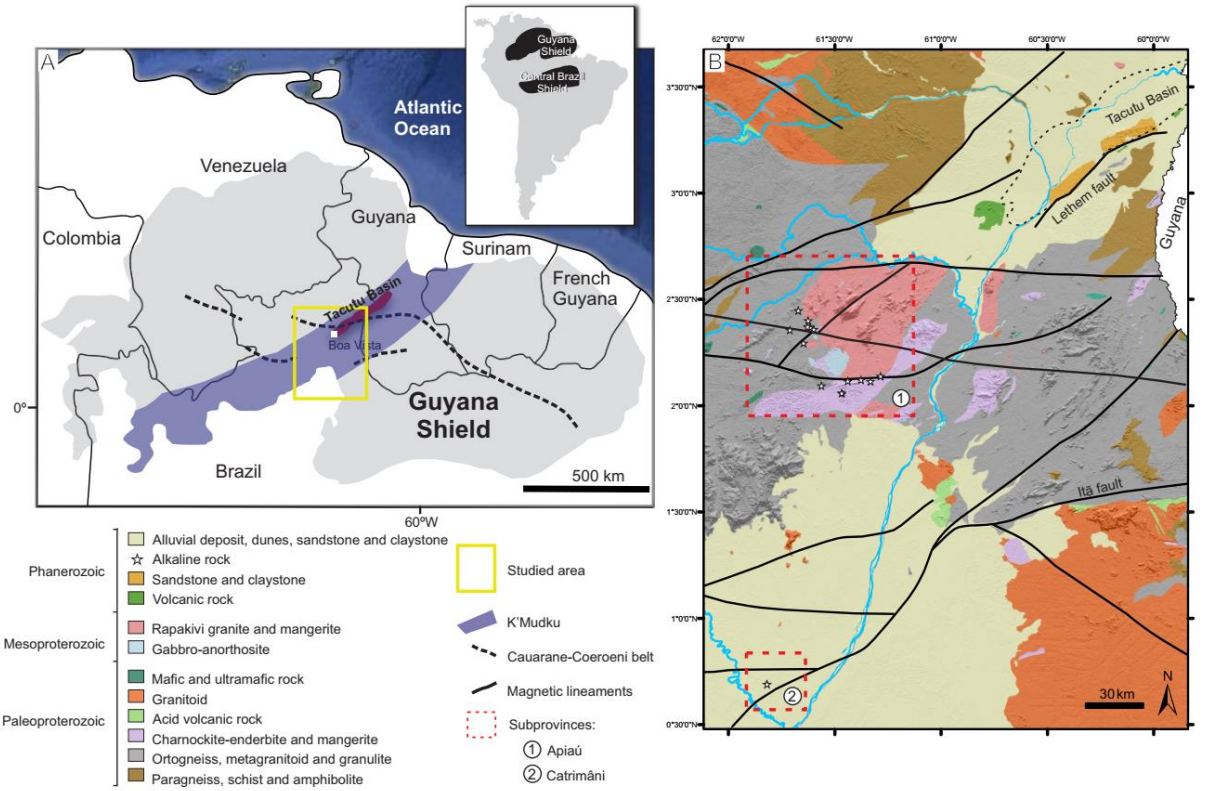

Figure 3.1: A) Map of Guyana Shield displaying Cauarane-Coeroeni Belt (Fraga et al., 2009) and K'Mudku event (Santos et al., 2000, 2006). B) Simplified geological map of the Roraima Alkaline Province, modified from Reis et al. (2004). White stars are alkaline rocks compiled from Figueiredo et al. (in prep) and Brandão and Freitas (1994).

3. Airborne magnetic and gamma-ray survey data

The study area is covered by 4 aerogeophysical surveys (Parima-Uraricoera, Centro-Leste de Roraima, Sudeste de Roraima and Catrimâni-Aracá). The aerogeophysical data used were provided by Brazilian Geological Survey – CPRM and included aeromagnetic and aeroradiometry data which were acquired in 2001, 2010, 2011 and 2012. The surveys were carried out with N-S-directed flight lines, spaced 500 m, and the tie flight lines directions were E-W, with 10 km spacing with both flight and control lines acquired with 100 m average ground clearance.

Data complies with magnetic and gamma-spectrometric data which are made available in reduced form. The reduced aerogeophysical data were interpolated using a square gridding cell of 125 m size. Gamma-ray data were interpolated using the minimum curvature method, and magnetometry data were interpolated by the bi-directional algorithm. We applied filters to eliminate tendencies across flight line direction, with a conjunct use of a Butterworth low pass filter and directional cosine. Both gamma-spectrometric and magnetic data were processed using Oasis Montaj software (GEOSOFT) v. 9.4.

The airborne geophysical data were analysed on a regional scale to contextualise the structures in the hosting basement to the RAP, and on a local scale to individualise the alkaline intrusions. We interpreted the gamma-ray spectrometry data as K, eU and eTh and Ternary RGB (K-Th-U) maps as proxies for the overall geochemistry of the surface materials and to map potential alkaline rock bodies. For the later we interpreted the maps for regions with K, eTh and eU signatures.

To get insight on the regional structural framework of the area and provide context to exam the relationship between Precambrian structures and emplacement of alkaline rocks we interpreted the aeromagnetic data. The interpretation of the aeromagnetometric products involved a visual interpretation of the Analytical Signal Amplitude (Nabighian, 1972; Roest et al., 1992) and Tilt Derivative (Miller and Singh, 1994) filters over the magnetic anomaly map, which aimed to enhance the representation of the magnetic fabric and potential field source bodies in the region. Faults and shear zones are represented either by magnetic anomaly or no magnetic anomaly signature and were recognized by displacement, dislocation, or termination of identifiable magnetic units (Isles and Rankin, 2013).

4. Geophysical characterization of the Roraima Alkaline Province

Given that most of the intrusive bodies are too narrow to be representative in the data we concentrated on the aerogeophysical data interpretation along seven previously known foid and foid-bearing syenites from RAP (Table 3.2). They are the major alkaline bodies, varying from hundreds of meters to 4 km in extension. Figure 3.2 shows the ternary radiometric image and analytical signal amplitude for each of studied alkaline body.

4.1 Radiometric data

The ternary image offers much in term of lithologic discrimination based on equivalent element abundancies. The rocks from RAP are characterized by high equivalent concentrations of Uranium (eU), Thorium (eTh) and Potassium (K) comparing to the surrounding hosts. Most of the alkaline intrusions represent a topographic high, but for some of them there is no relief representation. Some intrusions are characterized by circular or ovoid morphostructures as can be observed in the digital elevation model of Pupunha and Repartimento (Figure 3.2). Regardless of the altitude, all of them are marked by high radiometric values for all the three elements, which translate into white colour on the ternary RGB image.

To the east of the Pupunha body, there is a region with high radiometric values where dykes of lamprophyres, tephrites and phonolites exist intruding rapakivi granites (dashes in Fig 3.2A). It is an area of very dense forest and high altitudes, where we were unable to map in detail, but it is a region that requires attention due to the high favourability to other alkaline bodies.

The host rocks of alkaline rocks from Apiaú subprovince (northern area) are essentially Paleoproterozoic metagranites, orthogneisses and charnockites and Mesoproterozoic rapakivi granite (Fraga, 2002; Costa, 2005; Fraga et al., 2009). It is a very complex terrane and the composition of the basement is essentially granitic, which is difficult to differentiate among Precambrian metamorphic and igneous rocks in gamma-ray maps. Few Mesoproterozoic anorthosite-gabbro are also situated into the area and are marked by dark colours on ternary, meaning they have low content on the three elements. High eU values are observed in positive topography lineaments observed in digital elevation model and surrounding the studied alkaline bodies.

The southern area of RAP, which corresponds to Catrimâni subprovince (Figueiredo et al. in prep), shows low values of K, intermediate values of eU and intermediate to high concentrations of eTh that indicate a spatial correlation with areas covered by Cenozoic deposits which cover the Solimões Basin (Fig. 3.2C). The flat terrane of this covering is interrupted by a small elevation constituted by nepheline syenite and phonolite dykes. The nepheline syenite is characterized by their strong radiometric response, clearly visible on the composite radioelement image, and can be easily discriminated from the low radioactive rocks from Quaternary deposits. In addition, mutual low concentrations of eU, eTh and K are reflected by darker areas in the Catrimâni subprovince.

Owing to extensive Cenozoic covering, we have known only one plutonic alkaline occurrence exposed in the Catrimâni subprovince. However, the Figure 3.2C shows a wide ternary image for Catrimâni subprovince that exhibit punctual high radiometric values into the weakly radioactive sedimentary deposits. Based on the high radiometric values of the foid and foid-bearing syenites from RAP, Catrimâni's high values directed in bright colour (circle in Figure 3.2C) might be related to unmapped alkaline rocks.

4.2 Magnetic data

The alkaline bodies often occur close to or truncate unidimensional, line-like our broad regions of high magnetization gradient amplitude. The analytical signal amplitude (ASA) map shows that the alkaline bodies exhibit mostly low to intermediate amplitude (Fig. 3.2). The higher values probably reflect magnetization gradients associated with the structures that control the alkaline bodies emplacement. In the surrounding areas, there are contrasting of high amplitude which is mostly associated with gabbro and important shear zones. No significant contrast has been observed from the felsic alkaline rocks and granitic basement. The sedimentary cover in Catrimâni subprovince can be considered relatively magnetic transparent, and most of the anomalies observed can be attributed to the various metamorphic and igneous basement.

A structural map of the studied area developed from tilt derivative image from airborne magnetic data is presented in Figure 3.3. The magnetic signature of the structural framework of the RAP region shows a complex configuration, with long magnetic lineaments trending NE–SW, E–W and NW–SE. The NE and NW trends can be recognized by high and low magnetic lineaments, while E-W trend is marked by the strike-slip movement of those lineaments.

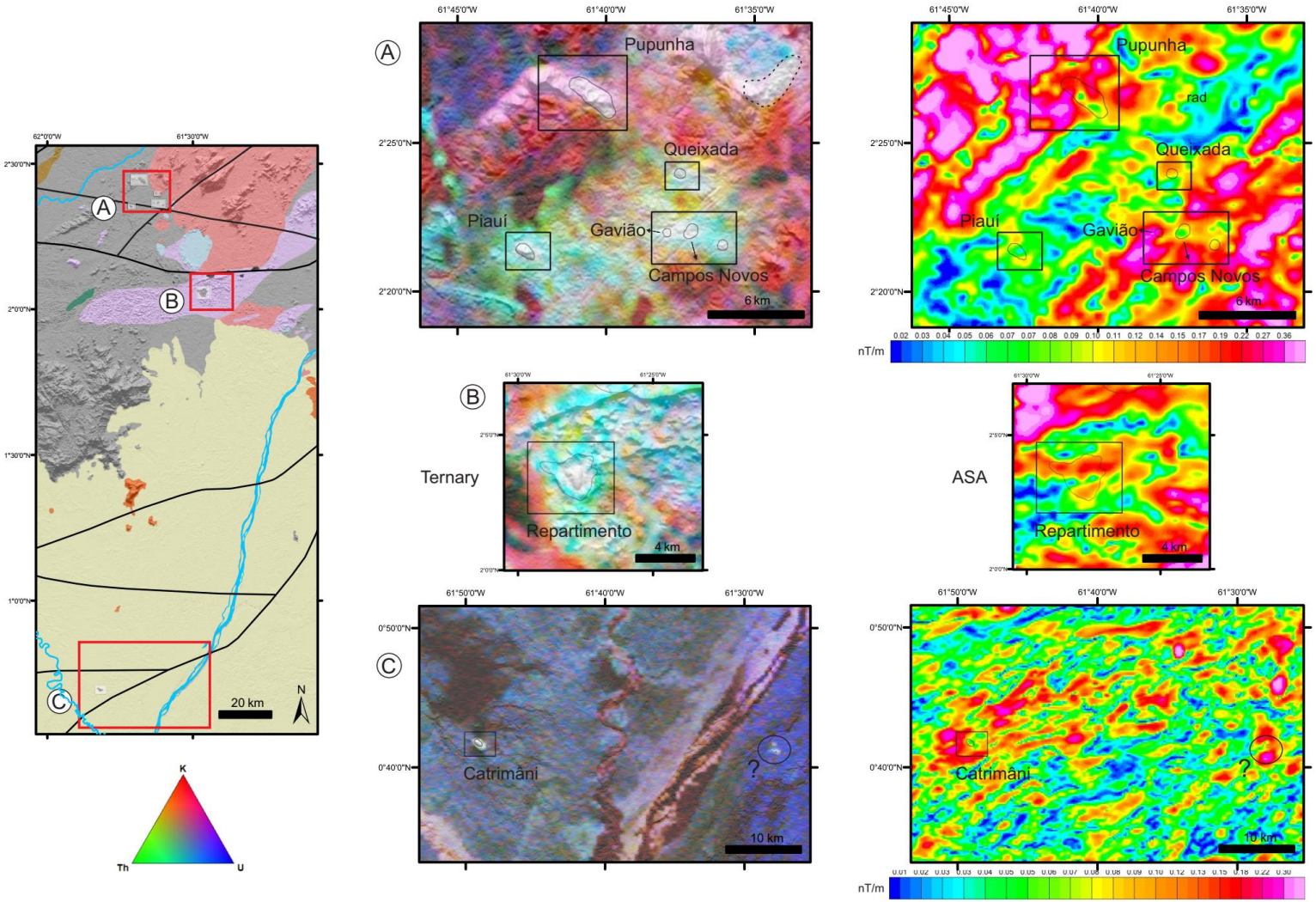

Figure 3.2: Geological map of the area of Roraima Alkaline Province highlighting the gamma-ray ternary image underlain by the digital elevation model and ASA of studied bodies. The images display high radiometric values and low to intermediate magnetic amplitude to foid and foid-bearing syenites. A and B are clipping of Apiaú subprovince where dashed line indicates area favorable to find other alkaline rocks. C is a clipping of Catrimâni subprovince and the circle indicates probable alkaline rock.

Table 3.1: Summary of the lithologies, their mineralogy (compilated from Figueiredo et al. in prep and Brandão and Freitas, 1994) and expression in airborne geophysical data. Afs – alkali feldspar, Aeg – aegirine, Agt – aegirine augite, Aug – augite, Arf – arfvedsonite, Ap – apatite, Aln – allanite, Bt – biotite, Cb – carbonate, Ccn – cancrinite, Ct – catapleiíte, Fl – fluorite, Nph – nepheline, Pl – plagioclase, Prg-Hst – pargasite hastigsite, Sdl – sodalite, Ttn – titanite, Woh – wohlerite, Zr – zircon.

Intrusion	**Lithology**	**Mineralogy**	**Airborne radiometric response**	**Airborne magnetic response**
Pupunha	Nepheline-bearing syenite	Afs, Pl, Nph, Prg-Hst, Bt, Zr, Aln	High values of K, eU and eTh	Low to high amplitudes
Piauí	Nepheline-bearing syenite	Afs, Bt, Agt, Aeg, Pl, Nph, Zr, Cb, Ttn	High values of K, eU and eTh	Low amplitudes
Queixada	Sodalite nepheline syenite and nepheline syenite	Afs, Sdl, Aeg, Aug, Ccn, Cb, Ap, Ct	High values of K, eU and eTh	Intermediate amplitudes
Gavião	Sodalite nepheline syenite	Afs, Sdl, Nph, Amp, Aug, Agt, Cb	High values of K, eU and eTh	High amplitudes
Campos Novos	Nepheline syenite	Afs, Nph, Arf, Agt, Pl, Bt, Ccn, Ttn, Fl, Aln, Woh	High values of K, eU and eTh	Low amplitudes
Repartimento	Lateritic crust and mafic dykes. The magnetic response indicates felsic rocks to Repartimento	unknown	High values of K, eU and eTh	Low to intermediate amplitudes.
Catrimâni	Nepheline syenite	Afs, Nph, Arf, Bt, Aeg, Agt, Prg-Hst, Pl, Ccn, Ttn, Cb, Sd, Ap, Zr	High values of K, eU and eTh	Intermediate amplitudes

5. The interplay between the Proterozoic structures and the alkaline magmatism

The rocks from RAP (Fig. 3.4A-C) are following main fault and shear zones from central-southern Guyana Shield, suggesting a tectonic control of magmatism by Precambrian crustal discontinuities. The emplacement of alkaline rocks would be favored by the proximity of a lineament or, even better, the intersection of several lineaments. The structural control is clearer in Apiaú subprovince, where the alkaline rocks are situated into the intersection of NE-SW and E-W faults (Fig. 3.3). Those weakness zones have played a major role on the alkaline magmatism emplacement during Mesozoic reactivation.

All those structures are related to the tectonic evolution of Guyana Shield during Precambrian. The central segment of Guyana Shield has been subject to multiple tectonic events such as: 1) Trans-Amazonian in Paleoproterozoic; 2) K'Mudku event during Mesoproterozoic; 3) Tacutu rift during Mesozoic. The NW magnetic signatures are probably related to Paleoproterozoic Cauarane-Coeroeni Belt (Fraga et al., 2009) which extends to Guyana and Suriname in a sinuous NW–SE/NE–SW/NW–SE structure, and according to Kroonemberg et al. (2016) is associated with Trans-Amazonian orogeny. The NE-SW trend is associated with both Cauarane-Coeroeni Belt and K'Mudku event. This trend is marked in deformation of Paleoproterozoic gneisses-metagranitoids, described by Fraga (2002) as D1 deformation event (Cauarane-Coeroeni Belt), and in deformation of Mesoproterozoic granites described by the same author as D2 event (K'Mudku, Fig.3.4D). Therefore, NE-SW trend was generated in the Paleoproterozoic Trans-Amazonian orogeny and reactivated during the Mesoproterozoic K'Mudku event.

The regional NE-SW trend inflected to E-W, which is also observed in outcrop scale (Fig. 3.4E). Fraga (2002) describes NE-SW to E-W trends in gneiss banding from Apiaú subprovince. Kroonemberg et al. (2016) also describe important E-W trend along Cauarane-Coeroeni Belt in Suriname. The NE and NW lineaments are dislocated by huge E-W trend which exceeds the extension of the studied area. Thus, the E-W orientation seems to have been suffered the last reactivation in central Guyana Shield, dislocating the NE and NW lineaments, which is obvious in Apiaú subprovince and Tacutu Basin. The recognized trends can also be observed in the digital elevation model (see Fig. 3.1).

Most alkaline rocks from RAP (Apiaú subprovince) are emplaced along S-C structures developed in the basement (Figure 3.3), marked by NE-SW and E-W lineaments. The dextral displacement of the lineaments that marks this shear zone (C-surface) is clear in aeromagnetic maps and kinematic indicators mapped in outcrop. Fraga (2002) also describes a

dextral transpression regime for this zone. In this context, the region is characterized by lithospheric-scale shear zones that have accommodated alkaline magmatism. During the Paleoproterozoic shear deformation, the central portion of the anastomosed zone presents a lower strain rate, consequently remaining more preserved. The location of the alkaline bodies along the S planes in the central portion of old shear zones is due to sinistral reactivations, which turned these surfaces into extensional zones, facilitating the magma rise during the Mesozoic. The crossing zones between the S surfaces and the E-W structures are an important structural control guide for locating alkaline bodies.

The NE- trending structures, related to Paleo and Mesoproterozoic events in Guyana Shield, are weakness zones where the Tacutu rift has incised. The Tacutu Basin is an intracratonic failed-rift basin and, although the rift setting is well known, it is not stated whether the magmatic event resulted from an upwelling deep mantle plume or was associated with stretching of the lithosphere and passive upwelling of the asthenosphere. The beginning of extension in central Guyana Shield is marked by NE-trending tholeiitic dykes from ~ 200 Ma associated with Central Atlantic Magmatic Province – CAMP (Marzolli et al., 1999) which is linked to the initial disruption of Pangea. This age is also coherent with the model of Labails et al. (2010), which suggests that the earliest seafloor spreading of the Central Atlantic occurred at 190 Ma. According to Lamotte et al. (2015), the long timing of the CAMP magmatism, as well as the width of the rift system and the role of heritage, are consistent with a passive mechanism initiated by lithospheric extensional stresses with mantle uplift.

With time, the Tacutu rift becomes more active, with effusion of flood basalts between 153-135 Ma (Leal et al., 2000; Reis et al., 2006). Timing of volcanic activity in Tacutu is coincident with accelerated seafloor spreading rates in the Central Atlantic (~ 154 Ma) which was asymmetrically much higher on the American plate (Labais et al., 2010). It is also concordant with the opening of the proto-Caribbean Basin around 145 Ma, forming a triple junction to the east between the mid-ocean ridge of the Central Atlantic and rift axis of the Equatorial/ South Atlantic (Seton et al. 2012).

Basalts were extruded on the floor of the Tacutu Basin and were conformably overlain by continental or littoral-type sediments (Berrangé and Dearnley, 1975). However, Vaz et al. (2007) describe some outcrops with intercalations of basalts and clastic sedimentary rocks that suggest different pulses of magmatic activity. It is worth noting that the ages were acquired by K-Ar and Ar-Ar from whole-rock methods highlighted by Nomade et al. (2007) as not accurate ages owing to alteration complications recognized in many CAMP zones.

In this context, the thinning episode in central Guyana Shield grew in Late Jurassic, marked by volcanic activity, and probably slowed down around Early Cretaceous time. Following the basalt eruptions, a period of tectonic quiescence occurred, allowing the generation of alkaline magmatism. Note that most rocks from RAP are emplaced into the intersection between NE-SW and E-W faults and the magnetic data show E-W sinistral movement as the last reactivation in central Guyana Shield (Fig. 3.3). The available geochronological data point to a time span between 100 and 116 Ma for the alkaline magmatic activity. These ages are in good agreement with the end of the salt deposition and the breakup within both the Central and Equatorial segments (The Aptian–Albian Boundary ~112 Ma, Moulin et al., 2010).

The Equatorial segment considered in this study is that proposed by Moulin et al. (2010) which is separated from the Central Atlantic Ocean by the Marathon Fracture Zones, to the north of the Demerara and Guinean plateaus. According to Gouyet et al. (1994), in Early Cretaceous a local high separated the Demerara from the Guinea plateau, thus isolating shallow marine gulfs open to the north, and consider the Tacutu as the southernmost graben related to this initial phase of rifting. Moreover, those authors argue that as early as middle Albian times, marine environments of deposition prevailed in response to the opening of the E-W-trending Equatorial Ocean. Based on seismic data from French Guiana margin, Greenroyd et al. (2007) state that the break-up geometry in this part of the Equatorial Atlantic has a significant transform/trans-tensional component.

Within a global perspective, the emplacement of the RAP on the Amazonian Craton coincided with the start of rifting in the Equatorial Atlantic (Figueiredo et al., 2018). Alkaline magmatism occurs concerning reactivation of Precambrian NE and NW-trending weakness zones and, subsequently, E-W strike-slip movements. Alkaline dykes with both NE and NW trending were mapped associated with foid and foid-bearing syenites (Fig. 3.4B-C). It indicates that the reactivation in RAP region occurred in all complex tectonic framework.

As stated by Matton and Jébrak (2009), changes in the velocity and geometry of spreading would imply changes in the intensity and orientation of the stresses acting on plate boundaries. Relationship between changes in plate dynamics and intraplate adjustments along lithospheric structures is described to Cabo Frio lineament in southern Brazil (Ferroni et al 2018). Alkaline intrusion related to changes in plate motion is also described in Africa margin. Moreau et al. (1996) argue that the emplacement of alkaline rocks from Los Archipelago in Guinea margin is related to the end of a transtensional tectonic regime during the early opening of the Equatorial Atlantic.

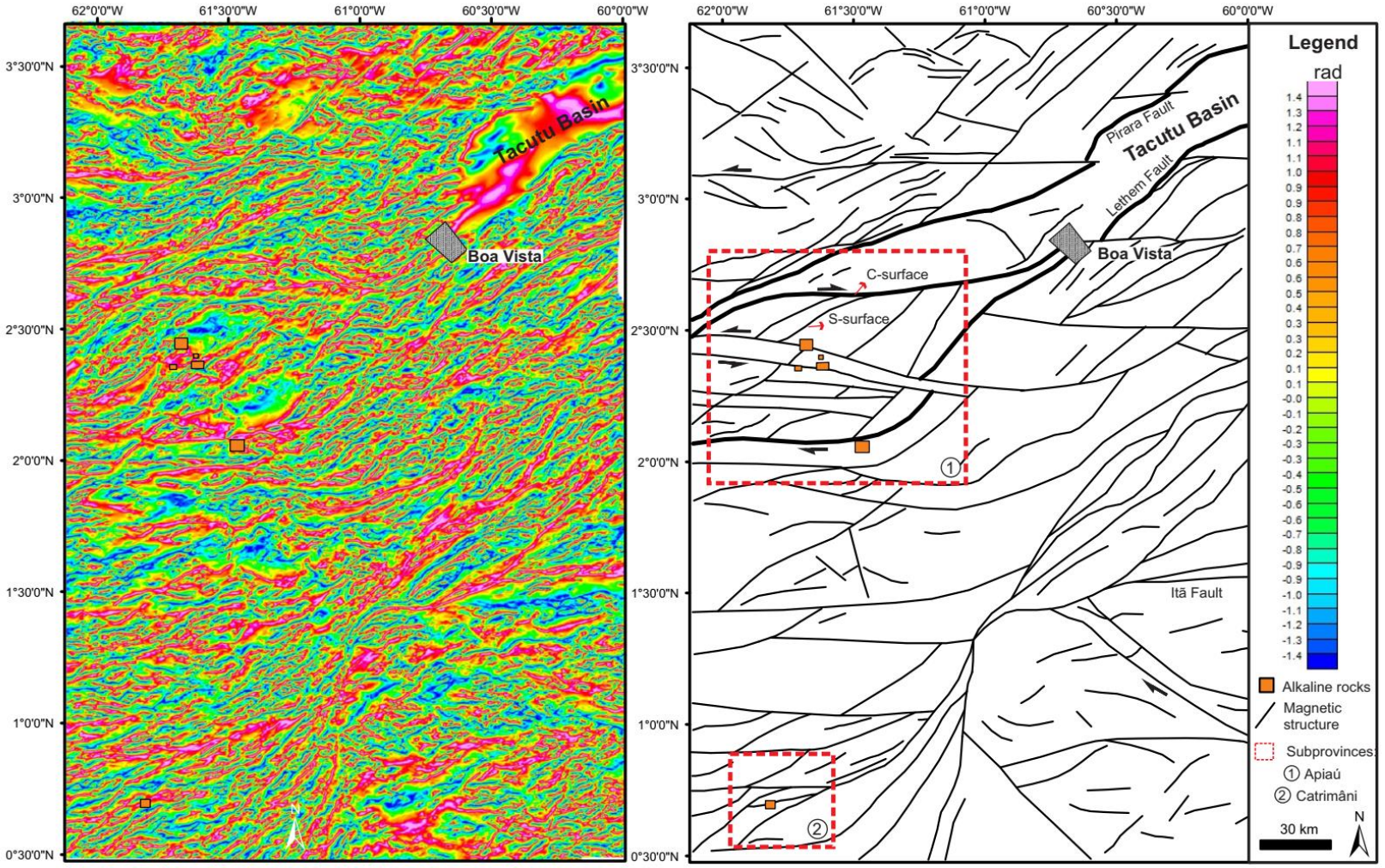

Figure 3.3: (a) Tilt derivative map of RAP region. Three sets of magnetic lineaments can be observed: NE-SW, NW-SE and E-W-trending anomalies. (b) Structural interpretation of map a. The NE-SW-trending magnetic lineaments appear to have been superimposed by the E-W magnetic dislocations.

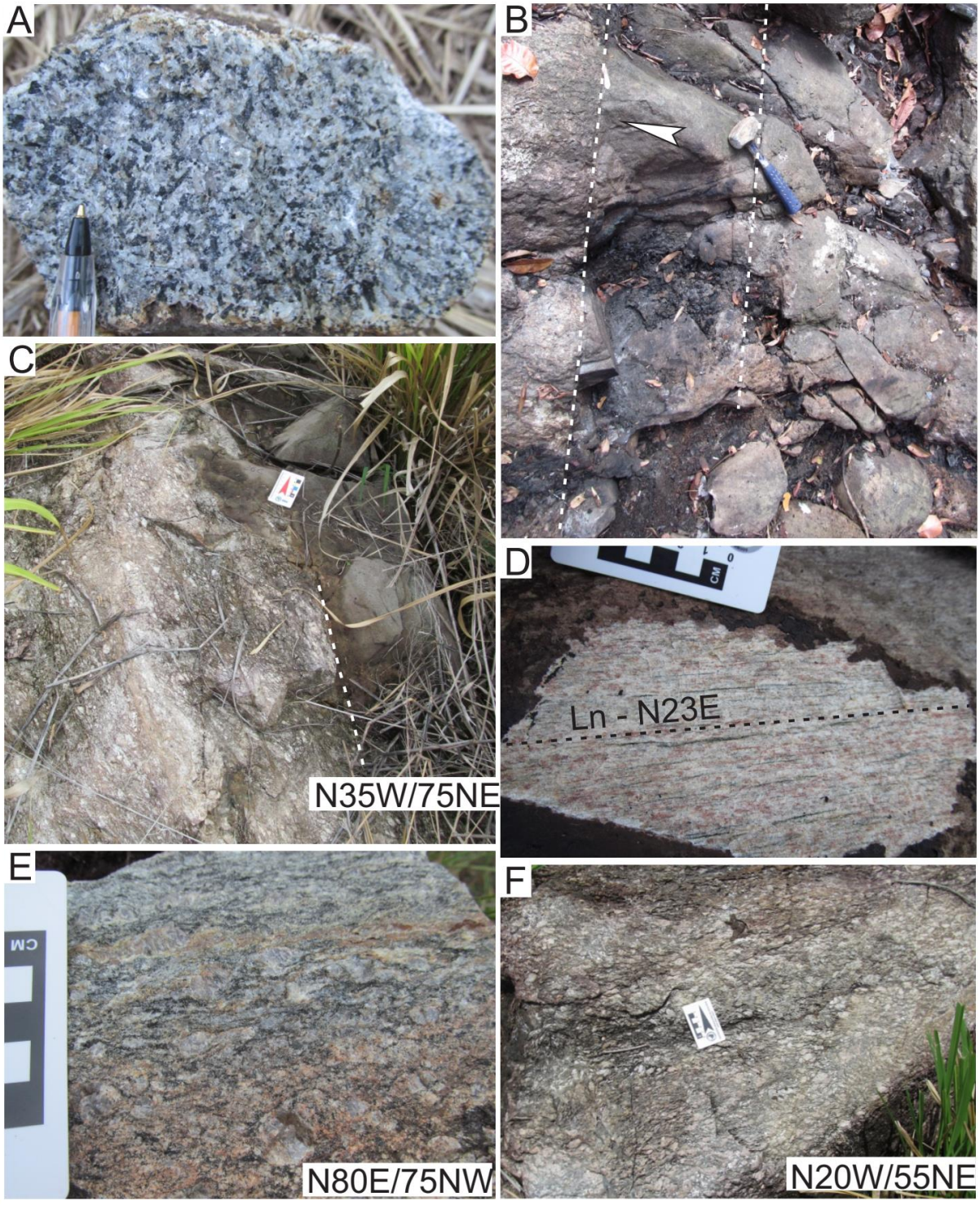

Figure 3.4: Outcrop field photographs. A) Macroscopic aspect of nepheline syenite from Campos Novos intrusion. B) Tephritic dyke crosscut rapakivi granite (N70E direction). C) NW-SE striking foliation in augen gneiss is crosscut by NW tephrite dyke. D) NE-SW mineral lineation in Mesoproterozoic granite. E) Paleoproterozoic augen gneiss composed of quartz, feldspars, biotite and hornblende, and present almost E-W striking foliation. F) Paleoproterozoic augen gneiss with NW-SE striking foliation.

6. Conclusions

Interpretations of gamma-ray spectrometry and magnetic data constrained by field observations proved to be efficient in identifying felsic alkaline rocks from the RAP and deciphering the regional structural framework in central Guyana Shield. The ternary image is the best product to individualize foid and foid-bearing syenites. The studied rocks are characterized by high concentrations of eU, eTh and K compared to the surroundings in both Apiaú and Catrimâni subprovinces. Since the analyse of gamma-ray spectrometry data, it was possible to delineate an area of high favourability to other alkaline bodies. Besides that, the ternary image is useful to differentiate the Precambrian granitic basement from the mafic basement. However, it is not useful to distinguish granites and orthogneisses. The alkaline bodies exhibit mostly low to intermediate amplitude in the ASA image. Nevertheless, the high values are probably reflex of structures in where the alkaline rocks are emplaced or reflex of Precambrian rocks such as gabbro.

The magnetic framework of the RAP can be reconciled with the structural evolution of the Guyana Shield following the major deformation events, such as Transamazonian, K'Mudku and Mesozoic reactivation, could be interpreted in airborne magnetic data. Alkaline magmatism occurs close to or in spatial association with pre-existing structures which are reactivated, particularly those with NE and NW directions and, subsequently, E-W strike-slip movements. Besides, the timing of emplacement of the RAP on the Amazonian Craton coincided with the start of rifting in the Equatorial Atlantic.

References

Almeida, F.F.M., 1986. Distribuição regional e relações tectônicas do magmatismo pós-paleozóico no Brasil. Revista Brasileira de Geociências 16, 325-349.

Begg G.C., Griffin W.L., Natapov L.M., O'Reilly S.Y., Grand S.P., O'Neill C.J., Hronsky J.M.A., Djomani Y.P., Swain C.J., Deen T., Bowden P. 2009. The lithospheric architecture of Africa: Seismic tomography, mantle petrology, and tectonic evolution. *Geosphere*, **5**: 23–50.

Black R., Lameyre J., Bonin B. 1985. The structural setting of alkaline complexes. *Journal of African Earth Sciences*, **3**: 5–16.

Borges F. R. 1990. Projeto Serra do Repartimento. *Relatório de Progresso*. Manaus: CPRM, 30 p.

Brandão R.L. and Freitas A.F.F. 1994. Serra do Ajarani: Folha NA.20-X- C- VI. *Relatório Final*. Manaus: CPRM, 153 p.

Chiwona, A. G., Cortés, J. A., Gaulton, R. G., Manning, D. A. C. 2020. Petrology and geochemistry of selected nepheline syenites from Malawi and their potential as alternative potash sources. Journal of African Earth Sciences, 164, 103769.

Cordani U.G., Fraga L.M., Tassinari C.C.G., Brito-Neves B.B. 2010. On the origin and tectonic significance of the intra-plate events of Grenvillian-type age in South America: A discussion. *Journal of South American Earth Science*, **29**: 143-159.

Costa S.S. 2005. *Delimitação do arcabouço tectônico do Cinturão Guiana Central, estado de Roraima, com base na análise integrada dos dados geofísicos, geológicos, isotópicos e imagens de satélite.* Tese (Doutorado). Instituto de Geociências – Universidade Estadual de Campinas, Campinas, 189 p.

Delor C., de Roever E.W.F, Lafon J.M., Lahondere D., Rossi P., Cocherie A., Potrel A. 2003. The Bakhuis ultra-high-temperature granulite belt (Suriname): II. Implications for the late Transamazonian crustal stretching in a revised Guiana Shield framework. Géologie de la France 2-3-4: 207–230.

Dutra, A. C., Marangoni, Y. R., Junqueira-Brod, T. C. 2012. Investigation of the Goiás Alkaline Province, Central Brazil: Application of gravity and magnetic methods. Journal of South American Earth Sciences, 33(1), 43–55.

Eiras, J.F., Kinoshita, E.M., 1988. Evidências de movimentos transcorrentes na Bacia do Tacutu. Boletim de Geociências da Petrobras 2, 193-208.

Ferroni, F. R., Mello, C. L., Destro, N. 2018. Tectonic control on the Cabo Frio anorogenic magmatic lineament, Southeastern Brazil. Journal of South American Earth Sciences, 83, 37–54.

Figueiredo, R. F. de, Santos, T. J. S. dos, Tonetto, E. M. 2018. Petrology, geochemistry and U-Pb zircon and baddeleyite ages of the alkaline rocks from the central-southern Guyana Shield, northern Amazonian Craton. Journal of South American Earth Sciences, 86, 461–474.

Fraga L.M.B. 2002. *A associação anortosito-mangerito-granito rapakivi (AMG) do Cinturão Guiana Central, Roraima, e suas encaixantes paleoproterozóicas: evolução estrutural, geocronologia e petrologia.* Tese (Doutorado). Centro de Geociências – Universidade Federal do Pará, Belém, 351 p.

Fraga L.M.B., Dall'Agnol R., Costa J.B.S., Macambira M.J.B. 2009. The Mesoproterozoic Mucajaí anorthosite-mangerite-rapakivi granite complex, Amazonian Craton, Brazil. *The Canadian Mineralogist*, **47**: 1469-1492.

Fraga L.M.B., Cordani U., Kroonenberg S., De Roever E., Nadeau S., and Maurer V.C. 2017. U-PB SHRIMP new data on the high-grade supracrustal rocks of the Cauarane Coeroeni Belt - insights on the tectonic Eo-Orosirian evolution of the Guiana Shield. In: 15º Simpósio De Geologia da Amazônia, *anais*, 486-490.

Gaudette H. E., Olszewski Jr. W. J., Santos J. O.S. 1996. Geochronology of Precambrian rocks from the northern part of Guiana Shield, State of Roraima, Brazil. *Journal of South American Earth Sciences***, 9** (3,4): 183- 195.

Gibbs A.K., Barron C.N. 1993. Geology of the Guiana shield. Oxford University Press (Oxford): 246 pp.

Gouyet, S., Unternehr, P., & Mascle, A. 1994. The French Guyana Margin and the Demerara Plateau: Geological History and Petroleum Plays. Hydrocarbon and Petroleum Geology of France, 411–422.

Greenroyd, C. J., Peirce, C., Rodger, M., Watts, A. B., & Hobbs, R. W. 2007. Crustal structure of the French Guiana margin, West Equatorial Atlantic. Geophysical Journal International, 169(3), 964–987.

Heinonen A.P., Fraga L.M., Rämö O.T., Dall'Agnol R., Mänttäri I., Andersen T. 2012. Petrogenesis of the igneous Mucajaí AMG complex, northern Amazonian Craton - Geochemical, U-Pb geochronological, and Nd-Hf-O isotopic constraints. *Lithos*, **151**:17–34.

Isles D.J. and Rankin R.L. 2013. *Geological interpretation of aeromagnetic data.* Australia, CSIRO Publishing, 357 p.

Katumwehe, A. B., Abdelsalam, M. G., and Atekwana, E. A. 2015. The role of pre-existing Precambrian structures in rift evolution: The Albertine and Rhino grabens, Uganda. Tectonophysics, 646, 117–129.

Kroonenberg S.B., 1976. Amphibolite facies and granulite facies metamorphism in the Coeroeni Lucie area, southwestern Surinam. PhD Thesis, University of Amsterdam. Mededelingen Geologisch. Mijnbouwkundige Dienst Suriname 25: 101–289.

Kroonenberg, S. B., De Roever, E. W. F., Fraga, L. M., Reis, N. J., Faraco, T., Lafon, J. M., Wong, T. E. 2016. Paleoproterozoic evolution of the Guiana Shield in Suriname: A revised model. Geologie En Mijnbouw/Netherlands Journal of Geosciences, 95(4), 491–522.

Kwayisi, D., Lehmann, J., and Elburg, M. 2020. The architecture of the Buem Structural Unit: Implications for the tectonic evolution of the Pan-African Dahomeyide Orogen, West Africa. Precambrian Research, 338, 105568.

Labails, C., Olivet, J. L., Aslanian, D., and Roest, W. R. 2010. An alternative early opening scenario for the Central Atlantic Ocean. Earth and Planetary Science Letters, 297(3–4), 355–368.

Lamotte, F. D., Fourdan, B., Leleu, S., Leparmentier, F., and De Clarens, P. 2015. Style of rifting and the stages of Pangea breakup. Tectonics, 34(5), 1009–1029.

Leal, A.B.M., Girardi, V.A.V., Leal, L.R.B., 2000. Petrologia e geoquímica do magmatismo básico mesozoico da Suíte Básica Apoteri, estado de Roraima. Geochimica Brasiliensis 14, 155-174.

Louro, V. H. A., Negrão, A. P., Castro, L. G., Ferreira, F. J. F. 2019. Canoas geophysical anomaly: A possible alkaline body or unusual anomaly caused by mafic dykes in the Ponta Grossa Arch, Brazil, Journal of Applied Geophysics, 170.

Matton, G. and Jébrak, M. 2009. The Cretaceous Peri-Atlantic Alkaline Pulse (PAAP): Deep mantle plume origin or shallow lithospheric break-up? Tectonophysics, 469(1–4), 1–12.

Marangoni, Y. R., Mantovani, M. S. M. 2013. Geophysical signatures of the alkaline intrusions bordering the Paraná Basin. Journal of South American Earth Sciences, 41, 83–98.

Marzoli A., Renne P.R., Piccirillo E.M., Ernesto M., Bellieni G., De Min A. 1999. Extensive 200-Million-Year-Old Continental Flood Basalts of the Central Atlantic Magmatic Province. Science 284, 616–618.

Miller H.G. and Singh V. 1994. Potential field tilt –a new concept for location of potential field sources. *Journal of Applied Geophysics*, **32**(2-3): 213-217.

Montalvão R. M.G., Muniz, M. C., Issler R. S., Dall'Agnol R., Lima M. I. C., Fernandes P. E. C. A, Silva G. G. 1975. *Projeto Radam Brasil: Folha NA.20- Boa Vista e parte das folhas NA.21 - Tumucumaque, NB.20 – Roraima e NB.21*, v.8, Rio de Janeiro, DNPM, 403 p.

Moreau, C., Ohnenstetter, D., Demaiffe, D., Robineau, B. 1996. The Los Archipelago nepheline syenite ring-structure: A magmatic marker of the evolution of the central and equatorial atlantic. Canadian Mineralogist, 34(2), 281–299.

Moulin, M., Aslanian, D., & Unternehr, P. 2010. A new starting point for the South and Equatorial Atlantic Ocean. Earth-Science Reviews, 98(1–2), 1–37.

Nomade, S., Knight, K. B., Beutel, E., Renne, P. R., Verati, C., Féraud, G., … Bertrand, H. 2007. Chronology of the Central Atlantic Magmatic Province: Implications for the Central Atlantic rifting processes and the Triassic-Jurassic biotic crisis. Palaeogeography, Palaeoclimatology, Palaeoecology, 244(1–4), 326–344.

Pinto, M. L., and Vidotti, R. M. 2019. Tectonic framework of the Paraná basin unveiled from gravity and magnetic data. Journal of South American Earth Sciences, 90, 216–232.

Pirajno, F., 2015. Intracontinental anorogenic alkaline magmatism and carbonatites, associated mineral systems and the mantle plume connection. Gondwana Research 27, 1181–1216.

Reis, N. J., Fraga, L.M., Faria, M.S.G., Almeida, M. E., 2003. A geologia de Roraima. Géologie de la France 2-3-4, 121-134.

Reis N.J., Faria M.S.G., Almeida M.E., Oliveira M.A. 2004. Folhas NA.20-Boa Vista e NB.20-Roraima. *In*: Schobbenhaus C., Gonçalves J.H., Santos J.O.S., Abram M.B., Leão Neto R., Matos G.M.M., Vidotti R.M., Ramos M.A.B., Jesus J.D.A. (Eds.) *Carta Geológica do Brasil ao Milionésimo, Sistema de Informações Geográficas-SIG. Programa Geologia do Brasil.* Brasília, CPRM, CD-ROM.

Reis, N.J, Szatmari, P, Wanderley Filho, J.R, York, D, Evensen, N.M, Smith, P.E., 2006. Dois eventos de magmatismo máfico mesozóico na fronteira Brasil-Guiana, Escudo das Guianas: enfoque à região do rifte Tacutu-North Savannas, in: 43º Congresso Brasileiro de Geologia, Aracaju, 459–46.

Riccomini C., Velázquez V.F., Gomes C.B. 2005. Tectonic controls of the Mesozoic and Cenozoic alkaline magmatism in central-southeastern Brazilian plataform. *In*: Comin-Chiaramonti P. & Gomes C.B. (Eds.) *Mesozoic to Cenozoic Alkaline Magmatism in the Brazilian Platform*. São Paulo, Edusp/Fapesp, p. 31-55.

Rocha, L. G. M., Pires, A. C. B., Carmelo, A. C., & Araújo Filho, J. O. de. 2014. Geophysical characterization of the Azimuth 125 lineament with aeromagnetic data: Contributions to the geology of central Brazil. Precambrian Research, 249, 273–287.

Salas N.J. & Santos J.O.S. 1974. Determinações geocronológicas pelo método da birrefringência em fonólito na área do Projeto Norte da Amazônia. *In*: SBG, 28º Congresso Brasileiro de Geologia. Porto Alegre, *Anais,* v. 6, p. 221-224.

Santos J. O. S., Hartmann L. A., Gaudette H. E., Groves D. I., Mcnaughton N. J., Fletcher I. R. 2000. A New Understanding of the Provinces of the Amazon Craton Based on Integration of Field Mapping and U-Pb and Sm-Nd Geochronology. *Gondwana Research*, **3** (4): 453-488.

Santos J.O.S., Faria M.S.G., Riker S.R., Souza M.M., Hartmann L.A., Almeida M.E., McNaughton N.J., Fletcher I.R. 2006. A faixa colisional K'Mudku (idade Greenvilliana) no norte do Cráton Amazonas: reflexo intracontinental do orógeno Sunsás na margem ocidental do cráton. *In*: SBG, 9º Simpósio de Geologia da Amazônia. Belém, *Anais,* CD-ROM.

Seton, M., Müller, R. D., Zahirovic, S., Gaina, C., Torsvik, T., Shephard, G., … Chandler, M. 2012. Global continental and ocean basin reconstructions since 200Ma. Earth-Science Reviews, 113(3–4), 212–270.

Spampinato, G. P. T., Betts, P. G., Ailleres, L., and Armit, R. J. 2015. Early tectonic evolution of the Thomson Orogen in Queensland inferred from constrained magnetic and gravity data. Tectonophysics, 651, 99–120.

Verduzco B., Fairhead J.D., Green C.M., Mackenzie C. 2004. New insights into magnetic derivatives for structural mapping. *The Leading Edge*, **23**(2): 116-119.

Vaz, P.T., Wanderley Filho, J.R., Bueno, G.V. 2007. Bacia do Tacutu. Boletim de Geociências da Petrobras 15, 289–297.

CAPÍTULO 4 – CONSIDERAÇÕES FINAIS

A Província Alcalina de Roraima - RAP foi proposta para reunir as ocorrências de rochas alcalinas cretáceas no estado de Roraima, norte do Cráton Amazônico. Trata-se da primeira província alcalina proposta para o Escudo das Guianas. Embora essas rochas venham sendo reportadas desde a década de 1970, essa tese é o primeiro trabalho que detalha e integra os dados petrográficos, geoquímicos, isotópicos e geofísicos dos diferentes corpos alcalinos. Em função das rochas aflorarem em duas áreas com cerca de 150 km de distância uma da outra, a província foi dividida em duas subprovíncias: Apiaú, ao norte, e Catrimâni, ao sul. As rochas afloram ao longo de 200 km de extensão, associadas a importantes falhas e zonas de cisalhamento do Escudo das Guianas. As idades obtidas para a RAP estão entre aproximadamente 100 e 116 Ma, indicando trata-se de um evento magmático de curta duração.

As rochas que compõem a província podem ser classificadas em dois grupos: i) fonolitos, traquitos e sienitos que predominam na região, ocorrendo como pequenos e grandes plutons e diques; ii) rochas alcalinas básicas, tais como lamprófiro, tefrito e tefrifonolito ocorrendo como pequenos e raros diques. Todas as rochas são insaturadas, variando entre metaluminosas e peralcalinas, com mineralogia que permite classificá-las em miaskíticas e agpaíticas. Os padrões geoquímicos das subprovíncias Apiaú e Catrimâni são muito parecidos. Eles indicam que as rochas evoluíram por cristalização fracionada, com olivina, espinélio, plagioclásio e apatita como fases iniciais, e feldspato alcalino como fase tardia. Com o intuito de verificar a possibilidade de relação entre magmas básicos e evoluídos da província, foram realizadas modelagens termodinâmicas utilizando o algoritmo MELTS. As modelagens indicaram que alguns fonolitos e sienitos podem ser resultado de 51 a 68% da cristalização de um magma tefrítico, com olivina, clinopiroxênio e espinélio como fases iniciais e feldspato e biotita como fases tardias.

Os dados petrográficos, geoquímicos, isotópicos e geocronológicos mostram que os processos de assimilação crustal influenciaram na petrogênese das rochas da RAP. Os efeitos da assimilação crustal são evidentes como texturas de desequilíbrio na maioria das rochas, tais como bordas de reação, clinopiroxênio zonado e *spongy texture*. Além disso, xenocristais e xenólitos crustais foram encontrados na petrografia. Em relação aos dados geoquímicos, altos valores de Sr, Rb e Ba, além da ausência de anomalia de Eu em algumas

amostras, indicam contribuição crustal do embasamento granítico. Ademais, existe uma grande variação entre as razões isotópicas de Sr (0,7029 a 0,7069). No modelo de mistura simples, as amostram plotam seguindo o trend de mistura, sugerindo um processo de mistura entre o magma alcalino e suas encaixantes. Outra evidência importante de contaminação é a presença de zircões mais antigos, herdados do embasamento meso e paleoproterozoico, encontrados nas rochas da RAP.

As assinaturas isotópicas das amostras menos contaminadas sugerem que a fonte está relacionada a mistura de dois componentes mantélicos, uma provável mistura entre um componente enriquecido e outro empobrecido. Além disso, as rochas da RAP apresentam assinatura similar aos basaltos da CAMP, que vem sendo considerado um magmatismo toleítico derivado de um manto heterogêneo e com contribuição crustal. As idades modelo da RAP também coincidem com as descritas para a CAMP, indicando um único evento metassomático para o magmatismo toleítico e alcalino, o qual ocorreu próximo ao início do rifteamento do Tacutu no Escudo das Guianas.

As interpretações dos dados aerogeofísicos, em conjunto com os dados geológicos de campo, mostraram ser muito eficientes na prospecção de rochas alcalinas félsicas. Além disso, foram importantes para decifrar a estruturação regional da porção central do Escudo das Guianas. A imagem ternária foi o melhor produto para a individualização dos sienitos alcalinos, visto que estes são caracterizados por altos valores de eU, eTh e K comparados as coberturas sedimentares e as rochas do embasamento. Embora não seja possível verificar todos os alvos em campo, os dados aerogamaespectrométricos permitiram definir áreas de favorabilidade para rochas alcalinas. Os corpos alcalinos exibem amplitude baixa a intermediária das imagens ASA, porém os valores mais altos refletem provavelmente as estruturas nas quais as rochas alcalinas estão alojadas ou, ainda, rochas máficas do embasamento.

A partir da assinatura magnética do Escudo das Guianas, foi possível identificar as estruturas relacionadas aos diferentes eventos tectônicos que afetaram a região, tais como Transamazônico, K'Mudku e a reativação mesozoica. A partir disso, buscou-se compreender as suas relações com o magmatismo alcalino cretáceo. A ascensão deste magmatismo está estreitamente associada a reativação das estruturas pré-cambrianas NE e NW e, posteriormente, a movimentos transcorrentes E-W. Além disso, ao correlacionar as estruturas com os dados geocronológicos disponíveis, conclui-se que o *emplacement* da RAP coincide com a movimentação tectônica do início da abertura do oceano Atlântico Equatorial.

REFERÊNCIAS GERAIS

Aarden, H.M., Holm, V., Iturralde de Arozena, J.M., Moticska, P., Navarro, J., Pasquali, Z.J., Sifontes, R.S. 1973. Aspectos geoeconomicos del Cerro Impacto: Congreso Latinoamericano de Geologia, 2nd, Caracas, Venezuela, Memoria; Ministerio de Energia y Minas, Dirección de Geologia Boletin de Geologia Publicación Especial 7, v. 5, pp. 3901-3902.

Ackerman, L., Ulrych, J., Řanda, Z., Erban, V., Hegner, E., Magna, T., Balogh, K., Frána, J., Lang, M., Novák, J. K. 2015. Geochemical characteristics and petrogenesis of phonolites and trachytic rocks from the České Středohoří Volcanic Complex, the Ohře Rift, Bohemian Massif. Lithos, 224–225(January), 256–271.

Almeida, F. F. M., 1983. Relações tectônicas das rochas alcalinas mesozoicas da região meridional da plataforma sul-americana. Revista Brasileira de Geociências 13,139-158.

Almeida, F.F.M., 1986. Distribuição regional e relações tectônicas do magmatismo pós-paleozóico no Brasil. Revista Brasileira de Geociências 16, 325-349.

Almeida, M. E., 2006. Evolução geológica da porção centro-sul do Escudo das Guianas com base no estudo Geoquímico, Geocronológico e Isotópico dos granitoides paleoproterozóicos do sudeste de Roraima, Brasil. PhD thesis, Federal University of Pará, 227 pp.

Almeida, M.E., Macambira, M.J.B., Valente, S. de C., 2008. New geological and single-zircon Pb evaporation data from the Central Guyana Domain, southeastern Roraima, Brazil: Tectonic implications for the central region of the Guyana Shield. Journal of South America Earth Science 26, 318–328.

Almeida, V. V., Janasi, V. A., Heaman, L. M., Shaulis, B. J., Hollanda, M. H. B. M., Renne, P. R. 2017. Contemporaneous alkaline and tholeiitic magmatism in the Ponta Grossa Arch, Paraná-Etendeka Magmatic Province: Constraints from U–Pb zircon/baddeleyite and 40Ar/39Ar phlogopite dating of the José Fernandes Gabbro and mafic dykes. Journal of Volcanology and Geothermal Research.

Angélica, R. S., Costa, M. L. 1993. Geochemistry of rare-earth elements in surface lateritic rocks and soils from the Maicuru complex, Para, Brazil. Journal of Geochemical Exploration, 47(1–3), 165–182.

Asimow, P.D., Ghiorso, M.S., 1998. Algorithmic modifications extending MELTS to calculate subsolidus phase relations. American Mineralogist 83, 1127–1131.

Azzone, R. G., Munoz, P. M., Enrich, G. E. R., Alves, A., Ruberti, E., Gomes, C. B. 2016. Petrographic, geochemical and isotopic evidence of crustal assimilation processes in the Ponte Nova alkaline mafic-ultramafic massif, SE Brazil. Lithos, 260, 58–75.

Azzone, R. G., Chmyz, L., Guarino, V., Alves, A., Gomes, C. de B., Ruberti, E. 2020. Isotopic clues tracking the open-system evolution of the Ponte Nova mafic-ultramafic alkaline massif, SE Brazil: The contribution of Pb isotopes. Chemie Der Erde, April, 125648.

Bailey, D.K. 1987. Mantle metasomatism – perspective and prospect. In: Fitton JG, Upton BGJ (eds) Alkaline rocks. Geol Soc Spec Publi 30: 1-14.

Bates, R.L., Jackson, J.A. 1987. Glossary of Geology. 3rd Edition, American Geological Institute, Alexandria, 788 p.

Baker, B.H. 1987. Outline of the petrology of the Kenya rift alkaline province. In: Fitton, J.G., Upton, B.G.J. (Eds.) Alkaline igneous rocks. Geological Society Special Publication 30, 293-311.

Barros, A.M., Alves, E.D.O., Araujo, J.F.V., Lima, M.I.C., Fernandes, C.S.C. 1977. Projeto Radam Brasil: Folha SB/SC18 Javari/Contama. DNPM, Rio de Janeiro, pp 161.

Beccaluva, L., Born, H., Brotzu, P., Coltorti, M., Conte, A.M., Garbarino, C., Gomes, C.B., Loss, E.L., Macciotta, G., Morbidelli, L., Ruberti, E., Siena, F., Traversa, G. 1992. Fractional crystallization and liquid immiscibility processes in the alkaline-carbonatite complex of Juquiá (São Paulo State, Brazil). Journal of Petrology, 33:1371-1404.

Begg G.C., Griffin W.L., Natapov L.M., O'Reilly S.Y., Grand S.P., O'Neill C.J., Hronsky J.M.A., Djomani Y.P., Swain C.J., Deen T., Bowden P. 2009. The lithospheric architecture of Africa: Seismic tomography, mantle petrology, and tectonic evolution. *Geosphere*, **5**: 23–50.

Bell, K., Simonetti, A. 1996. Carbonatite magmatism and plume activity: Implications from the Nd, Pb and Sr isotope systematics of Oldoinyo Lengai. Journal of Petrology, 37(6), 1321–1339.

Berger, J., Ennih, N., Mercier, J.-C. C., LiéGeois, J.P., Demaiffe, D. 2009. The role of fractional crystallization and late-stage peralkaline melt segregation in the mineralogical evolution of Cenozoic nephelinites/phonolites from Saghro (SE Morocco). Mineralogical Magazine, 73(1), 59–82.

Berger, J., Ennih, N., Ligeois, J. P. 2014. Extreme trace elements fractionation in Cenozoic nephelinites and phonolites from the Moroccan Anti-Atlas (Eastern Saghro). Lithos, 210, 69–88.

Berrangé J.P. & Dearnley R. 1975. The apoteri volcanic formation – tholeiitic flows in the North Savannas Graben of Guyana and Brazil. Sttutgart, Geologische Rundschau, 64 (1): 883-899.

Black R., Lameyre J., Bonin B. 1985. The structural setting of alkaline complexes. *Journal of African Earth Sciences*, **3**: 5–16

Borges, F.R., 1990. Projeto Serra do Repartimento. Technical report, CPRM, 30 pp.

Brandão, R.L., Freitas, A.F.F., 1994. Serra do Ajarani: Folha NA.20-X- C- VI. Technical report, CPRM, 153 pp.

Brooks, E.W., Orris, G.J., Wynn, J.C. 1983. Deposits formed in supracrustal rocks and epizonal plutons: carbonatite deposits. In: Wynn, J.C., Gray, F., Page, N.J. (Eds), Geology and mineral resource assessment of the Venezuelan Guayana Shield, USGS, pp.73-74.

Brotzu P., Gomes C.B., Melluso L., Morbidelli L., Morra V., Ruberti E. 1997. Petrogenesis of coexisting SiO2-undersaturated to SiO2- oversaturated felsic igneous rocks: the alkaline complex of Itatiaia, southeastern Brazil. Lithos, 40:133-156.

Chiwona, A. G., Cortés, J. A., Gaulton, R. G., Manning, D. A. C. 2020. Petrology and geochemistry of selected nepheline syenites from Malawi and their potential as alternative potash sources. Journal of African Earth Sciences, 164, 103769.

Comin-Chiaramonti, P. et al. 1999. Early Cretaceous-Tertiary Magmatism in Eastern Paraguay (Western Parana Basin): Geological, Geophysical and Geochemical Relationships. Journal of Geodynamics 28(4–5): 375–91.

Comin-Chiaramonti, P., Gomes, C.B., Velázquez, V.F., Censi, P., Antonini, P., Comin-Chiaramonti, F., Punturo., R. 2005. Alkaline complexes from southeastern Bolivia. In: Comin-Chiaramonti, P., Gomes, C.B. (Eds.), Mesozoic to Cenozoic Alkaline Magmatism in the Brazilian Platform. Edusp/Fapesp, São Paulo, pp. 159 - 212.

Comin-Chiaramonti, P., De Min, A., Girardi, V.A.V., Ruberti, E., 2011. Post-Paleozoic magmatism in Angola and Namibia: a review. Geological Society of America (GSA) Special Paper 478, 223–247.

Cordani U.G., Teixeira W., D'Agrella-Filho M.S., Trindade R.I. 2009. The position of the Amazonian Craton in supercontinents. Gondwana Research, 15: 396–407.

Cordani, U.G., Fraga, L.M., Tassinari, C.C.G., Brito-Neves, B.B., 2010. On the origin and tectonic significance of the intra-plate events of Grenvillian-type age in South America: A discussion. Journal of South American Earth Science 29, 143-159.

Corfu, F., Polteau, S., Planke, S., Faleide, J. I., Svensen, H., Zayoncheck, A., Stolbov, N. 2013. U-Pb geochronology of cretaceous magmatism on svalbard and franz josef land, barents sea large igneous province. Geological Magazine, 150(6), 1127–1135.

Costa, J.B.S., Pinheiro, R.V.L., Reis, N.J., Pessoa, M.R., Pinheiro, S.S., 1991. O hemigraben do Tacutu: uma estrutura controlada pela geometria do Cinturão de Cisalhamento Guiana Central. Geociências 10, 119-130.

Costa, M. L., Fonseca, L. R., Angélica, R. S., Lemos, V. P., Lemos, R. L. 1991. Geochemical exploration of the Maicuru alkaline-ultramafic-carbonatite complex, northern Brazil. Journal of Geochemical Exploration, 40(1–3), 193–204.

Costa, S.S., 2005. Delimitação do arcabouço tectônico do Cinturão Guiana Central, estado de Roraima, com base na análise integrada dos dados geofísicos, geológicos, isotópicos e imagens de satélite. PhD thesis, University of Campinas, 189 pp.

Cotta, A.J.B., Enzweiler, J., 2011. Classical and new procedures of whole rock dissolution for Trace Element determination by ICP-MS. Geostandards and Geoanalytical Research, 1-24.).

Crawford F. D., Szelewski C. E., Alvey G. D. 1984. Geology and exploration in the Takutu Graben of Guyana. Beaconsfield, Journal Petroleum Geology, 8 (1): 5-36.

Delor C., de Roever E.W.F, Lafon J.M., Lahondere D., Rossi P., Cocherie A., Potrel A. 2003. The Bakhuis ultra-high-temperature granulite belt (Suriname): II. Implications for the late Transamazonian crustal stretching in a revised Guiana Shield framework. Géologie de la France 2-3-4: 207–230.

Deckart, K., Bertrand, H., Liégeois, J. P. 2005. Geochemistry and Sr, Nd, Pb isotopic composition of the Central Atlantic Magmatic Province (CAMP) in Guyana and Guinea. Lithos, 82(3-4 SPEC. ISS.), 289–314.

De Min, A., Piccirillo, E.M., Marzoli, A., Bellieni, G., Renne, P.R., Ernesto, M., Marques, L.S. 2003. The Central Atlantic Magmatic Province (CAMP) in Brazil: petrology, geochemistry, 40Ar/39Ar ages, paleomagnetism and geodynamic implications. In: Hames, W., McHone, J.G., Renne, P.R., Ruppel, C. (eds.). The Central Atlantic Magmatic Province. AGU Geophysical Monograph, 136, p. 91-128.

Downes, Hilary et al. 2005. "Petrogenetic Processes in the Ultramafic, Alkaline and Carbonatitic Magmatism in the Kola Alkaline Province: A Review." Lithos 85(1-4 SPEC. ISS.): 48–75.

Dunworth, E. A. 2001. "The Turiy Massif, Kola Peninsula, Russia: Isotopic and Geochemical Evidence for Multi-Source Evolution." Journal of Petrology 42(2): 377–405.

Dutra, A. C., Marangoni, Y. R., Junqueira-Brod, T. C. 2012. Investigation of the Goiás Alkaline Province, Central Brazil: Application of gravity and magnetic methods. Journal of South American Earth Sciences, 33(1), 43–55.

Eiras, J.F., Kinoshita, E.M., 1988. Evidências de movimentos transcorrentes na Bacia do Tacutu. Boletim de Geociências da Petrobras 2, 193-208.

Eiras, J.F., Kinoshita E.M., 1990. Geologia e perspectivas petrolíferas da Bacia do Tacutu. In: Gabaglia, G.P.R, Milani, E.J (Eds), Origem e Evolução de Bacias Sedimentares. Petrobras, Rio de Janeiro, pp 197-220.

Elburg, M. A., Cawthorn, R. G. 2017. Source and evolution of the alkaline Pilanesberg Complex, South Africa. Chemical Geology, 455, 148–165.

Ferroni, F. R., Mello, C. L., Destro, N. 2018. Tectonic control on the Cabo Frio anorogenic magmatic lineament, Southeastern Brazil. Journal of South American Earth Sciences, 83, 37–54.

Figueiredo, R.F., 2016. Contexto tectônico do Complexo Alcalino Apiaú– Roraima: Aerogeofísica, petrologia e geocronologia U-Pb. M.S. thesis, University of Campinas, 102 pp.

Figueiredo, R. F. de, Santos, T. J. S., Tonetto, E. M. 2018. Petrology, geochemistry and U-Pb zircon and baddeleyite ages of the alkaline rocks from the central-southern Guyana Shield, northern Amazonian Craton. Journal of South American Earth Sciences, 86, 461–474.

Fitton, J.G., Upton, B.G.J., 1987.Alkaline igneous rocks. Geological Society of London, London, 568 pp.

Fletcher, C.J.N., Beddoe-Stephens, B. 1987. The petrology, chemistry and crystallization history of the Velasco alkaline province, eastern Bolivia. In: Fitton, J.G., Upton, B.G.J. (Eds.) Alkaline igneous rocks. Geological Society Special Publication 30, 403-413.

Fraga, L.M.B., Almeida, M.E., Macambira, M.J.B., 1997. First lead-lead zircon ages of charnockitic rocks from Central Guiana Belt (CGB) in the state of Roraima, Brazil, in: South American Symposium on Isotope Geology, Campos do Jordão, SP, 115-117.

Fraga, L.M.B., 2002. A associação anortosito-mangerito-granito rapakivi (AMG) do Cinturão Guiana Central, Roraima, e suas encaixantes paleoproterozóicas: evolução estrutural, geocronologia e petrologia. PhD thesis, Federal University of Pará, 351 pp.

Fraga, L.M., Dall'Agnol, R., Costa, J.B.S., Macambira, M.J.B., 2009. The Mesoproterozoic Mucajaí anorthosite-mangerite-rapakivi granite complex, Amazonian Craton, Brazil. The Canadian Mineralogist 47, 1469-1492.

Fraga L.M.B., Cordani U., Kroonenberg S., De Roever E., Nadeau S., and Maurer V.C. 2017. U-PB SHRIMP new data on the high-grade supracrustal rocks of the Cauarane Coeroeni Belt - insights on the tectonic Eo-Orosirian evolution of the Guiana Shield. In: 15º Simpósio De Geologia da Amazônia, anais, 486-490.

Gaudette, H. E., Olszewski Jr., W. J., Santos, J.O.S., 1996. Geochronology of Precambrian rocks from the northern part of Guiana Shield, State of Roraima, Brazil. Journal of South American Earth Sciences 9, 183- 195.

Guarino, V., Wu, F. Y., Lustrino, M., Melluso, L., Brotzu, P., Gomes, C. de B., Svisero, D. P. 2013. U-Pb ages, Sr-Nd- isotope geochemistry, and petrogenesis of kimberlites, kamafugites and phlogopite-picrites of the Alto Paranaíba Igneous Province, Brazil. Chemical Geology, 353, 65–82.

Gibson, S.A., Thompson, R.N., Leonardos, O.H., Dickin, A.P., Mitchell, J.G., 1995. The Late Cretaceous impact of the Trindade mantle plume: Evidence from large volume, mafic potassic magmatism in SE Brazil. Journal of Petrology 36, 189-229.

Gibson, S.A., Thompson, R.N., Leonardos, O.H., Dickin, A.P., Mitchell, J.G., 1999. The limited extent of plume-lithosphere interactions during continental flood-basalt genesis: Geochemical evidence from Cretaceous magmatism in southern Brazil. Contributions to Mineralogy and Petrology 137, 147-169.

Gibson, S. A., R. N. Thompson, and J. A. Day. 2006. "Timescales and Mechanisms of Plume-Lithosphere Interactions: 40Ar/39Ar Geochronology and Geochemistry of Alkaline Igneous Rocks from the Paraná-Etendeka Large Igneous Province." Earth and Planetary Science Letters 251(1–2): 1–17.

Gibbs A.K., Barron C.N. 1993. Geology of the Guiana shield. Oxford University Press (Oxford): 246 pp.

Ghiorso, M.S., Sack, R.O., 1995. Chemical mass transfer in magmatic processes. IV. A revised and internally consistent thermodynamic model for the interpolation and extrapolation of liquid–solid equilibria in magmatic systems at elevated temperatures and pressures. Contributions to Mineralogy and Petrology 119, 197–212.

Gillespie, M.R., Stephenson, D., Millward, D. 2008. BGS classification of lithodemic unit: Proposals for classifying units of intrusive rocks. *British Geological Survey Research Report RR/08/05*.

Gomes, C.B., Ruberti, E., Morbidelli, L., 1990. Carbonatite complexes from Brazil: A review. Journal of South American Earth Sciences 3, 51-63.

Gomes, C.B., Comin-Chiaramonti, P., 2005. An introduction to the alkaline and alkaline-carbonatitic magmatism in and around the Paraná Basin. In: Comin-Chiaramonti, P., Gomes, C.B. (Eds.), Mesozoic to Cenozoic Alkaline Magmatism in the Brazilian Platform. Edusp/Fapesp, São Paulo, pp. 21-29.

Gomes, C. B., Ruberti E., Comin-Chiaramonti P., and Azzone, R. G. 2011. "Alkaline Magmatism in the Ponta Grossa Arch, SE Brazil: A Review." Journal of South American Earth Sciences 32(2): 152–68.

Gomes, C. B., Comin-Chiaramonti, P. 2017. Magmatismo alcalino continental da região meridional da Plataforma Brasileira. São Paulo: Edusp. 595 p.

Gouyet, S., Unternehr, P., & Mascle, A. 1994. The French Guyana Margin and the Demerara Plateau: Geological History and Petroleum Plays. Hydrocarbon and Petroleum Geology of France, 411–422.

Hall, A. 1987. Igneous petrology. Longman Scientific Technical, 573 p

Hamilton, D.L., MacKenzie, W.S. 1965. Phase equilibrium studies in the system NaAlSiO4 (nepheline)-KAlSiO4 (kalsilite)-SiO2-H2O. Mineralogical Magazine, 34:214-231.

Heaman, L. M., Easton, R. M., Hart, T. R., Hollings, P., MacDonald, C. A., Smyk, M. C. 2007. Further refinement to the timing of Mesoproterozoic magmatism, Lake Nipigon region, Ontario. Canadian Journal of Earth Sciences, 44(8), 1055–1086.

Heaman, L.M., 2009. The application of U–Pb geochronology to mafic, ultramafic and alkaline rocks: an evaluation of three mineral standards. Chemical Geology 261, 43–52.

Heinonen, A.P., Fraga, L.M., Rämö, O.T., Dall'Agnol, R., Mänttäri, I., Andersen, T., 2012. Petrogenesis of the igneous Mucajaí AMG complex, northern Amazonian craton - Geochemical, U-Pb geochronological, and Nd-Hf-O isotopic constraints. Lithos 151, 17–34.

Isles D.J. and Rankin R.L. 2013. *Geological interpretation of aeromagnetic data.* Australia, CSIRO Publishing, 357 p.

Issler, R. S., 1974. Projeto Radam Brasil: Folha SA.22- Belém. DNPM, Rio de Janeiro, 503 pp.

Issler, R.S., Lima, R.M.G., Montalvao, G.G. 1975. Magmatismo alcalino no craton Guianense, in: Anais Décima Conferência Geológica Interguianas, Belém, Brazil, pp 103–122.

Issler, R.S., Silva, G.G., 1980. The Seis Lagos carbonatite complex. In: Congresso Brasileiro de Geologia 31, Camboriu, vol. 3, pp. 1564-1572.

Iwanuch, W. 1976. Idades Rb-Sr das alcalinas do "Domo do Sucunduri", AM. In: Congresso Brasileiro de Geologia XXIX, anais, p. 196.

Iwanuch, W. 1981. Geologia da região do domo do Sucunduri. Master thesis, University of São Paulo, pp 151.

Justo, L.J.E.C., Souza, M.M., 1986. Jazida de Niobio do Morro dos Seis Lagos, Amazonas. In: Schobbenhaus, C., Coelho, C.E.S. (Eds.), Principais Depositos Minerais do Brasil. Departamento Nacional de Produção Mineral, Brasília, pp. 463-468.

Katumwehe, A. B., Abdelsalam, M. G., and Atekwana, E. A. 2015. The role of pre-existing Precambrian structures in rift evolution: The Albertine and Rhino grabens, Uganda. Tectonophysics, 646, 117–129.

Kogarko, L.N. 1987. Alkaline rocks of the eastern part of the Baltic Shield (Kola Peninsula). In: Fitton, J.G., Upton, B.G.J. (Eds.) Alkaline igneous rocks. Geological Society Special Publication 30, 293-311.

Kramm, U., Kogarko, L. N. 1994. Nd and Sr isotope signatures of the Khibina and Lovozero agpaitic centres, Kola Alkaline province, Russia. Lithos, 32(3–4), 225–242.

Kroonenberg S.B., 1976. Amphibolite facies and granulite facies metamorphism in the Coeroeni Lucie area, southwestern Surinam. PhD Thesis, University of Amsterdam. Mededelingen Geologisch. Mijnbouwkundige Dienst Suriname 25: 101–289.

Kroonenberg, S. B., De Roever, E. W. F., Fraga, L. M., Reis, N. J., Faraco, T., Lafon, J. M., Wong, T. E. 2016. Paleoproterozoic evolution of the Guiana Shield in Suriname: A revised model. Geologie En Mijnbouw/Netherlands Journal of Geosciences, 95(4), 491–522.

Kwayisi, D., Lehmann, J., and Elburg, M. 2020. The architecture of the Buem Structural Unit: Implications for the tectonic evolution of the Pan-African Dahomeyide Orogen, West Africa. Precambrian Research, 338, 105568.

Labails, C., Olivet, J. L., Aslanian, D., and Roest, W. R. 2010. An alternative early opening scenario for the Central Atlantic Ocean. Earth and Planetary Science Letters, 297(3–4), 355–368.

Lamotte, F. D., Fourdan, B., Leleu, S., Leparmentier, F., and De Clarens, P. 2015. Style of rifting and the stages of Pangea breakup. Tectonics, 34(5), 1009–1029.

Leal, A.B.M., Girardi, V.A.V., Leal, L.R.B., 2000. Petrologia e geoquímica do magmatismo básico mesozoico da Suíte Básica Apoteri, estado de Roraima. Geochimica Brasiliensis 14, 155-174.

Leal, J.W.L., Silva, G.H., Santos, D.B., Teixeira, W., Fernandes, C.A.C., Pinto, A.C. 1978. Projeto Radam Brasil: Folha SC.20 Porto Velho. DNPM, Rio de Janeiro, 403 pp.

Legendre, C., Maury, R.C., Caroff, M., Guillou, H., Cotton, J., Chauvel, C., Bollinger, C., Hémond, C., Guille, G., Blais, S., Rossi, P., Savanier, D. 2005. Origin of exceptionally abundant phonolites on Ua Pou Island (Marquesas, French Polynesia): partial melting of basanites followed by crustal contamination. Journal of Petrology, 46:1925-1962.

Lemos, V. P., Costa, M. L., 1987. Partição das terras raras nos lateritos fosfáticos de Maicuru, PA. Anais, Congresso Brasileiro de Geoquímica, Porto Alegre 1, 83-102.

Le Maitre, R. W., 2002. Igneous Rocks: A classification and glossary of terms. Cambridge University Press, New York, 236 pp.

Litherland, M., Annels, R.N., Appleton, J.D., Berrange, J.P., Bloomfield, K., Burton, C.C., Darbyshire, D.P.F., Fletcher, C.J.N., Hawkins, M.P., Klink, B.A., Llanos, A., Mitchell, W.I., O'Connor, E.A., Pitfield, P.E., Power, G.,Webb, B.C. 1986. The geology and mineral resources of the Bolivian Precambrian Shield. Keyworth Overseas Memoir 9, British Geological Survey, 153p.

Louro, V. H. A., Negrão, A. P., Castro, L. G., Ferreira, F. J. F. 2019. Canoas geophysical anomaly: A possible alkaline body or unusual anomaly caused by mafic dykes in the Ponta Grossa Arch, Brazil, Journal of Applied Geophysics, 170.

Ludwig, K.R. 1991. ISOPLOT; a plotting and regression program for radiogenic-isotope data; version 2.53. USGS Open-File Report 91-445.

Lustrino, M., Wilson, M. 2007. "The Circum-Mediterranean Anorogenic Cenozoic Igneous Province." Earth-Science Reviews 81(1–2): 1–65.

Macciotta, G., Almeida, A., Barbieri, M., Beccaluva, L., Brotzu, P., Coltorti, M., Conte, A., Garbarino, C., Gomes, C. B., Morbidelli, L., Ruberti, E., Siena, F., & Traversa, G. 1990. Petrology of the tephrite-phonolite suite and cognate xenoliths of the Fortaleza district (Ceará, Brazil). European Journal of Mineralogy, 2(5), 687–710.

Marangoni, Y. R., Mantovani, M. S. M. 2013. Geophysical signatures of the alkaline intrusions bordering the Paraná Basin. Journal of South American Earth Sciences, 41, 83–98.

Markl, G., Marks, M.W., Schwinn, G., Sommer, H., 2001. Phase equilibrium constraints on intensive crystallization parameters of the Ilímaussaq Complex, South Greenland. Journal of Petrology 42, 2231–2257.

Marks, M. A. W., Hettmann, K., Schilling, J., Frost, B. R., Markl, G., 2011. The mineralogical diversity of alkaline igneous rocks: Critical factors for the transition from miaskitic to agpaitic phase assemblages. Journal of Petrology 52, 439–455.

Marks, M. A. W., Markl, G. 2017. A global review on agpaitic rocks. Earth-Science Reviews, 173(July), 229–258.

Marsh, J. S. 2010. The geochemistry and evolution of Palaeogene phonolites, central Namibia. Lithos, 117(1–4), 149–160.

Marzoli A., Renne P.R., Piccirillo E.M., Ernesto M., Bellieni G., De Min A. 1999. Extensive 200-Million-Year-Old Continental Flood Basalts of the Central Atlantic Magmatic Province. Science 284, 616–618.

Matheus, G.F. 2019. Geocronologia U-Pb em badeleíta aplicado às rochas alcalinas do sul do estado de São Paulo. Dissertação de mestrado. Instituto de Geociências – Universidade Estadual de Campinas, 98 p.

Matton, G. and Jébrak, M. 2009. The Cretaceous Peri-Atlantic Alkaline Pulse (PAAP): Deep mantle plume origin or shallow lithospheric break-up? Tectonophysics, 469(1–4), 1–12.

McDonough, W.F., Sun, S., 1995. The composition of the Earth. Chemical Geology 120, 223-253.

Middlemost, E.A.K., 1975. The basalt clan. Earth Science Reviews 11, 337-364.

Miller H.G. and Singh V. 1994. Potential field tilt –a new concept for location of potential field sources. *Journal of Applied Geophysics*, **32**(2-3): 213-217.

Montalvão, R. M.G., Muniz, M. C., Issler R. S., Dall'Agnol R., Lima M. I. C., Fernandes P. E. C. A, Silva G. G. 1975. Projeto Radam Brasil 8v: Folha NA.20- Boa Vista e parte das folhas NA.21 - Tumucumaque, NB.20 – Roraima e NB.21. DNPM, Rio de Janeiro, 403 pp.

Morbidelli, L., Gomes, C.B., Beccaluva, L., Brotzu, P., Conte, A.M., Ruberti, E., Traversa, G., 1995. Mineralogical, petrological and geochemical aspects of alkaline and alkaline carbonatite associations from Brazil. Earth Sciences Review 39, 135-168.

Moreau, C., Ohnenstetter, D., Demaiffe, D., Robineau, B. 1996. The Los Archipelago nepheline syenite ring-structure: A magmatic marker of the evolution of the central and equatorial atlantic. Canadian Mineralogist, 34(2), 281–299.

Moulin, M., Aslanian, D., & Unternehr, P. 2010. A new starting point for the South and Equatorial Atlantic Ocean. Earth-Science Reviews, 98(1–2), 1–37.

Navarro, M.S., Tonetto, E.M., Oliveira, E.P., 2015. LA-SF-ICP-MS U-Pb zircon dating at University of Campinas, Brazi. In: IAG, Geoanalysis 2015. Leoben, CD-ROM.

Ngonge, E. D., de Hollanda, M. H. B. M., Pimentel, M. M., Oliveira, D. C. 2016. Petrology of the alkaline rocks of the Macau Volcanic Field, NE Brazil. Lithos, 266–267, 453–470.

Nomade, S., Knight, K. B., Beutel, E., Renne, P. R., Verati, C., Féraud, G., … Bertrand, H.

2007. Chronology of the Central Atlantic Magmatic Province: Implications for the Central Atlantic rifting processes and the Triassic-Jurassic biotic crisis. Palaeogeography, Palaeoclimatology, Palaeoecology, 244(1–4), 326–344.

Oliveira, A.S., Fernandes, C.A.C., Issler, R.S., Abreu, A.S., Montalvão., R.M.G., Teixeira, W. 1975. Projeto Radam Brasil: Folha NA.21- Tumucumaque e parte da folha NB.21. DNPM, Rio de Janeiro, pp 361.

Peate, D.W. 1997. The Paraná-Etendeka Province. In: Mahoney, J.J. & Coffin, M.F. (eds.) Large igneous provinces: continental, oceanic and planetary flood volcanism. Geophysical Monograph, AGU 100, 217-246.

Petronilho L.A. 2009. Método Sm-Nd no CPGeo-IGc-USP: procedimentos analíticos atualmente em rotina. In: Simpósio 45 anos de Geocronologia no Brasil, Boletim de Resumos Expandidos, 116-118.

Pinto, V. M., Santos, J. O. S., Ronchi, L. H., Hartmann, L. A., Bicudo, C. A., de Souza, V. 2017. Field and geochemical constraints on the relationship between the Apoteri basalts (northern Brazil, southwestern Guyana) and the Central Atlantic Magmatic Province. Journal of South American Earth Sciences, 79, 384–393. https://doi.org/10.1016/j.jsames.2017.08.015.

Pirajno, F., 2015. Intracontinental anorogenic alkaline magmatism and carbonatites, associated mineral systems and the mantle plume connection. Gondwana Research 27, 1181–1216.

Premoli, C., Kroonenberg, S. B. 1984. Radioactive Mineral Potential of Carbonatites in Western Parts of the South American Shields. Geology and Metallogenesis of Uranium Deposits in South America: Proceedings of Working Group Meeting, San Luis, Argentina, pp 245-268.

Reis, N. J., Fraga, L.M., Faria, M.S.G., Almeida, M. E., 2003. A geologia de Roraima. Géologie de la France 2-3-4, 121-134.

Reis N.J., Faria M.S.G., Almeida M.E., Oliveira M.A. 2004. Folhas NA.20-Boa Vista e NB.20-Roraima. In: Schobbenhaus, C., Gonçalves, J.H., Santos, J.O.S., Abram, M.B., Leão Neto, R., Matos, G.M.M., Vidotti, R.M., Ramos, M.A.B., Jesus, J.D.A.de. (Eds.) Carta Geológica do Brasil ao Milionésimo, Sistema de Informações Geográficas-SIG, Programa Geologia do Brasil. CPRM, Brasília, CD-ROM.

Reis, N.J, Szatmari, P, Wanderley Filho, J.R, York, D, Evensen, N.M, Smith, P.E., 2006. Dois eventos de magmatismo máfico mesozóico na fronteira Brasil-Guiana, Escudo das Guianas: enfoque à região do rifte Tacutu-North Savannas, in: 43º Congresso Brasileiro de Geologia, Aracaju, 459–46.

Riccomini, C., Velázquez, V.F., Gomes, C.B., 2005. Tectonic controls of the Mesozoic and Cenozoic alkaline magmatism in Central-Southeastern Brazilian Platform. In: Comin-Chiaramonti, P., Gomes, C.B. (Eds.), Mesozoic to Cenozoic Alkaline Magmatism in the Brazilian Platform. Edusp/Fapesp, São Paulo, pp. 31 - 55.

Rocha, L. G. M., Pires, A. C. B., Carmelo, A. C., & Araújo Filho, J. O. de. 2014. Geophysical characterization of the Azimuth 125 lineament with aeromagnetic data: Contributions to the geology of central Brazil. Precambrian Research, 249, 273–287.

Rock, N. M.S. 1981. “How Should Igneous Rocks Be Grouped?” Geological Magazine 118(5): 449–61.

Rooney, T. O. 2017. The Cenozoic magmatism of East-Africa: Part I — Flood basalts and pulsed magmatism. Lithos, 286–287, 264–301.

Rossoni, M. B., Bastos Neto, A. C., Souza, V. S., Marques, J. C., Dantas, E., Botelho, N. F., Pereira, V. P. 2017. U-Pb zircon geochronologycal investigation on the Morro dos Seis Lagos Carbonatite Complex and associated Nb deposit (Amazonas, Brazil). Journal of South American Earth Sciences, 80, 1–17.

Salas, N. J., Santos, J. O. S., 1974. Determinações geocronológicas pelo método da birrefringência em phonolite na área do Projeto Norte da Amazônia, in: 28º Congresso Brasileiro de Geologia, Porto Alegre, 221-224.

Santos, J. O. S., Hartmann, L. A., Gaudette, H. E., Groves, D. I., Mcnaughton, N. J., Fletcher, I. R., 2000. A new understanding of the Provinces of the Amazon Craton based on integration of field mapping and U-Pb and Sm-Nd Geochronology. Gondwana Research 3, 453-488.

Santos, J.O.S., Faria, M.S.G., Riker, S.R., Souza, M.M., Hartmann, L.A., Almeida, M.E., McNaughton, N.J., Fletcher, I.R., 2006b. A faixa colisional K’Mudku (idade Greenvilliana) no norte do Cráton Amazonas: reflexo intracontinental do orógeno Sunsás na margem ocidental do Cráton, in: 9º Simpósio de Geologia da Amazônia, Belém, CD-ROM.

Santos J.O.S. 2003. Geotectônica dos Escudos das Guianas e Brasil Central. In: Bizzi L.A., Schobbenhaus C., Vidotti R.M., Gonçalves J.H (Eds.) Geologia, Tectônica e Recursos Minerais do Brasil: texto, mapas e SIG. Brasilia, CPRM, p. 169–226.

Seton, M., Müller, R. D., Zahirovic, S., Gaina, C., Torsvik, T., Shephard, G., … Chandler, M. 2012. Global continental and ocean basin reconstructions since 200Ma. Earth-Science Reviews, 113(3–4), 212–270.

Shand, S. J., 1943. Eruptive rocks: Their genesis, composition, classification, and their relation to ore-deposits with a chapter on Meteorite. John Wiley & Sons, New York, 488 pp.

Sial, A.N. 1987. The Tertiary alkaline province of Fortaleza, State of Ceará, Brazil: oxygen isotopes and REE-geochemistry. Geoch. BrasiL, 1, 41-51.

Silva, H.G., Leal, J.W.L., Salum, O.A.L., Dall’Agnol, R., Basei, M.A.S. 1974. Esboço Geológico de parte da Folha SC21 Juruena. In: XXVIII Congresso Brasileiro de Geologia, v.4, pp 309-320.

Spinelli, F.P., Gomes, C.B. 2009. A ocorrência alcalina de Cananeia, litoral sul do Estado de São Paulo: petrologia e geoquímica. Revista Brasileira de Geociências, 39:304-323.

Silveira, F.V., 2006. *Magmatismo cenozóico da porção central do Rio Grande do Norte, NE do Brasil.* Tese (doutorado). Universidade Federal do Rio Grande do Norte, Natal, 220 pp.

Silva, A.B., Liberal, G.S., Grossi Sad, J.H., Issa Filho, A., Rodrigues, C.S. and Riffel, B.F. (1988) Geologia e petrologia do complexo Angico dos Dias (Bahia, Brasil), uma associação carbonatitica Precambriana. Geochimica Brasiliensis, 2, 81 –108.

Silva, M.G, Porsani M.J. 2006. Aplicação de balanceamento espectral e DMO no processamento sísmico da Bacia do Tacutu. Revista Brasileira de Geofísica, 24: 273–290.

Soares, M.A., 1985, Estudio petrografico de la estructura alcalina La Churuata, Territorio Federal Amazonas: Congreso Geologico Venezolano, 6th, Caracas, Memoria, v. 4, pp. 2117-2158.

Söderlund, U., Johansson, L., 2002. A simple way to extract baddeleyite (ZrO2). Geochemistry, Geophysics and Geosystems 3, 1-7.

Souza S.L. 2009. Métodos radiométricos Rb-Sr e Sm-Nd no CPGeo IGc-USP. In: Simpósio 45 anos de Geocronologia no Brasil, Boletim de Resumos Expandidos, 137-139.

Souza, V. D. S., Souza, A. G. H., Dantas, E. L., Valério, C. D. S., 2015. K'Mudku A-type magmatism in the southernmost Guyana shield, central-north Amazon Craton (Brazil): The case of Pedra do Gavião syenogranite. Brazilian Journal of Geology 45, 293–306.

Spampinato, G. P. T., Betts, P. G., Ailleres, L., and Armit, R. J. 2015. Early tectonic evolution of the Thomson Orogen in Queensland inferred from constrained magnetic and gravity data. Tectonophysics, 651, 99–120.

Streck, M.J., 2008. Mineral textures and zoning as evidence for open system processes. Reviews in Mineralogy and Geochemistry 69, 595–622.

Svensen, H., Corfu, F., Polteau, S., Hammer, Ø., Planke, S. 2012. Rapid magma emplacement in the Karoo Large Igneous Province. Earth and Planetary Science Letters, 325–326, 1–9.

Tassinari, C.C.G. 1996. O mapa geocronológico do Cráton Amazônico no Brasil: revisão dos dados isotópicos. Habilitation thesis, University of São Paulo, 139 pp.

Tassinari, C. C. G., Macambira, M. J. B., 1999. Geochronological Provinces of the Amazonian Craton. Episodes 22, 174-182.

Tassinari, C. C. G.; Bettencourt, J. S.; Geraldes, M. C.; Macambira, M. J. B.; Lafon, J. M. 2000. The Amazonian cráton. In: Cordani, U. G.; Milani,E. J.; Thomaz Filho, A.; Campos, D. A. (Eds.)Tectonic evolution of South America. Rio de Janei-ro, s.n. p. 41-95.

Tassinari, C.C.G., Macambira M.J.B., 2004. A evolução tectônica do Cráton Amazônico. In: Neto, V. M.; Bartorelli, A.; Carneiro, C.D.R.; Neves, B.B.B. (Eds.), Geologia do Continente Sul-Americano: Evolução da obra de Fernando Flávio Marques de Almeida. Beca, São Paulo, 471-485.

Teixeira, W., 1978. Significação tectônica do magmatismo anorogênico básico e alcalino na região amazônica. M.S thesis, University of São Paulo, 99 p.

Teixeira, W., Tassinari, C.C.G., Cordani, U.G., Kawashita, K. 1989. "A Review of the Geochronology of the Amazonian Craton: Tectonic Implications." Precambrian Research 42(3–4): 213–27.

Thompson, R.N., Gibson, S.A., Mitchell, J.G., Dickin, A.P., Leonardos, O.H., Brod, J.A., Greenwood, J.C., 1998. Migrating Cretaceous–Eocene magmatism in the Serra do mar Alkaline Province, SE Brazil: melts from the deflected Trindade mantle plume? Journal of Petrology 39, 1493–1526.

Torsvik, Trond H., Mark A. Smethurst, Kevin Burke, and Bernhard Steinberger. 2008. "Long Term Stability in Deep Mantle Structure: Evidence from the ~ 300 Ma Skagerrak-Centered Large Igneous Province (the SCLIP)." Earth and Planetary Science Letters 267(3–4): 444–52.

Ulbrich, H.H.G.J, Gomes, C.B., 1981. Alkaline rocks from continental Brazil. Earth-Science Reviews 17, 135–154.

Vaz, P.T., Wanderley Filho, J.R., Bueno, G.V. 2007. Bacia do Tacutu. Boletim de Geociências da Petrobras 15, 289–297.

Vendemiatto, M.A., Enzweiler, J., 2001. Routine control of accuracy in silicate rock analysis by X-Ray Fluorescence Spectrometry. Geostandards and Geoanalytical Research. 25, 283-291.

Verduzco B., Fairhead J.D., Green C.M., Mackenzie C. 2004. New insights into magnetic derivatives for structural mapping. *The Leading Edge*, **23**(2): 116-119.

Wilson, M., and Downes, H. 1991. "Tertiary - Quaternary Extension-Related Alkaline Magmatism in Western and Central Europe." Journal of Petrology 32(4): 811–49.

Wilson, M., and Downes, H. 1992. "Mafic Alkaline Magmatism Associated with the European Cenozoic Rift System." Tectonophysics 208(1–3): 173–82.

Wohlgemuth-Ueberwasser, C.C., Söderlund, U., Pease, V., Nilsson, M.K.M., 2015. Quadrupole LA-ICP-MS U/Pb geochronology of baddeleyite single crystals. Journal of Analytical Atomic Spectrometry 30, 1191-1196.

Woolley, A.R. 1987. Alkaline rocks and carbonatites of the World. Part I: North and South America. London: British Museum (Natural History), 216p.